PROTECTION OF ULTRA LONG HVDC TRANSMISSION LINES

By

Divoloshanan Naidoo BSc (Eng)

A dissertation submitted to the Discipline of Electrical Engineering at the University of KwaZulu-Natal in partial fulfilment for the requirements of the degree of Master of Science (Engineering)(Power and Energy).

UNIVERSITY OF
KWAZULU-NATAL

Supervisor

Professor N.M. Ijumba

BSc (Hons) Eng (Dar-es-Salaam), MSc (Salford), PhD (Strathclyde),

PrEng, CEng, MIEE, MIEEE, REng (Kenya and Tanzania)

March 2005

Declaration

I, the undersigned, hereby declare that the material presented in this dissertation is my own work, except where specific acknowledgement is made in the form of a reference.

_____

D. Naidoo

Abstract

HVDC transmission is today widely used in modern Power Systems as an alternative to HVAC. Current trends indicate that many future conventional HVDC systems will be systems of increasing power ratings, delivered over larger distances as well as multi-terminal systems. In order to ensure the security and dependability of such systems, the current protection schemes need to be evaluated to assess their ability to provide adequate protection for the envisaged HVDC systems.

This research work firstly reviews the present HVDC transmission line protection systems, and highlights their advantages and disadvantages, including factors that adversely influence their performance. The author critically evaluates the current protection schemes and reveals the drawbacks and other factors that render them unsuitable for the protection of long dc transmission lines.

The author then goes on to propose and develop an HVDC line protection system that will be able to provide adequate protection for proposed long HVDC transmission lines. The proposed protection system is able to make decisions based solely on local detection increasing its overall reliability. The author then recommends that the proposed protection system be used in conjunction with the existing main protection system in order to optimise the protection response times for both close in and distant faults. The author also proposes and develops a method of further enhancing the reliability of the protection system by the use of the telecommunication infrastructure when available.

Finally the performance and feasibility of the proposed protection system is evaluated using the results obtained from the extensive fault simulations performed in EMTDC and Matlab. The simulations are performed using a bipole model of an HVDC System on which the required line and protection systems are modelled. The simulation results obtained are very favourable and promote the use of this proposed protection system, for the protection of long HVDC transmission lines.

Acknowledgements

I would like to take this opportunity to thank my employer, Eskom Distribution, as well as the HVDC Centre for fully supporting and funding this research work, which made the realization of this dissertation possible.

My special thanks go out to my family and friends for their continued support, patience and motivation during this study phase of my life.

A special word of thanks goes out to my supervisor, Professor N.M. Ijumba for his invaluable help and guidance in putting this research work together.

I would also like to extend a word of thanks to Dr D. Muthumuni, from the Manitoba HVDC Research Centre in Canada, for his help in acquiring the bipole HVDC case model.

Finally, I would like to thank Ms Leena Rajpal and the rest of HVDC Centre personnel for their continued help and support.

Abbreviations

AC : Alternating Current

ACCF : Auxiliary Cross-Correlation Function

C : Capacitance

CCF : Cross-Correlation Function

DC : Direct Current

D_f : Distance to fault

EMTDC : Electromagnetic Transients including DC

G : Conductance

GPS : Global Positioning System

HVDC : High Voltage Direct Current

I : Current

K_r : Reflection Coefficient

K_t : Refraction\Transmission Coefficient

L : Inductance

LL : Line Length

NP-G : Negative Pole to Ground

P1 : Pole 1

P2 : Pole 2

P-G : Pole to Ground

PLC : Power Line Carrier

P-P : Pole to Pole

PP-G : Positive Pole to Ground

P-P-G : Pole to Pole to Ground

P_s : Protection Starter

pu : Per Unit

R : Resistance

SCCF : Standard Cross-Correlation Function

SCR : Short Circuit Ratio

U : Voltage

v : Velocity

Z : Impedance

Table of Contents

Abstract iii
Acknowledgements iv
Abbreviations v
Table of Figures viii
Table of Tables xiv

Chapter 1: Introduction 1
1.1. Background 1
1.2. Problem Identification 4
1.3. Research Problem 5
1.4. Hypothesis 6
1.5. Objective 6
1.6. Research Design and Methodology 6
1.7. Dissertation Outline 7

Chapter 2: Literature Survey 8
2.1 HVDC Line Protection 8
2.1.1. Causes of HVDC Line Faults 8
2.1.2. HVDC Line Fault Development 8
2.1.3. Role of HVDC Line Protection 9
2.1.4. Methods of HVDC Line Protection 10
2.1.4.1. Voltage derivative protection 10
2.1.4.2. Travelling Wave Protection 12
2.1.4.3. Current Differential Protection 14
2.1.4.4. DC Voltage level Protection 16
2.1.5. Cable Section Fault Detection 17
2.1.6. Fault Clearing and Recovery 18
2.1.7. HVDC Line Protection Telecommunications Requirements 19
2.1.8. Security and Reliability of Current HVDC Line Protection 20
2.2. Travelling Waves 21
2.2.1. Theory 21
2.2.2. Reflection of Travelling Waves 24
2.2.3. Attenuation and Distortion of Travelling Waves 28
2.2.4. Successive Reflection of Travelling Waves 29
2.2.5. Termination Waveform Frequency Dominance 31
2.2.6. Multiconductor Systems 35

Chapter 3: Proposed Protection Methods 39
3.1. Introduction 39
3.2. Local fault Detection Method 39
3.2.1. Method Formulation 39
3.2.2. Cross-Correlation 45
3.2.3. Protection Starter Requirements 49
3.2.4. Possible Protection Starters 51
3.2.5. Bipolar System Considerations 54
3.2.6. Limitations of Standard Cross-Correlation Function 56
3.2.7. Auxiliary Cross-Correlation Function 59
3.2.8. Cross-Correlation Fault Location Strategy 60

3.2.9. Functioning of Complete Local Detection Protection System 62
3.3. Method of Using Telecommunications for Optimization. 64
3.4. Proposed Complete DC Line Main Protection Scheme 67

Chapter 4: Research Design and Methodology 68
4.1. Introduction 68
4.2. PSCAD/EMTDC 68
4.3. HVDC System Model 69
4.4. HVDC Transmission Line Model 73
4.4.1. Transmission Line Details 74
4.4.2. PSCAD/EMTDC Modelling of a Transmission Line 76
4.4.3. Modelling the Proposed HVDC Transmission Line in PSCAD 79
4.4.4. Incorporating the Line Model into HVDC System Model 81
4.5. DC Side Filters 82
4.6. Protection Modelling 84
4.6.1. Calculation of Modal Voltages and Currents 84
4.6.2. Protection Starter Modelling 85
4.6.3. Calculation of Relaying Signals 86
4.6.4. Protection System Algorithm 89
4.7. External Fault Modelling 92
4.8. Simulation Procedure 93

Chapter 5: Simulation Results and Discussion 94
5.1. Startup and Steady State Operating Conditions 94
5.2. Protection Starter and Correlation Settings 97
5.3. Sampling Interval 98
5.4. Fault Simulations 99
5.4.1. Pole to Ground Faults 99
5.4.2. Bipole Faults 122
5.4.3. Startup Faults 128
5.4.3.1. Faults existing prior to Startup\Restart 128
5.4.3.1. Faults Occurring During Startup 129
5.4.4. Close in Faults 131
5.4.5. External Faults 134
5.4.5.1. External Faults behind the Relaying Point 134
5.4.5.2. External Faults in Front of the Relaying Point 136
5.4.6. Effect of the DC Filters on the Correlation Function. 138
5.4.7. Effect of the Control System on the Correlation Function. 139
5.4.8. Fault Detection using Telecommunications Method 141
5.4.9. Fault Detection with One Pole Out of Service 146

Chapter 6: Conclusion and Recommendations 148
6.1. Conclusion 148
6.2. Recommendations for Further Work 151

References 152
Appendix A 158
Appendix B 164
Appendix C 168

Table of Figures

Fig. 2.1. High level Block Diagram of a Voltage Derivative Protection Scheme 11
Fig. 2.2. Example of different measurements used to determine existence of dc line fault 12
Fig. 2.3. Differential current calculation for two terminal point to point HVDC system 14
Fig. 2.4. Differential current calculation for parallel multi-terminal HVDC system 14
Fig. 2.5. Block Diagram of Differential current scheme used to protect HVDC transmission lines 15
Fig 2.6. Schematic diagram of an elemental section of a single phase transmission line 22
Fig. 2.7. Travelling voltage and current waves leaving the disturbed area 24
Fig. 2.8. Reflection of Travelling waves at a discontinuity 25
Fig. 2.9. Bewley Lattice Diagram of System in Fig 2.7 29
Fig 2.10. Simple Transmission Line 31
Fig 2.11. Surge propagation on a simple line with large source impedance 33
Fig 2.12. Surge propagation on a simple line with small source impedance 33
Fig 2.13. Positive and Zero Sequences Waves on HVDC Bipolar Transmission Lines 36
Fig 3.1. HVDC Transmission Line Fault with zero fault resistance with total reflection at terminations 40
Fig 3.2. HVDC Transmission Line Fault with finite fault resistance and total reflection at terminations 42
Fig 3.3. HVDC Transmission Line Fault with finite fault resistance located at the centre of the line 44
Fig 3.5. Fault located beyond the transmission line in front of the relay pointing 50
Fig 3.6. Fault located behind relaying point 50
Fig 3.7. Illustration of the Modal/Sequence Networks 55
Fig 3.8. Bewley Lattice Diagram illustrating possible cause of inaccuracy in cross-correlation function 56
Fig 3.9. Connection of modal networks for pole to ground fault 58
Fig 3.10. Flowchart of correlation process 61
Fig 3.11. Flowchart of fault location and detection process 62

Fig 3.12 Flowchart of Complete Local Protection System 63
Fig 3.13. Block Diagram of Complete DC Line Main Protection Scheme 67
Fig 4.1. Schematic Diagram of the Electrical System Model 70
Fig 4.2. Schematic Diagram of the Rectifier Control System Model 71
Fig 4.3. Schematic Diagram of the Pole Inverter Control System Model 72
Fig 4.4. Currently used line model in HVDC System 73
Fig 4.5. HVDC Transmission Line and Tower Configuration 75
Fig 4.6. HVDC Transmission Line Modelling in PSCAD 76
Fig 4.7. Complete Line Model with Auxiliary Components Required for Fault Simulation 80
Fig 4.8. Incorporating the Proposed Line Model into the HVDC System Model 81
Fig 4.9. High Pass and 12th Harmonic DC Filters 83
Fig 4.10. Implementation of DC Filters on the Positive Pole 83
Fig 4.11. Calculation of Modal Voltages and Currents 84
Fig 4.12. Time Shifting of Modal Voltages and Currents 85
Fig 4.13. Protection Starter Implementation 86
Fig 4.14. Output of Line Constants Program 87
Fig 4.15. Calculation of DELTA_U1_pu and DELTA_I1_pu 88
Fig 4.16. Calculation of Relaying Signals S_F and S_B 88
Fig 4.17. AC System Fault Modelling 92
Fig 5.1. Startup and Steady State Operating DC Voltage and Current 94
Fig 5.2. Power Transfer per Pole in pu 95
Fig 5.3. Modal Line Voltages and Currents 95
Fig 5.4. Relaying Signal from Startup to Steady State 96
Fig 5.5. Protection Starter Values from Startup to Steady State 97
Fig 5.6. Modal Voltages and Currents for PP-G Fault Located 350kms from Relaying Point 100
Fig 5.7. Calculated Starter values for PP-G Fault at 10% of Line Length 100
Fig 5.8. Relaying Signals for PP-G Fault Located 350kms from Relaying Point 101
Fig 5.9. SCCF output for PP-G fault located at 350kms 101
Fig 5.10. Normalized SCCF output for a PP-G Fault located at 350kms 104
Fig 5.11. Modal Voltages and Currents for NP-G Fault Located 350kms from Relaying Point 105
Fig 5.12. Calculated Starter values for NP-G Fault at 10% of Line Length 105

Fig 5.13. Relaying Signals for NP-G Fault Located 350kms from Relaying Point 106
Fig 5.14. SCCF output for a NP-G Fault located at 350kms 106
Fig 5.15. SCCF output for a PP-G Fault located at 350kms with a 50Ω Fault Resistance 108
Fig 5.16. SCCF output for a PP-G Fault located at 350kms with a 100Ω Fault Resistance 108
Fig 5.17. SCCF output for a PP-G Fault located at 350kms with a 200Ω Fault Resistance 109
Fig 5.18. ACCF output for a PP-G Fault located at 350kms with a 200Ω Fault Resistance 109
Fig 5.19. SCCF output for a PP-G Fault located at 350kms with a 400Ω Fault Resistance 110
Fig 5.20. ACCF output for a PP-G Fault located at 350kms with a 400Ω Fault Resistance 111
Fig 5.21. SCCF output for a PP-G Fault located at 1750kms 116
Fig 5.22. ACCF output for a PP-G Fault located at 1750kms 116
Fig 5.23. SCCF output for a NP-G Fault with 400Ω Fault Resistance located at 1750kms 118
Fig 5.24. ACCF output for a NP-G Fault with 400Ω Fault Resistance located at 1750kms 118
Fig 5.25. Correlation Process with Additional Check added to detect midpoint faults 120
Fig 5.26. SCCF output for a P-G Fault Located at 1740kms 121
Fig 5.27. SCCF output for a P-G Fault Located at 1760kms 121
Fig 5.28. Modal Quantities for a Bipole Fault at 0.85s located at 1750kms 123
Fig 5.29. SCCF Output for a Bipole Fault at 1750kms 123
Fig 5.30. SCCF Output for a P-P Fault with 400Ω Bipole Fault Resistance at 1750kms 124
Fig 5.31. Schematic of P-P-G Fault Illustrating the Fault Resistances Present 125
Fig 5.32. Modal Quantities for unbalanced fault at 1750kms 125
Fig 5.33. SCCF Output for unbalanced P-P-G Fault with 400Ω between poles at 1750kms 126

Fig 5.34. SCCF Output for unbalanced P-P-G Fault with 400Ω in both fault paths at 1750kms 127
Fig 5.35. SCCF Output for P-G Fault at 20kms 131
Fig 5.36. SCCF Output for P-G Fault with a 400Ω Fault Resistance at 20kms 132
Fig 5.37. Modal Quantities for a Fault behind the Relaying Point 135
Fig 5.38. Starter and Relaying Signals for Fault behind the Relaying Point 136
Fig 5.39. SCCF Output for External P-P Fault in Front of the Relaying Point 137
Fig 5.40. ACCF Output for External P-P Fault in Front of the Relaying Point 137
Fig 5.41. SCCF Output for P-G Fault at 80% of Line with DC Filters 138
Fig 5.42. SCCF Output for P-G Fault at 80% of Line without DC Filters 139
Fig 5.43. SCCF Output for P-G Fault at 100% of Line with Control Action 140
Fig 5.44. SCCF Output for P-G Fault at 100% of Line without Control Action 140
Fig 5.45. Calculated Rectifier Starter Values for a Fault at the 350km 141
Fig 5.46. Calculated Inverter Starter Values for a Fault at the 350km 141
Fig 5.47. SCCF for P-G Fault at 1750km under Monopole Condition 147
Fig B.1. Modified HVDC System Model 165
Fig B.2. Protection System Modelling 166
Fig B.3. AC and DC Fault Modelling 167
Fig C.1. SCCF output for a P-G Fault located at 700kms 169
Fig C.2. SCCF output for a P-G Fault located at 700kms with 50Ω fault resistance. 169
Fig C.3. SCCF output for a P-G Fault located at 700kms with 100Ω fault resistance 169
Fig C.4. SCCF output for a P-G Fault located at 700kms with 200Ω fault resistance 170
Fig C.5. ACCF output for a P-G Fault located at 700kms with 200Ω fault resistance 170
Fig C.6. SCCF output for a P-G Fault located at 700kms with 400Ω fault resistance 170
Fig C.7. ACCF output for a P-G Fault located at 700kms with 400Ω fault resistance 171
Fig C.8. SCCF output for a P-G Fault located at 1400kms 171

Fig C.9. SCCF output for a P-G Fault located at 1400kms with 50Ω fault resistance 171
Fig C.10. SCCF output for a P-G Fault located at 1400kms with 100Ω fault resistance 172
Fig C.11. SCCF output for a P-G Fault located at 1400kms with 200Ω fault resistance 172
Fig C.12. ACCF output for a P-G Fault located at 1400kms with 200Ω fault resistance 172
Fig C.13. SCCF output for a P-G Fault located at 1400kms with 400Ω fault resistance 173
Fig C.14. ACCF output for a P-G Fault located at 1400kms with 400Ω fault resistance 173
Fig C.15. SCCF output for a P-G Fault located at 2100kms 173
Fig C.16. SCCF output for a P-G Fault located at 2100kms with 50Ω fault resistance 174
Fig C.17. SCCF output for a P-G Fault located at 2100kms with 100Ω fault resistance 174
Fig C.18. SCCF output for a P-G Fault located at 2100kms with 200Ω fault resistance 174
Fig C.19. ACCF output for a P-G Fault located at 2100kms with 200Ω fault resistance 175
Fig C.20. ACCF output for a P-G Fault located at 2100kms with 400Ω fault resistance 175
Fig C.21. ACCF output for a P-G Fault located at 2100kms with 400Ω fault resistance 175
Fig C.22. SCCF output for a P-G Fault located at 2800kms 176
Fig C.23. SCCF output for a P-G Fault located at 2800kms with 50Ω fault resistance 176
Fig C.24. SCCF output for a P-G Fault located at 2800kms with 100Ω fault resistance 176
Fig C.25. ACCF output for a P-G Fault located at 2800kms with 100Ω fault resistance 177
Fig C.26. SCCF output for a P-G Fault located at 2800kms with 200Ω fault resistance 177

Fig C.27. ACCF output for a P-G Fault located at 2800kms with 200Ω fault resistance 177
Fig C.28. SCCF output for a P-G Fault located at 2800kms with 400Ω fault resistance 178
Fig C.29. ACCF output for a P-G Fault located at 2800kms with 400Ω fault resistance 178

Table of Tables

Table 3.1. Changes in local quantities at the relaying location for various faults 52
Table 4.1. Specification of Bipole HVDC System under Study 69
Table 4.2. HVDC Transmission Line Information 75
Table 4.3. Frequency Dependent Model Parameters 77
Table 4.4. Comparison of Steady State Operating Conditions 82
Table 5.1. Fault Location Results for a NP-G Fault located at 350kms 112
Table 5.2. Fault Location Results for a Pole to Ground Fault located at 700kms 112
Table 5.3. Fault Location Results for a Pole to Ground Fault located at 1400kms 113
Table 5.4. Fault Location Results for a Pole to Ground Fault located at 2100kms 113
Table 5.5. Fault Location Results for a Pole to Ground Fault located at 2800kms 114
Table 5.6. Fault Location Results for a Pole to Ground Fault located at 3150kms 114
Table 5.7. Fault Location Results for a Pole to Ground Fault located at 3500kms 115
Table 5.8. Fault Location Results for a Bipole Faults located at 875kms 127
Table 5.9. Fault Location Results for a Bipole Faults located at 3325kms 128
Table 5.10. Fault Location Results for a Fault Existing Prior to Startup 129
Table 5.11. Fault Location Results for a P-G Faults occurring at Startup 130
Table 5.12. Fault Location Results for a Pole to Pole Faults occurring at Startup 131
Table 5.13. Fault Location Results for Close up Faults 133
Table 5.14. Fault Location Results using the TI for P-G Faults at 350kms 143
Table 5.15. Fault Location Results using the TI for Bipole Faults at 350kms 143
Table 5.16. Fault Location Results using TI for Faults at different locations 144
Table 5.17. Fault Location Results using TI for Startup Faults at different locations 145

Chapter 1: Introduction

1.1. Background

"Since the first commercial HVDC system installation in 1954 a huge amount of HVDC transmission systems have been installed" and successfully integrated into transmission networks around the world for almost 50 years [1]. "During the last 20 years, HVDC has become the dominating technology for long distance transmission of bulk power" [2].

"In the 1960s and 1970s, 800kV HVAC was introduced in several countries. But that technology has come to a halt. In contrast, HVDC technology has developed rapidly and so has the confidence in it, resulting in a shift from ac to dc for bulk power transmission systems" [2].

Apart from long distance transmission, HVDC technology provides the possibility of interconnecting asynchronous systems together allowing power to be transferred between these different systems. HVDC Transmission also has the advantage that there is no limit in terms of the length of submarine or underground cables through which power can be transmitted as opposed to HVAC Transmission which has a limit of around 50km [3].

Furthermore the current industry trend of interconnecting major transmission systems for improving reliability [4] and a quantum leap in efforts to conserve the environment tend to favour HVDC transmission over HVAC transmission due to [1],[5]:

- Its excellent control of power flow between dissimilar power systems.
- Its ability to provide stability improvements to the surrounding system by fast dynamic control.
- Its ability to provide a source of power injection without increasing the fault level at the connection point. "This means that it will not be necessary to change the circuit breakers in the existing network" [1].

- Its ability to rapidly change the direction of power flow.
- Its smaller environmental impact. HVDC as opposed to HVAC requires a smaller servitude for the same transmitted power.
- Its "higher availability and reliability rate, shown by more than 30 years of operation" [1].

HVDC transmission is, therefore, becoming today more and more attractive and is currently being widely used in modern power systems as an alternative to HVAC in applications that involve but not limited to the following [6], [7]:

- Bulk power transmission over long distances.
- Power transmission between asynchronous systems.
- Submarine and underground power transmission over long distances.

With the increasing demand for clean, renewable energy, utilities around the world are looking to exploit hydropower resources that are available [8], [9]. However, in most instances these hydropower resources are located in very remote areas which means that remote hydro generating plants would need to be established to harness this energy and long distance transmission would be required to transport this energy to the load centres. HVDC technology will in many cases be the only feasible option for the transmission of this bulk power [8-11]. The increasing need to transport bulk power from more distant and remote locations will result in the need for longer transmission lines, higher voltages, higher power ratings and in some cases multi-terminal HVDC systems [8-11].

A typical example of the above is the proposed Westcor Project where two 3000 - 3500km bipole HVDC lines will be built to carry bulk power from the Democratic Republic of Congo (DRC) to Southern Africa [11]. The first phase will use a 500kV HVDC link to transport around 3GW (1.5GW per bipole) to Southern Africa [11]. "The 800kV HVDC voltage will be introduced in the second phase to assist with the higher power transfers" [11].

In order to ensure the security and dependability of such systems, the current protection philosophies and systems need to be evaluated to assess their suitability to adequately protect future HVDC systems.

HVDC System protection can be divided into two major groups [7]:

- AC side protection functions.
- DC side protection functions

The AC side protection involves protection of the converter transformers, ac filters, shunt capacitors, shunt reactors and busbars. The DC side protection involves the protection of the valves, smoothing reactor, dc filters and dc line.

If one combines all the AC protection functions with the all the DC protection functions except for the protection of the dc transmission line, we can then associate these protection functions with the converter station. We can therefore break up the protection of the HVDC scheme into two more relevant components viz.

- Converter Station Protection
- DC Transmission Line Protection

The converter station protection systems are conventional and are in general either unit type protection or protection based on simple voltage and current thresholds. These protection functions should not be adversely influenced by the proposed future HVDC systems.

The DC line protection schemes however, especially the main protection schemes, are based on the system transients that occur during the fault condition. These dynamics are influenced by numerous factors, one of which being the transmission line lengths [12]. Therefore, it is expected that the existing main protection schemes will be influenced by increasing transmission line lengths [12].

1.2. Problem Identification

The most commonly used HVDC line protection systems include voltage derivative, travelling wave, current differential and voltage level protection [7], [13-16].

Voltage derivative and travelling wave protection are based on system transients (travelling waves) that occur during the fault condition. One of these protection schemes is normally used as the DC line main protection system [15], [16].

DC voltage level protection is generally used as backup to either the voltage derivative protection or travelling wave protection [15]. This protection system is not expected to be significantly influenced by the future changes in the HVDC system. The reason for the above is explained in 2.1.4.4.

Current differential protection can be used as either as a main or backup protection system, but is generally used as a backup protection system mainly because of its reliance on the telecommunication infrastructure [7], [15].

In general as the HVDC transmission line lengths increase, the cost involved with providing a telecommunication infrastructure increases. Now in order to use current differential protection as the main protection system a certain degree of reliability and redundancy is required by the telecommunications infrastructure. As illustrated in [17] the cost involved in providing the required reliability and redundancy, will in most cases not be financially viable. Current differential protection in these cases, will, therefore, only at best be able to be used as a backup protection system.

Fault detection in voltage derivative and travelling wave protection schemes are based on the amplitude and gradient of the incident travelling waves approaching the relaying point from the fault point on the line. However, as the fault distance from the relaying point increases and/or the fault impedance increases, the travelling waves become more damped and therefore, faults close to the inverter or high impedance faults become difficult to detect using this method [14]. This implies that the fault coverage of this type of protection scheme is limited and will, therefore, not be able to adequately protect the expected future HVDC systems with long transmission lines.

The above is further confirmed in [12] where the DLP 110 (voltage derivative protection) and DLP 120 (Travelling wave protection) algorithms were evaluated using an HVDC simulator. The system simulated was a 500kV bipole system with the details and line configurations as given in [12]. Problems in detection were experience with faults located beyond 2000km when using the DLP 110 algorithm [12]. The DLP 120 algorithm also experienced problems in detection when faults were located beyond 2300km [12]. The above problem has not yet been an issue because there is no HVDC transmission line in service that exceeds 2000km. The longest HVDC transmission line currently in service is 1700km (Inga-Shaba) [7], [8]. However, with the Westcor project projected to have a transmission length of 3000-3500km the above mentioned reach problems will become a major issue.

It can be therefore deduced that the currently used HVDC transmission line main protection systems will not be able to adequately protect the proposed HVDC systems with long transmission lines without any enhancements or modifications. Also in order to improve the reliability, any enhanced, modified or new schemes should not rely on a telecommunication infrastructure to make protection decisions i.e. all protection decisions must be based on the available local quantities [18].

This research work is, therefore, focused on developing a method of enhancing and/or modifying the existing main protection schemes, which will increase the existing protection coverage of the protection scheme in order to provide an adequate level of protection, for the proposed future HVDC systems with long transmission lines. The protection scheme must use locally available quantities to make all protection decisions and telecommunication should only be used to enhance the overall performance of the protection scheme.

1.3. Research Problem

Development of a method of enhancing and/or modifying the existing HVDC transmission line main protection schemes in order to provide the required level of protection for point to point two terminal HVDC Systems with long dc transmission lines between converter stations.

1.4. Hypothesis

The current HVDC line main protection systems based on travelling waves can be enhanced/modified using local quantities available at the relaying point in order to provide the required degree of reliability that will make them suitable for the protection of two terminal point to point HVDC systems with long dc transmission lines up to 3500km.

1.5. Objective

The objective of this research is to develop a protection method that is suitable for the protection of long dc transmission lines. In order to achieve this goal travelling waves initiated by fault conditions will be reviewed to determine ways in which these quantities can be used for fault detection. Ultimately the knowledge gained will be used to develop a protection method that will be able to provide adequate protection for ultra long HVDC transmission lines.

1.6. Research Design and Methodology

A brief description of the design and methodology adopted is outlined below:

- Firstly all possible methods in which the local quantities and/or any calculated quantities at the relaying point can be used for fault detection were investigated.
- Possible methods of enhancing the existing main protection system were then developed.
- Generic working model HVDC System in EMTDC had to be obtained.
- DC transmission line was then modelled in EMTDC using a suitable line model for transient simulations.
- Line model and HVDC system model were then integrated and performance evaluated to ensure acceptable performance under both steady state and transient conditions.

- All relevant simulations studies were thereafter conducted to determine whether or not the protection methods proposed will be able to reliably protect the long HVDC transmission line.

1.7. Dissertation Outline

The dissertation as been structured as follows:

- Chapter 1: Introduction – this chapter provides the background and motivation for the research. It identifies the specific problem and outlines the approach taken in order to try resolve this problem.

- Chapter 2: Literature Survey – this chapter presents an overview of the literature available on the current dc line protection systems and travelling waves.

- Chapter 3: Proposed Protection Methods – the formulation of new proposed protection methods of enhancing the current protection systems are discussed in this chapter.

- Chapter 4: Research Design and Methodology – this chapter provides an overview of the HVDC system modelling in EMTDC in order to evaluate the new proposed protection methods.

- Chapter 5: Simulation Results and Discussion – the results of the simulations are presented and discussed in this chapter.

- Chapter 6: Conclusion and Recommendations – conclusions that were drawn from the research work, recommendations and further work are presented in this chapter.

- References

- Appendices

Chapter 2: Literature Survey

2.1 HVDC Line Protection

The purpose of this section is to illustrate the importance of a reliable and dependable HVDC line protection system. This section attempts to cover this by first considering the common causes of faults and the fault development in HVDC lines. The common types of DC line protection systems will be then discussed with emphasis on the operating principles, advantages and disadvantages of the different methods. The method of fault clearance and re-energizing philosophies together with the telecommunication requirements are then touched upon and the section is concluded with an analysis of the current protection systems.

2.1.1. Causes of HVDC Line Faults

The protection of the DC line during line faults is of vital importance in assuring the continuity of power transmission. Although the DC transmission line is designed to be safe from any flashover by proper design, the possibility of short circuits due to the presence of trees, insulator pollution and bush fires is very high, especially in the remote areas through which the lines run and where efficient inspection and maintenance is not always possible. Moreover, weather conditions such as high temperature, humidity and strong winds favour the occurrence of flashovers when some of the aforementioned causes of short circuits have taken place [13].

2.1.2. HVDC Line Fault Development

The main characteristic of a dc line short circuit is that once started, it will not extinguish by itself until the current is brought down to zero and the arc deionised [14], [19]. DC line faults caused by lightning on overhead lines are often self-clearing, because they can deionise at the current zeros due to the line oscillations. However, this cannot be guaranteed [14] and the current must therefore be brought down to zero by control action to ensure fault clearance.

On occurrence of the dc fault the line voltage collapses and rectifier current rises, while the inverter current will tend to fall. The rectifier will then increase its firing angle to try and maintain the preset current value. At the inverter end, normal control action will cause the firing angle to decrease, even to less than 90° into rectification to try and maintain the inverter current. The above condition is, however, not normally allowed to occur in most HVDC systems for the various reasons given in [14] and [20]. The inverter end converters are prevented from going into rectification mode by monitoring the inverter extinction angle and ensuring that it is not allowed to exceed a specific maximum value.

Thus normal converter control is not adequate to reduce the fault current to zero. The reduction of the fault current down to zero is achieved by driving both converters into inversion once protection has detected the presence of a line fault.

2.1.3. Role of HVDC Line Protection

The role of the dc line protection is, therefore, to detect any line faults and by means of control action extinguish the fault and restore the system as fast as possible, if the fault is not permanent. If the fault is permanent, the protection systems must lockout only the faulted line.

Studies conducted in [21] confirm that majority of the DC line faults are transient in nature and are cleared after short de-energisation of faulted pole. These transient fault currents are much lower in HVDC systems (approx 2 to 3pu) than in ac systems [14], [18], [20]. This low fault current combined with the low impedance of the dc line, results in low voltages on the entire system even for distant faults [22].

These low voltages imply that the maximum power that can be transmitted during the fault condition is very low. "It is thus important to disconnect the faulty line and re-energize the system with the shortest possible delay" [22]. Also depending on the ac system strength and the power transported before the fault, the loss of the power injection provided by the HVDC system could threaten the receiving systems stability because of the sudden mismatch between load and available power. In order to

minimise any stability problems the dc injection should be re-established as soon as possible which, again stresses the importance of fast fault clearance and system recovery.

2.1.4. Methods of HVDC Line Protection

The most commonly used methods today in the protection of HVDC lines are:

- Voltage derivative protection.
- Travelling wave protection.
- Differential protection.
- DC Voltage level protection.

This section will briefly discuss each of these methods of protection illustrating their operating principles, advantages, disadvantages and also identify the possible gaps.

2.1.4.1. Voltage derivative protection

When a dc line fault occurs, the travelling waves initiated by the fault cause the dc voltage and line current to decrease and increase at a certain rate respectively. This method makes use of this travelling wave concept and is normally used as the dc line main protection. The dc voltages and currents are measured and the derivatives dU/dt and dI/dt are then obtained either by the use of a differentiator circuit or suitable algorithm.

The sign of dI/dt is used to indicate whether the fault is located on the line or in the DC yard i.e. a positive dI/dt at the rectifier terminal indicates that the fault is on the line side of the current transducer and a negative dI/dt indicates that the fault is in the DC yard. The opposite is true for the inverter terminal.

A weighted sum of the derivatives is then calculated using (1) and compared to a set threshold [14]. If this threshold is exceeded the protection will operate. Fig. 2.1 shows a block diagram of the most commonly used voltage derivative protection scheme.

$$\epsilon = K_1 \frac{dU}{dt} + K_2 \frac{dI}{dt} \quad (1)$$

Where

K_1 and K_2 are the assigned weights and ϵ is the weighted sum of the derivatives.

The protection is normally active in both the rectifier and inverter stations. In the event of a fault detected by the inverter protection, a signal is transmitted to the rectifier terminal via the interstation telecommunication system to initiate the fault clearing and restart logic [15].

In a bipolar dc line, a monopole fault will also induce over-voltage on the healthy pole due to mutual coupling. The location of the fault as well as the line and terminal characteristics affect this over-voltage magnitude at the terminals but the converter controls have practically no effect on the first wave reflections at the terminals, which in general involve the peak overvoltages [14]. Therefore, in order to ensure correct operation, each pole of a bipolar line will require this type of detection.

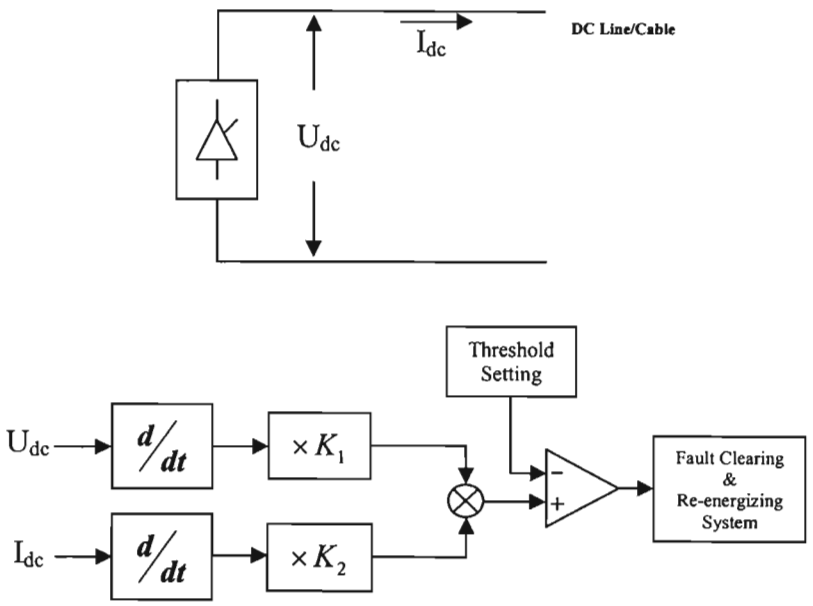

Fig. 2.1. High level Block Diagram of a Voltage Derivative Protection Scheme.

The voltage derivative detection method is very fast and provides fault detection within 2-3ms [14]. Determination of the settings, however, involves detailed network studies to be carried out in order to ensure that the protection only operates for dc line

faults [23], and is stable for all other disturbances (e.g. commutation failures and lightning surges not resulting ground faults).

A major disadvantage of this method is that $\partial U/\partial t$ is dependent on the fault loop impedance and, therefore, high impedance faults and faults close to the inverter on long lines are difficult to detect using this method.

2.1.4.2. Travelling Wave Protection

This method of protection is based on travelling wave theory and thus the name. It is also normally used as the dc line main protection. Fig 2.2 has been extracted from [16] to illustrate how the travelling wave protection method used by ABB functions.

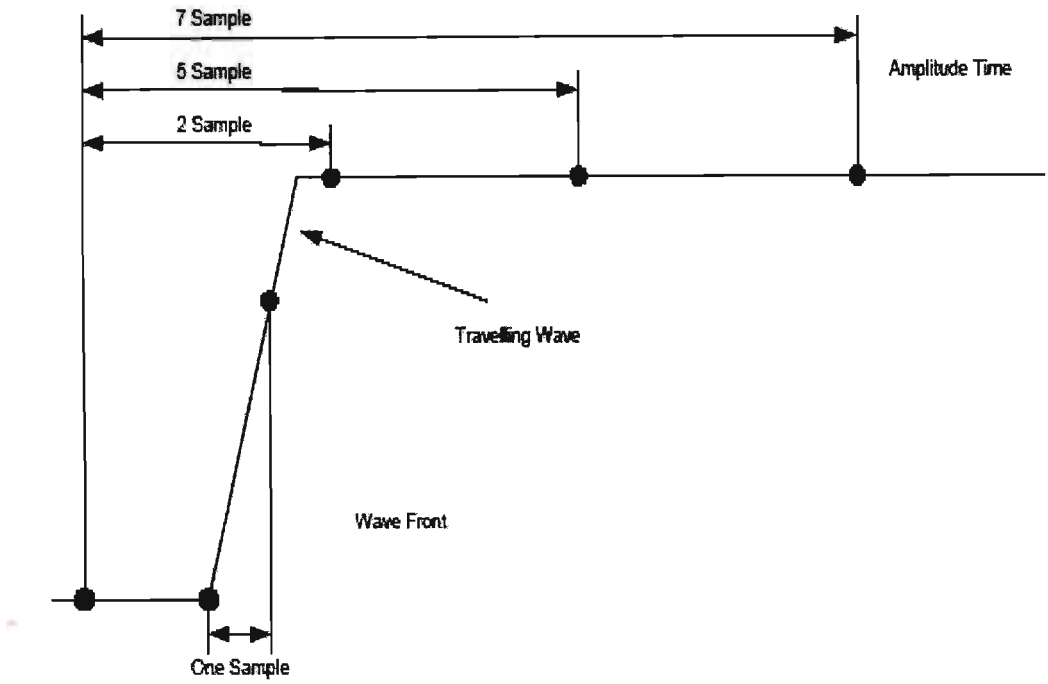

Fig. 2.2. "Example of different measurements used to determine existence of dc line fault. 1st measurement calculates wave difference between just before the wave front and after 2 samples (0.2ms). The 2nd and 3rd measurement calculates the wave difference between just before the wave front and after 5 and 7 samples" [16].

In this method the instantaneous voltages and currents are continuously sampled. In order to detect the wave front, the difference between two samples is measured as shown in Fig 2.2. "If this difference is greater than the threshold the protection is initiated and three different sample measurements will start to determine if the wave

has sufficient amplitude for a specific time" [16]. "If all these measurements are greater than the set thresholds, a line fault is detected" [16]. Fig. 2.2, shows an example of these different measurements.

In a bipolar HVDC line the travelling waves setup on the faulted pole will induce travelling waves on the healthy pole. In order to simplify the analysis of the travelling waves the total wave is split up into a pole mode (positive sequence) wave and a ground mode (zero sequence) wave [16], [24-26]. A more detailed discussion of this is given in 2.2.6. Now in order to prevent shutdown of both poles for a monopole fault the polarity of the ground mode wave is used to determine the faulted pole [16].

This type of protection is normally only active in the rectifier terminal. The settings should ensure that inadvertent protection operation is avoided in the following cases [16]:

- AC faults at rectifier and inverter terminal.
- Start and stop of the pole.
- Commutation failure at the inverter.
- Ground faults on other poles.
- Transients induced by thunderstorms not leading to flashover.
- Switching transients, especially connection of redundant filters in either station.

The strength of the algorithm is that both current and voltage contribute to the fault detection. However the longer the line, the more the waves are damped and difficulties in detecting the waves may arise for extremely long lines or relevantly high impedance faults.

2.1.4.3. Current Differential Protection

The differential line protection is generally used as backup protection and involves the measuring and comparing of the currents at both line ends. This information is relayed to the converter stations via a telecommunication infrastructure. The difference between the two measured currents is known as the differential current and if it exceeds a set threshold for a predefined time the protection will operate. This is a relatively simple method of fault detection that provides good reliability and protection coverage. Fig. 2.3, illustrates how the differential current is normally calculated. The differential protection method can also be relatively easily applied to multi-terminal HVDC Systems and Fig. 2.4 illustrates how the differential current is calculated for a parallel multi-terminal system. Fig 2.5, shows the block diagram of a differential current scheme used at the rectifier end. A similar differential current scheme is used at the inverter end.

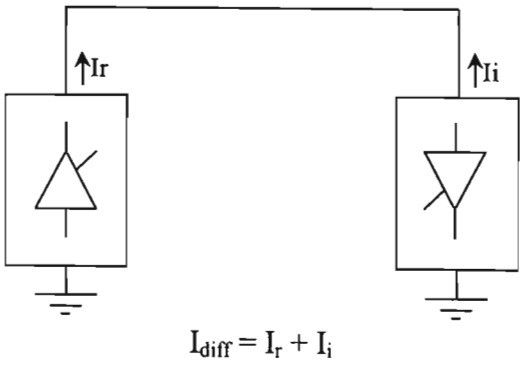

Fig. 2.3. Differential current calculation for two terminal point to point HVDC system.

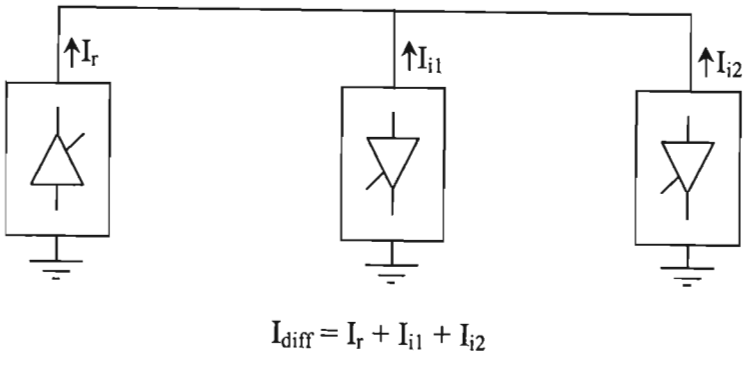

Fig. 2.4. Differential current calculation for parallel multi-terminal HVDC system.

The disadvantage of this method is that because of the line lengths used in HVDC systems (especially in cable systems), errors are introduced at each line end. These errors are due to the charging and discharging currents caused by any voltage variations [27]. The above errors limit the sensitivity settings that can be applied in order to avoid malfunctions and hence the ability of the protection to detect high impedance faults is reduced.

A proposed solution to this problem has been presented and results verified using simulators [27]. The paper presents the design for a circuit that will remove the capacitive currents from the current measurements at each end before the differential current is computed. The above circuit will allow the use of more sensitive settings, but may increase the requirements on the telecommunication infrastructure.

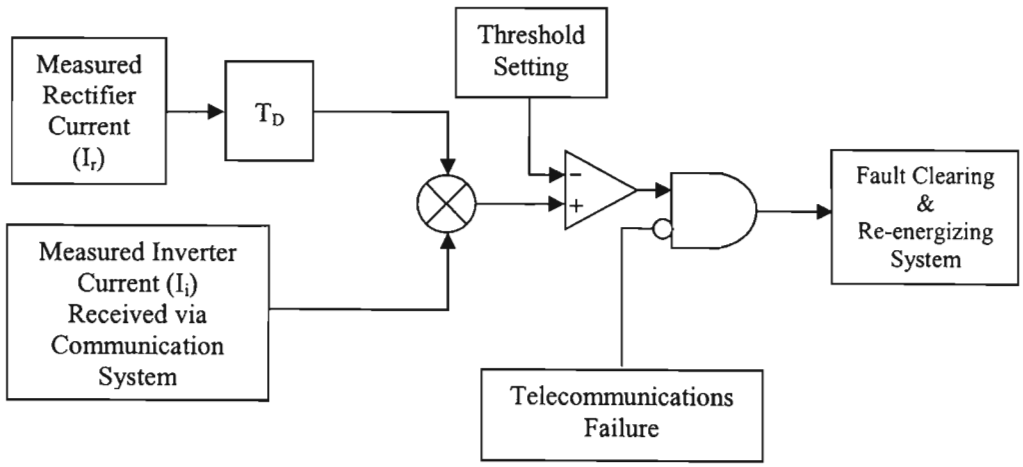

NB: The Delay Function T_D is required to compensate for the time required to transmit signals from one station to the other.

Fig. 2.5. Block Diagram of Differential current scheme used to protect HVDC transmission lines.

Since the information regarding line currents needs to be transmitted to the various converter stations, the signal propagation time greatly influences the response time of this method. A major disadvantage of this method is that the reliability of this type of protection is directly related to the reliability of the telecommunication infrastructure chosen.

2.1.4.4. DC Voltage level Protection

DC voltage level protection is used to respond to voltage depressions over a large time interval to detect high impedance faults or faults close to the inverter terminal. This method provides good protection coverage and is normally used as a backup to voltage derivative or travelling wave protection.

The level and time delays are selected such that normal switching operations or any other voltage transients that are not initiated by dc line faults will not cause the protection to operate. Some of these conditions include:

- Rectifier and inverter ac system faults
- Rectifier and inverter blocking
- Inverter commutation failures

The protection operating level is normally chosen as high as possible considering the lowest normal operating voltages. The scheme can, via the telecommunication infrastructure, receive information from the commutation failure protection at the inverter terminal thus allowing the level protection to be blocked in the event of a commutation failure.

The above will allow the time delays to be optimized and only in the event of a telecommunication failure does the time delay need to be increased to give the commutation failure protection at the inverter terminal a chance to operate first, if there is a commutation failure present. The level protection together with the restart logic is normally only applied at the rectifier terminal.

The voltage level protection response times for close up faults should be optimized. The above can be achieved by implementing the protection with multiple level and time settings, so that deeper voltage depressions will have much shorter response times. This type of setup will allow the voltage level protection to provide a more optimized fault detection time in the event of main protection failure. The implementation of multiple levels should not be a problem on newer systems as it will just involve slight changes to the algorithm. However, on older system which use

electronic circuits multiple level implementation may not be possible.

As indicated previously the response time of this method can be optimized with telecommunications. However, the reliability of the method is not influenced by telecommunication. Therefore, in the event of telecommunication failure this protection system will still operate correctly should a fault occur. The only difference is that the response time will be longer. The voltage level protection can be set to cover a wide range of voltage depressions and should, therefore, be able to provide satisfactory backup protection for the HVDC transmission line.

2.1.5. Cable Section Fault Detection

There are instances in which the HVDC transmission line comprises of both overhead conductor and cables e.g. Hokkaido-Honshu HVDC Link [27]. In these cases the protection system must be able distinguish between a cable and overhead line fault because cable faults are normally permanent in nature and a restart must not be allowed in the event of a cable fault.

The authors in [28] have developed a method of distinguishing cable faults from overhead line faults on dc transmission lines that contain cable sections. The method is based on the changes in current that occur at the rectifier side and inverter side of the cable at the instant of the fault [28]. The detection system is based on the fact that the currents change in opposite direction for internal (cable) faults and the currents change in the same direction for external faults.

The system only requires a communication channel capable of transmitting ON/OFF signals between the two cable ends and is currently being successfully used on the Hokkaido-Honshu HVDC Link.

2.1.6. Fault Clearing and Recovery

As already explained earlier normal control action alone is not sufficient to clear dc line faults. Therefore on detection of a dc line fault by the protection system, the rectifier firing angle (α) is advanced into the inverting region. Normally rectifier firing angles of between 120° to 135° are used [14].

The inverter maintains the correct polarity because as explained earlier the inverter is prevented from going in rectification by restricting the range of the extinction angle (γ) to less than 90°. Thus, both converters are forced to operate in the inverting mode. This is the fastest way of forcing the dc current to zero as all the energy trapped in the dc system is discharged into the ac system. The system is kept in this state until arc extinction and deionisation are likely to be completed [14].

On completion of the deionization period, a restart procedure can commence in order to restore the normal voltage and prefault power. During the restart, the current order is normally ignored and the bridge is started with minimal current and slowly brought up to the current order, to restore the prefault power. The success of the restart attempt is determined by monitoring the line voltage during restart period [13].

Normally between 1 and 4 restart attempts are made to try and restore the system before the pole is lockout by tripping the converter bridges at the rectifier end. Tripping the converter bridges isolates the faulted pole/s and prevents any restart attempts on the faulted pole/s. It also allows personnel to safely try and locate the fault or determine the reason for the pole/s trip.

2.1.7. HVDC Line Protection Telecommunications Requirements

All the rectifier and inverter stations in a HVDC scheme will have some sort of telecommunications infrastructure between them to relay vital control and protection information between the stations.

The availability of a secure high speed high quality telecommunications system provides a range of possibilities for high speed relaying. Essential decision making information can be rapidly transferred from one end to the other.

One might then ask, "Why is differential protection mainly used as the backup protection", especially after the work done in [27]. It can even be easily implemented in multi-terminal schemes as illustrated in 2.1.4.3.

The main reason for the above is the cost of providing the high quality, high speed telecommunication infrastructure with total redundancy required to use this system as the main protection. In most cases the cost of providing the above mentioned telecommunication infrastructure cannot be financially justified [17]. Therefore, a compromise has to be made which generally results in a less secure telecommunication infrastructure been adopted [17].

A commonly used telecommunication medium is the power line carrier (PLC). With the PLC for example, the signal to noise ratio is dependent on external factors such as weather conditions, corona and line faults [17]. This implies that the PLC is more prone to failure during line faults when its operation is most essential.

Clearly, the dependence of protection on the telecommunication system greatly increases the chance of failure or mal-operation of the protection system. The dc line main protection should, therefore as far as possible, avoid dependence on telecommunication in order to ensure correct fault detection, irrespective of the status of the communication infrastructure. All protection decisions must be able to be based on local detections when necessary and telecommunications should only be used to optimize the response of the overall protection system [18].

2.1.8. Security and Reliability of Current HVDC Line Protection

HVDC transmission lines are provided with both main and backup protection for added security. Both main and backup systems should, therefore, be able to provide adequate protection coverage for the entire transmission line.

Both currently used main protection schemes viz. derivative voltage and travelling wave protection are dependent on fault loop impedance. This limits the protection coverage because the greater the fault loop impedance the more damped the waves are and the more difficult they are to detect without causing mal-operation. Obviously as the length of transmission lines increase, the percentage of line not covered by the main protection increases, thus reducing the reliability of the system. The above discussion is further reinforced by the results obtained in [12] which, indicate the distances up to which the currently used main protection methods will function satisfactorily.

DC voltage level protection should provide adequate backup protection if implemented as described in 2.1.4.4. The response times could be enhanced by the telecommunication system when available, by relaying the converter station protection activity.

Differential protection has the ability to detect very high impedance faults and should, therefore, provide more than adequate protection coverage [21]. The major disadvantage of this method is that its reliability is based on the reliability of the telecommunication infrastructure. This implies that the protection system will be unavailable every time there is a communications failure. It is for this reason that differential protection is generally used as backup protection.

The main focus of this research is therefore to look into methods of increasing the protective coverage of current main protection schemes and determine their suitability for the protection of ultra long dc transmission lines. Since all the methods to be explored will be based on travelling wave theory, the next section will be dedicated to outlining the theory of travelling waves and its application.

2.2. Travelling Waves

As described in the previous section, both of the currently used dc line main protection schemes viz. travelling wave protection and voltage derivative protection, are based on travelling wave theory.

In these systems the fault detection is based on the magnitude and gradient of the first travelling waves arriving at the terminations. This method has the advantage that the peak overvoltages are detected. This helps in improving the maximum possibility of detecting the wavefront. The method also has the advantage that the HVDC control system has practically no impact on these first wave reflections. Therefore its impact on the protection system does not need to be considered when using this method.

As described in sections 2.1.4.1 and 2.1.4.2, the disadvantage of the above systems, is their dependence on the fault loop impedance. This implies that their protection coverage is limited and will, therefore, not be able to adequately protect the proposed future HVDC systems [12].

Both currently used main protection systems adopt the use of first incident wave reflections to detect the presence of a fault on the transmission line [15], [16]. This approach proves to provide fast but limited protection coverage. The purpose of this section is, therefore, to review travelling wave theory in an attempt to discover another method in which travelling waves can be used to detect faults on ultra long HVDC transmission lines.

2.2.1. Theory

Any disturbance on a transmission line results in the initiation of travelling waves which travel along the transmission line in both directions. These travelling waves are the result of changes in the stored energy in the line capacitance and inductance [29]. The waves propagate along the line causing high frequency oscillations that are continually being attenuated and distorted by corona and other losses until they die

out [24]. The frequency and damping of these oscillations are dependent on the line parameters and fault loop impedance.

Fig 2.6 below, shows a line section of a lossless transmission line. The length of the line section is Δx meters and is located at a distance x meters from the sending end. The transmission line has a series inductance L in H/m and a shunt capacitance C in F/m. Therefore, the line section has a series inductance $L\Delta x$ H and a shunt capacitance $C\Delta x$ F as shown in Fig 2.6.

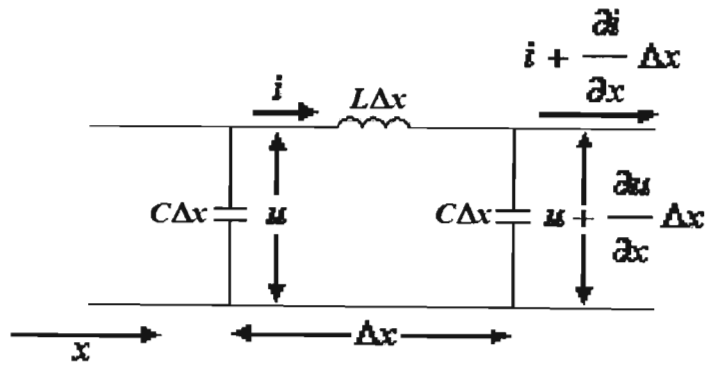

Fig 2.6. Schematic diagram of an elemental section of a single phase transmission line.

Note that both the voltage u and current i are functions of time t and distance x. Therefore, partial derivatives need to be used. The series voltage drop across element Δx is given by [4], [30]:

$$(L\Delta x)\cdot\frac{\partial i}{\partial t} \tag{2}$$

Therefore, from Fig 2.6, we can write

$$\frac{\partial u}{\partial x}\Delta x = -\left(L\frac{\partial i}{\partial t}\right)\Delta x \tag{3}$$

Similarly from Fig 2.6, we can write

$$\frac{\partial i}{\partial x}\Delta x = -\left(C\frac{\partial u}{\partial t}\right)\Delta x \tag{4}$$

We now divide both equations (3) and (4) by Δx to give us (5) and (6) below.

$$\partial u/\partial x = -L\,\partial i/\partial t \tag{5}$$

$$\partial i/\partial x = -C\,\partial u/\partial t \tag{6}$$

The voltage and current at any distance x on a lossless transmission line will obey the partial differential equations (5) and (6) respectively [4], [30], [31].

Rearranging equations (5) and (6), eliminating the current i and taking partial derivatives with respect to x and t yields the travelling wave equation of a lossless transmission line as given in (7) below [4].

$$\frac{1}{LC}\cdot\frac{\partial^2 u}{\partial x^2} = \frac{\partial^2 u}{\partial t^2} \tag{7}$$

The solution to the travelling wave equation is a function of $(x - vt)$ and the voltage and currents can be expressed as [31-33]:

$$u(x,t) = u_f(x-vt) + u_r(x+vt) \tag{8}$$

$$i(x,t) = \frac{1}{Z_c}\left[u_f(x-vt) + u_r(x+vt)\right] \tag{9}$$

Where

$Z_c = \sqrt{L/C}$ is the characteristic impedance of the transmission line.

$v = \dfrac{1}{\sqrt{LC}}$ is the velocity of propagation of the wave.

Figure 2.7, shows the forward (u_{fl} and i_{fl}) and backward (u_{rl} and i_{rl}) travelling waves as they leave the faulted area and travel at a velocity v towards the ends of the transmission line.

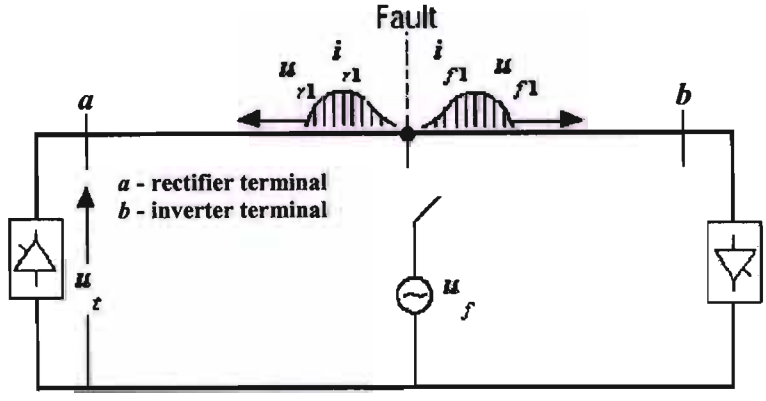

Fig. 2.7. Travelling voltage and current waves leaving the disturbed area.

2.2.2. Reflection of Travelling Waves

The travelling waves leaving the disturbed area will eventually reach some type of discontinuity e.g. busbars, generators, other transmission lines, an open or short circuit, termination. At this discontinuity, a part of the wave will be reflected and a part may pass to other sections. The voltage and/or current at the discontinuity may be anything from zero to double the magnitude of the travelling wave, depending on the terminal characteristics [24].

Let us consider the example in Fig 2.8 below, in which a transmission line with characteristic impedance Z_c is terminated through impedance Z_t. At some time t a disturbance, results in the initiation of travelling waves in the transmission line with the forward travelling wave u_i heading towards the termination as shown in Fig 2.8.

The incident (forward) voltage and current waves of a lossless line are related by the characteristic impedance of the line as follows [24]:

$$\frac{u_i}{i_i} = Z_c \qquad (10)$$

Where

u_i is the incidence (forward) voltage travelling wave.

i_i is the incidence (forward) current travelling wave.

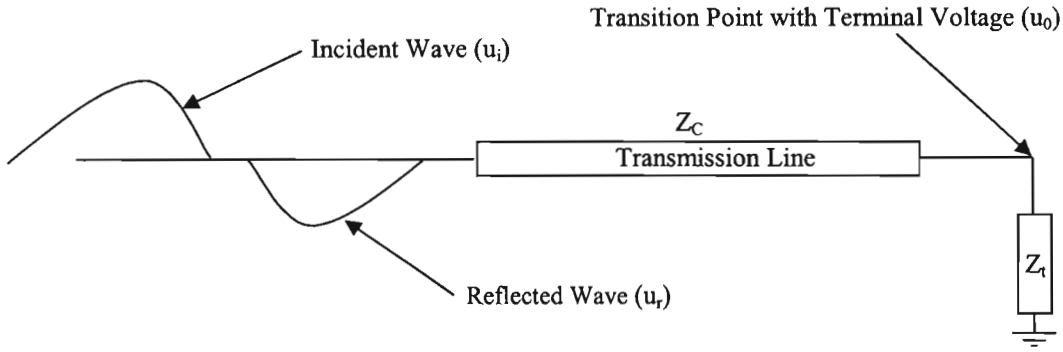

Fig. 2.8. Reflection of Travelling waves at a discontinuity.

Now at the discontinuity the voltage and current travelling waves will be reflected. The reflected (backward) waves for a lossless line are related to characteristic impedance as follows [24]:

$$\frac{u_r}{i_r} = -Z_c \qquad (11)$$

Where

u_r is the reflected (backward) voltage travelling wave.

i_r is the reflected (backward) current travelling wave.

Therefore the voltage u_0 and current i_0 at the termination are given by:

$$i_0 = i_i + i_r \tag{12}$$

$$u_0 = u_i + u_r = Z_t i_0 \tag{13}$$

Where

Z_t is the impedance seen by the surge at the discontinuity or transition point.

The case of a direct termination down to ground was chosen for simplicity. Note that in cases were the transmission line is not just terminated by an impedance to ground but instead connects to another transmission line, busbar, other parallel lines or a combination of these, Z_t will then be the equivalent impedance seen by the surge.

Now substituting (10) and (11) into (12) and (13) yields the following equations for the reflected waves and total voltage and current:

$$u_r = \frac{Z_t - Z_c}{Z_t + Z_c} u_i = K_{rv} u_i \tag{14}$$

$$u_0 = \frac{2Z_t}{Z_t + Z_c} u_i = K_{tv} u_i \tag{15}$$

$$i_r = -\frac{Z_t - Z_c}{Z_t + Z_c} i_i = K_{ri} i_i \tag{16}$$

$$i_0 = \frac{2}{Z_t + Z_c} u_i = \frac{2Z_c}{Z_t + Z_c} i_i = K_{ti} i_i \tag{17}$$

Where

K_{rv} is the reflection coefficient for voltage travelling waves.

K_{ri} is the reflection coefficient for current travelling waves.

K_{tv} is the refraction coefficient for voltage travelling waves.

K_{ti} is the refraction coefficient for current travelling waves.

The currently used main protection systems for the HVDC transmission lines monitor the terminal voltages U and currents I and use the changes in these signals (ΔU and ΔI) caused by the first wave reflections to detect the presence of line faults. These voltages and currents are given in equations (15) and (17) above.

The changes in ΔU and ΔI recorded on the waveforms at the terminations, are dependent on the incident wave and the reflection coefficients (K_{rv} and K_{ri}). The incident wave arriving at the termination is dependent on a number of factors viz. pre-fault voltages, fault resistance, attenuation due to line losses, corona and distortion. As described in 2.1, these factors affect the amplitude, gradient and shape of the travelling waves and, therefore, limit the protection coverage of a system based solely on first wave reflections.

Note that from a fault detection point of view the higher the voltage reflection coefficient at the terminal the better as it improves the possibility of fault detection [26]. The above is due to the fact that following a fault condition the incident travelling wave arrives at the terminal and is immediately reflected. Note the resultant wave, due to the combination of the incident and reflected waves, is what causes the instantaneous change in terminal voltage. So the higher the voltage reflection coefficient the larger the magnitude of the resultant wave and the greater the instantaneous change in terminal voltage. A greater instantaneous change in terminal voltage implies that the voltage gradient will be steeper and since the existing main protection systems are based on the steepness of the voltage gradient, the possibility of fault detection is improved. However, a higher voltage reflection coefficient means higher over voltage magnitudes at the terminations and hence increases the insulation costs.

2.2.3. Attenuation and Distortion of Travelling Waves

So far we have assumed a lossless transmission line, however, practical transmission lines have finite energy losses. These losses cause attenuation and in some cases distortion of the travelling wave as it propagates along the transmission line [24], [30].

There are different mathematical formulae to describe the attenuation phenomenon, some of which can be found in [24], however generally to avoid much undue complexity the attenuation is normally represented by a constant factor α. So if we assume that the transmission line considered in Fig 2.6. is still distortionless (i.e. $R/L = G/C$ [24]) but no longer lossless with a finite series resistance R in Ω/m and a finite shunt conductance G in S/m, equations (8) and (9) can be rewritten as (18) and (19) respectively to include the influence of attenuation [30].

$$u(x,t) = u_f(x-vt)e^{-\alpha x} + u_r(x+vt)e^{\alpha x} \tag{18}$$

$$i(x,t) = \frac{1}{Z}\left[u_f(x-vt)e^{-\alpha x} + u_r(x+vt)e^{\alpha x}\right] \tag{19}$$

Where

$\alpha = \sqrt{RG}$ is the attenuation constant.

On practical transmission lines the voltage and currents can be represented by (18) and (19) at high frequencies [24], [30] but at low frequencies, the typical transmission lines are not distortionless and thus equations (18) and (19) do not hold true. Methods of taking this distortion into account are provided in [24].

Distortion causes the associated voltage and current waves to no longer be exact replicas of each other except when they are initially initiated or reflected. So for all other times (10) and (11) do not hold true. Thus for a line with distortion the reflected and total voltage given by (14) and (15) become [24]:

$$u_r = \frac{Z_c}{Z_t + Z_c}\left[Z_t i - u_i\right] \tag{20}$$

$$u_0 = \frac{Z_t}{Z_t + Z_c}\left[Z_c i + u_i\right] \tag{21}$$

2.2.4. Successive Reflection of Travelling Waves

The travelling waves initiated by any disturbance will be continuously reflected and refracted until they die out and a new stable system state is achieved. The easiest way to keep track of these successive reflections is with the aid of time space diagram known as a lattice or bewley diagram. It shows at a glance the position and direction of every incident, reflected and refracted wave on the system at every instant in time [24]. The effects of attenuation and distortion can also be entered on the lattice diagram.

In order to illustrate this, let us consider Fig 2.7. in 2.2.1. above where K_{rva} and K_{rvb} represent the reflection coefficients at terminals a and b respectively. τ_a and τ_b represents the time taken by the travelling wave to travel from the fault to the discontinuity at a and b respectively. For simplicity we will assume full reflection at terminations and at the fault point (zero impedance fault).

Therefore we can construct the lattice diagram for Fig 2.7. as shown below.

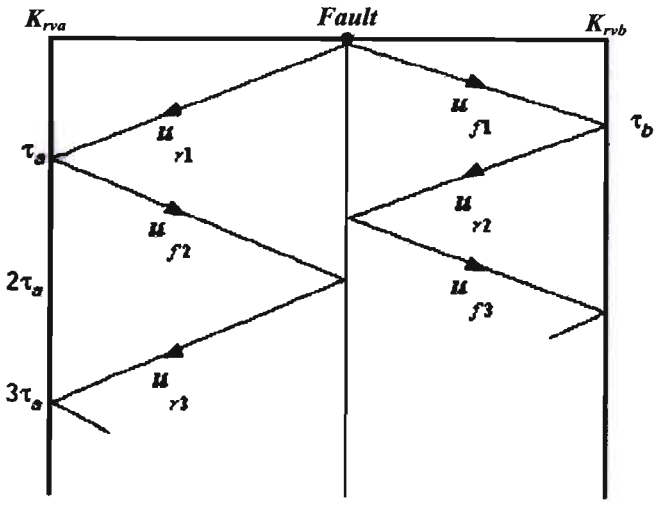

Fig. 2.9. Bewley Lattice Diagram of System in Fig 2.7.

Let us consider the termination at *a*, the incident wave will take τ_a milliseconds to reach *a*, were it would be reflected. The current HVDC main protection systems would react to this change and based on its setting, it will make a decision as to whether a fault is present or not. Problems with this method for the proposed future systems have been already discussed earlier.

Looking at Fig 2.9, if the time at which the first reflected wave u_{f2} leaves termination *a* is known and the time at which the subsequent reflected wave from the fault u_{r3} returns is known, the time difference ($3\tau_a$ - τ_a) can be easily calculated to reveal the total travel time t_D. The total travel time t_D represents the time taken by the travelling wave to travel from terminal *a* to the fault and back to terminal *a*. If the total travel time t_D and the velocity of propagation *v* is known, the distance to fault can be calculated by (22) below.

$$D_f = \frac{v \cdot (3\tau_a - \tau_a)}{2} = \frac{v \cdot t_D}{2} \qquad (22)$$

Where

D_f is the distance to fault in km

t_D is the total travel time in ms

v is the propagation velocity in km/ms

This property will be used in the next chapter to look into ways of improving the protective reach of the currently used dc line main protection systems and thus improving their applicability to future HVDC systems.

2.2.5. Termination Waveform Frequency Dominance

The continuous reflection of the travelling waves at the terminations, following a line fault results in the appearance of a dominant frequency component in the post fault voltage and current signals. This dominant frequency is a function of the distance to fault and is dependent on the termination and fault impedance [34].

To illustrate the above property let us consider the simple case in Fig. 2.10, in which a lossless transmission line with a characteristic impedance of Z_c is connected to a DC source with an internal impedance of Z_s. For simplicity we will assume the source impedance to be purely resistive. Now if at time t, equal to zero, the ideal switch at B is closed causing a line fault, a negative voltage travelling wave will be initiated in order to cancel the voltage at the fault. This surge will travel back towards the source cancelling the voltage as it travels towards A. When the surge hits the discontinuity at A, it will be reflected. The sign of the reflection will depend on the sign of the reflection coefficient at A.

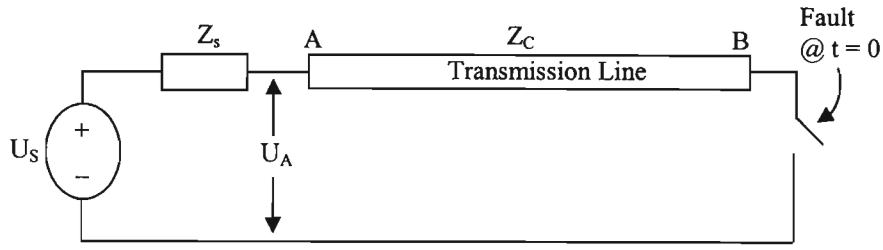

Fig 2.10. Simple Transmission Line.

Let us first consider the case with Z_s being large i.e. $Z_s > Z_c$. In this case the reflection coefficient K_{rv} as defined in (14) would be positive. Therefore, the voltage waveform will be reflected with the same sign and travel back to the fault as a negative surge. At the fault this negative surge will be reflected with a reverse sign and travel towards A as a positive surge. At A the surge will be reflected again with the same sign and travel towards the fault point as a positive surge and again at the fault location the surge will be reflected with the reverse sign and travel back to A as a negative surge.

We are now back to the original state, viz. a negative surge travelling towards A. This completes one cycle, which takes 4τ seconds to complete. Therefore, we can conclude that for this case the dominant frequency will be [34]:

$$f_{dom} = \frac{1}{4\tau} Hz \tag{23}$$

Now let us consider the case were Z_s is small i.e. $Z_s < Z_c$. In this case the reflection coefficient at A is negative and, therefore the voltage surge will be reflected with the opposite sign and travel back towards the fault as a positive surge. At the fault location the surge will again be reflected with the opposite sign and travel back to A as a negative surge.

We are now back to the original state, viz. a negative surge travelling towards A. Since the surge is reflected with opposite signs at both ends, a cycle is completed in 2τ seconds. Therefore we can conclude that for this case the dominant frequency will be [34]:

$$f_{dom} = \frac{1}{2\tau} Hz \tag{24}$$

For a relay located at A the voltage surges for both cases are shown in Fig 2.11 and Fig 2.12. The "gap" shown in Fig 2.12, approaches zero as the source impedance approaches zero. This implies that a relay located behind an ideal source will record no fluctuations in the voltage wave. This is a very important point to note as it affects the fault detection ability of a travelling wave based protection system. It also determines which waveform (voltage, current or both) can be used for fault detection. Obviously a voltage travelling wave based protection system will not be appropriate for a relaying point close to a strong source, in this case a current travelling wave protection system will be more appropriate.

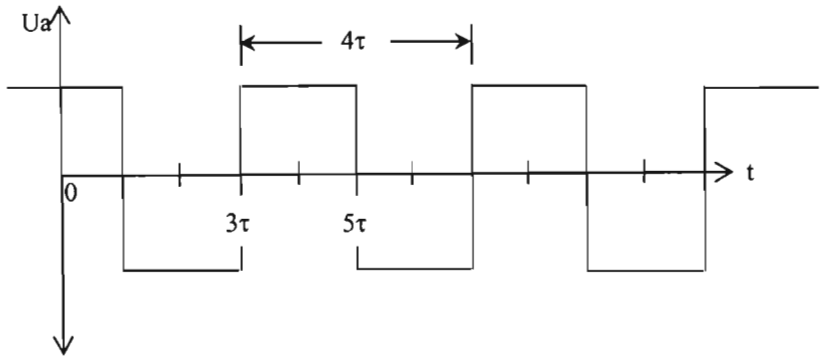

Fig 2.11. Surge propagation on a simple line with large source impedance.

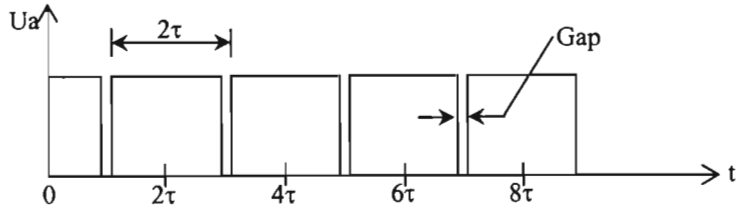

Fig 2.12. Surge propagation on a simple line with small source impedance.

Thus far we have assumed the source impedance Z_s to be purely resistive. In this case determining whether Z_s is small or large is easily accomplished be comparing the magnitude of Z_s to the magnitude of Z_c. However, in the practical case were Z_s is complex the above method cannot be directly used because the impedance seen by the surge is dependent on the time constant of Z_s and Z_c. This is due to the fact that a travelling wave reaching an inductive termination will firstly encounter a large impedance as the inductance tries to oppose the change in current, but after some time as the current is allowed to flow, the impedance seen by the surge will decrease. The opposite is true for a capacitive termination.

A basis of deciding on whether Z_s is large or small when Z_s is complex is given in [34]. This method compares the "time constant of the source inductance L_s plus characteristic impedance Z_c to the wave travel time τ " to make a decision [34]. According to [34] τ must be compared to (L_s/Z_c) in order to determine whether the source impedance Z_s seen by the incoming travelling wave is small or large.

The travel time τ varies with the fault distance. The previous statement implies that the impedance seen by the incoming travelling wave, on the same transmission line, can vary from small to large based on the location of the fault [34]. Thus the existence of a fault and the fault distance can not be easily determined by analyzing the dominant frequency components only.

Possible causes of errors in multi phase/pole systems include the existence of multi-velocity travelling waves which introduce different dominant frequency components. These different sets of dominant frequency components must be considered when analysing the frequency spectrum of the respective waveform after a fault. Other sources of error include the interference of reflected and refracted waves with each another.

Bearing all this in mind, the dominant frequency of the faulted waveform should not be solely used as a basis for fault detection. It can however be used in conjunction with other relaying information to determine the existence of a fault and initiate protective action.

2.2.6. Multiconductor Systems

So far we have only considered single phase/pole systems, however in the physical system, you rarely find these single phase/pole circuits. Most AC systems are three phase networks and most HVDC systems are bipolar systems. Since the main focus is on HVDC systems, this section will be focused on bipolar HVDC transmission.

In most cases both pole conductors of the bipolar system run in parallel and are in close proximity to each another. This therefore, represents a coupled system where any surge on one of the pole conductors will result in induced surges on the other pole conductor.

In order to simplify the analysis of these surges on bipolar systems, it is common practice to transform the coupled circuits in two balanced modal circuits that are not coupled viz. a positive sequence and zero sequence network [25]. This implies that a surge impressed on one conductor will propagate as two waves on both conductors (one for each mode).

The positive sequence waves in both conductors have equal and opposite amplitude while the zero sequence waves in both conductors have equal amplitude with the same polarity [26]. The zero sequence circuit involves ground return, whereas the positive sequence circuit does not, being a balanced metallic circuit [25]. The positive sequence waves are, therefore, not significantly affected by ground and fault impedance and have much lower attenuation and a higher propagation velocity than the zero sequence waves.

Fig 2.13, shows a surge initiated at point *A* on pole 1. It can be seen that both the resultant incident, and induced surges are a combination of the positive and zero sequence waves. Both the positive and zero sequence waves have the same polarity on the pole on which the surge was initiated while the positive and zero sequence waves are of opposite polarity on the healthy pole. This is an important property and is used in the system described in 2.1.4.2 to determine the faulted pole.

The pole conductors represented in Fig 2.13 below are assumed to be ideal. This is purposefully done to isolate the distortion and apparent attenuation effect caused by the separation of the two different velocity components.

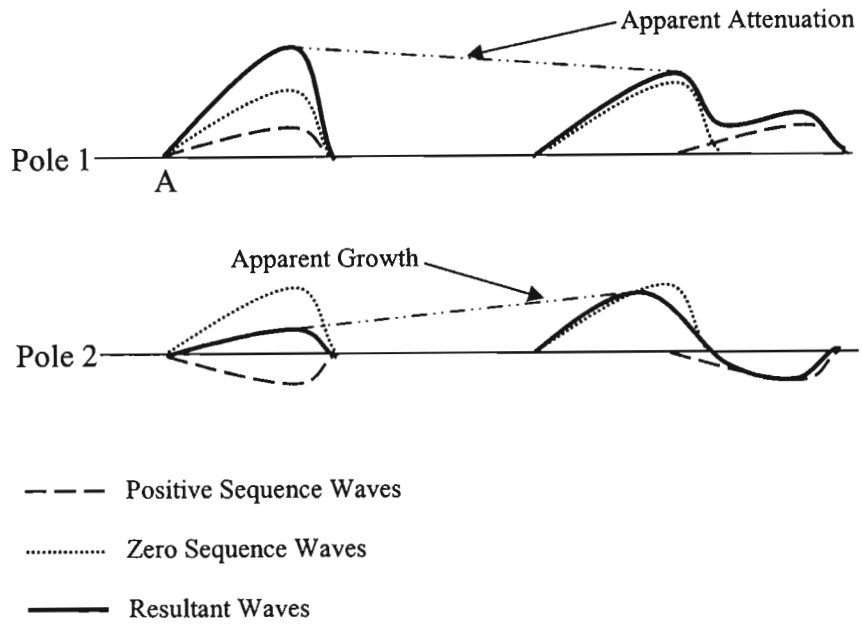

Fig 2.13. Positive and Zero Sequences Waves on HVDC Bipolar Transmission Lines.

Now with reference to Fig 2.13 above, we can calculate the modal voltages and currents. The resultant travelling waves on pole 1 and pole 2 two can be written as follows:

$$u_{p1} = u_0 + u_1 \tag{25}$$

$$u_{p2} = u_0 - u_1 \tag{26}$$

Where

u_{p1} is the resultant voltage travelling wave on pole 1.

u_{p2} is the resultant voltage travelling wave on pole 2.

u_1 is the positive sequence voltage travelling wave.

u_0 is the zero sequence voltage travelling wave.

Thus, the current travelling waves can be written as:

$$i_{p1} = i_0 + i_1 \tag{27}$$

$$i_{p2} = i_0 - i_1 \tag{28}$$

Where

i_{p1} is the resultant current travelling wave on pole 1.

i_{p2} is the resultant current travelling wave on pole 2.

i_1 is the positive sequence current travelling wave.

i_0 is the zero sequence current travelling wave.

Therefore, the modal components in terms of actual quantities are expressed as follows

$$u_0 = \frac{u_{p1} + u_{p2}}{2} \tag{29}$$

$$u_1 = \frac{u_{p1} - u_{p2}}{2} \tag{30}$$

$$i_0 = \frac{i_{p1} + i_{p2}}{2} \tag{31}$$

$$i_1 = \frac{i_{p1} - i_{p2}}{2} \tag{32}$$

The positive and zero sequence impedance are then simply given by [25]:

$$Z_1 = \frac{u_1}{i_1} = Z_{ss} - Z_m \tag{33}$$

$$Z_0 = \frac{u_0}{i_0} = Z_{ss} + Z_m \tag{34}$$

Where

Z_1 is the positive sequence impedance.

Z_0 is the zero sequence impedance.

Z_{ss} is the conductor self impedance.

Z_m is the mutual impedance between the two conductors.

The equations (25) to (32) allow conversion from actual quantities to symmetrical quantities and vice versa. This is of extreme importance in the analysis of faults on bipolar HVDC systems as it allows the use of per pole analysis methods, which would not be possible otherwise. The finer details on the use of sequence circuits will be discussed in later chapters.

Now equipped with the basic theory, the next chapter attempts to build on this and explore the various ways in which travelling waves can be used to detect the presence of DC line faults on HVDC systems with ultra long transmission lines.

Chapter 3: Proposed Protection Methods

3.1. Introduction

As mentioned previously, we can expect HVDC systems with very long transmission lines in the future e.g. the proposed Westcor Project, the details of which were given in Chapter 1. It has been indicated previously that the main protection systems currently used for the protection of HVDC transmission lines have inherently limited protection coverage and will, therefore, not be able to provide adequate protection for HVDC systems with very long transmission lines. There is, therefore, a need to address this challenge.

In the previous chapter, emphasis was placed on the fact that, in order to improve the security and reliability of the protection system, all protection decisions must be able to be made using locally available quantities in the event of telecommunication failure.

Travelling wave theory was introduced in Chapter 2. This chapter builds on the theory and discusses how the theory can be developed upon in order to formulate a reliable method of protecting long HVDC transmission lines. Later in the chapter, methods of using telecommunication in order to optimize the protection systems are discussed and the chapter is concluded with a block diagram of the proposed dc line main protection system.

3.2. Local fault Detection Method

3.2.1. Method Formulation

The concept of travelling wave reflection was introduced in sections 2.2.2 through to 2.2.4. It was illustrated that any disturbance on a transmission line would give rise to travelling waves that will be continuously reflected and refracted until they die out and give rise to a steady state condition. With this in mind, let us consider Fig 3.1,

which represents a HVDC transmission line with a zero impedance fault located D_f kilometres from terminal A. For simplicity, we have assumed that no refraction occurs at the terminals A and B.

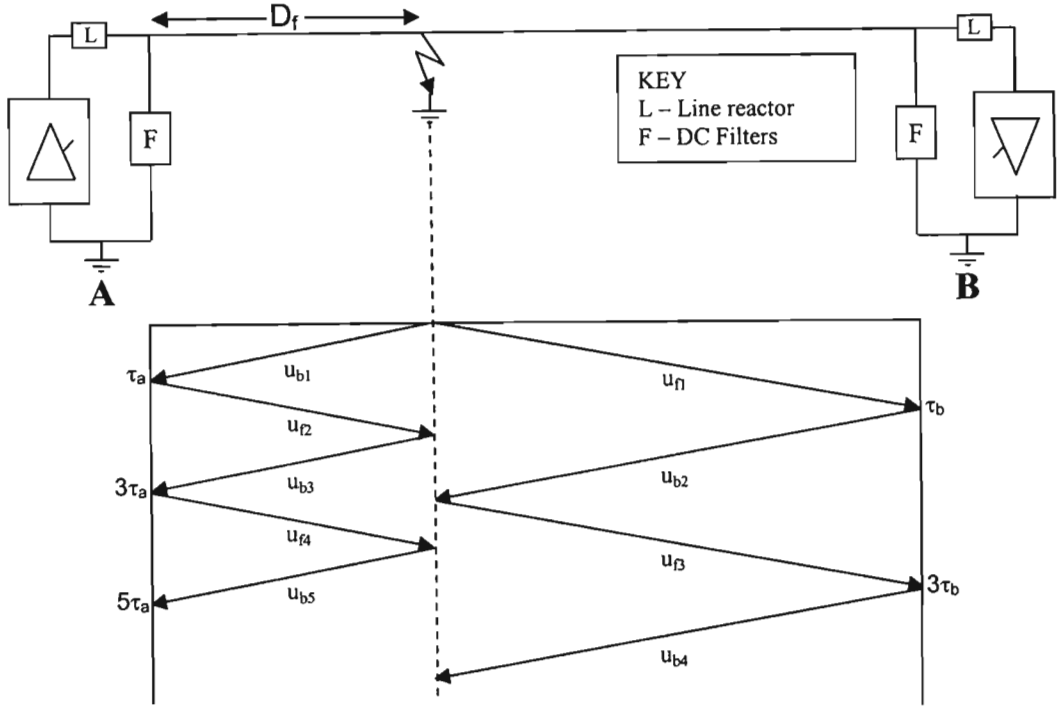

Fig 3.1. HVDC Transmission Line Fault with zero fault resistance with total reflection at terminations.

On occurrence of the fault, voltage and current travelling waves are initiated that travel along the transmission line towards both terminals. Fig 3.1 shows only the voltage travelling waves with subscripts "b" and "f" representing the backward and forward voltage travelling waves respectively. It can be noticed from Fig 3.1, that the zero impedance fault simplifies the analysis as it divides the transmission line into 2 zones, in which the travelling waves on the left hand side are reflected and propagate independently from those on the right hand side i.e. there is no coupling between the waves on either side.

Assuming our relaying point to be at terminal A, the incident voltage wave or first backward wave u_{b1} will arrive at the relaying point after time τ_a. This incident wave will be reflected at terminal A and give rise to a forward travelling wave u_{f2}, travelling towards the fault point. At the fault point, the forward travelling wave u_{f2} is reflected and gives rise to a backward travelling wave u_{b3} travelling back towards the relaying

point at terminal A. This travelling wave u_{b3} will reach the relaying point at time $3\tau_a$ after the initiation of the fault. As discussed in 2.2.4 if the time at which u_{f2} leaves the relaying point and time at which u_{b3} returns to the relaying point is known the time travel can be calculated and used in (22) to calculate the distance to the fault.

These times have to be determined from the local voltage and/or current waveforms measured at the relaying point. It has become common practice to use both, the voltage and current changes at the relaying point for fault location [20], [29], [35-37]. In order to accomplish this, let us define two relaying signals S_F which is the value of the forward travelling wave as it leaves the relaying point heading into the transmission line and S_B which is the value of the backward travelling wave as it arrives at the relaying point from the transmission line. Equations (35) and (36) derived from (8), (9), (10) and (11) are used to calculate the instantaneous values of forward and backward travelling waves from the physically measured voltage and current at the relaying point [37].

$$S_F = u(t) + Z_c i(t) \tag{35}$$

$$S_B = u(t) - Z_c i(t) \tag{36}$$

Where

Z_c is the characteristic impedance of the transmission line.

Now consider the fault in Fig. 3.1, the forward travelling wave u_{f2} will be reflected at the fault point and return to the relaying point after twice the travel time ($2D_f/v$) has elapsed. So assuming a lossless line, we can then write:

$$S_B(t + {}^{2D_f}\!/_{v}) = K_{rv} S_F(t) \tag{37}$$

Where

K_{rv} is the reflection coefficient as defined in (14) with Z_f equal to zero in this case because zero fault resistance has been assumed.

The equation is valid for $t>0$ and assumes that the fault occurred at time $t = -D_f/v$.

The basic relationship in (37) together with (35) and (36) defining the wave signals constitute the line equations on which protection schemes are based [35]. The basic relationship states that in case of a fault, the two wave signals S_F and S_B are exactly congruent except for a constant time shift, $(2D_f/v)$, proportional to the fault distance and a constant scaling factor, K_{rv} [35].

So far, we have assumed that the current backward travelling wave u_{b3} is due to the reflection of the previous forward travelling wave u_{f2}. This is not always the case especially when there is significant fault impedance. To illustrate this concept let us consider Fig 3.2, which represents an HVDC transmission line, this time, with a fault having a fault resistance R located D_f kilometres from terminal A.

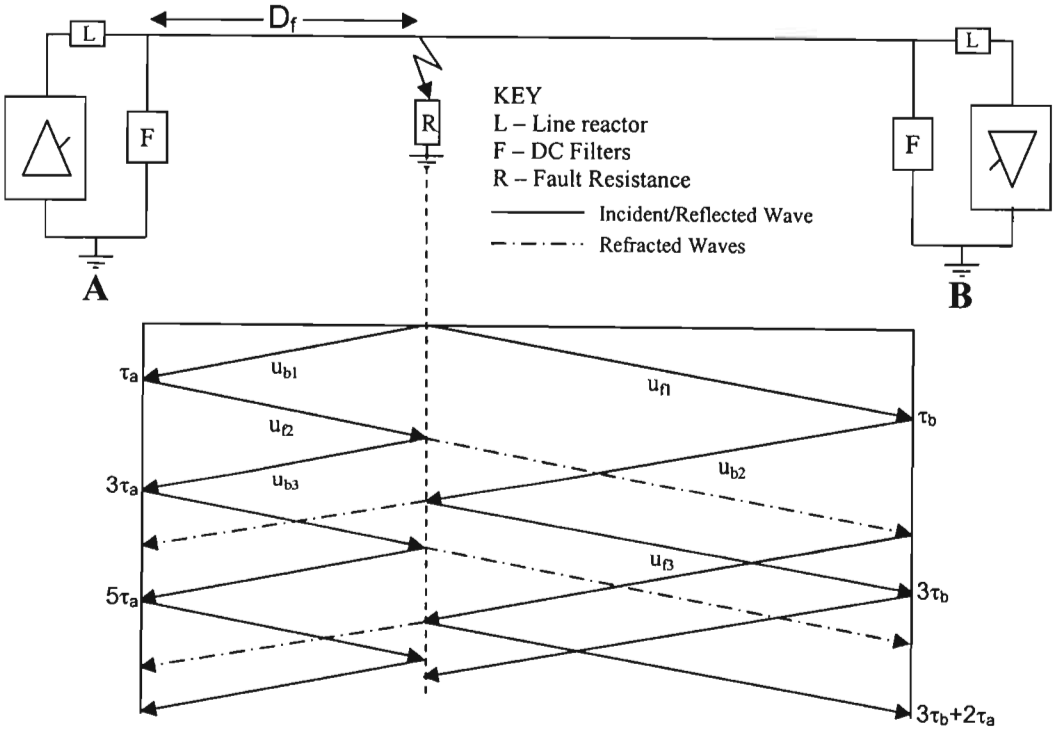

Fig 3.2. HVDC Transmission Line Fault with finite fault resistance and total reflection at terminations.

Firstly, notice that there now are reflected and refracted waves. Therefore, the travelling waves on either side of fault point are no longer independent of each other as they were in Fig 3.1. The coupling across the fault in Fig 3.2, is due to the fault

impedance on a monopole line, however on bipolar HVDC lines this coupling is also caused by mutual coupling with the unfaulted pole as described in 3.2.6. These refracted waves can have an effect on the calculated total travel time t_D from the relaying signals and hence provide an incorrect fault location.

Remembering that the relaying location is at terminal A, Fig 3.2 indicates that, the detection of the correct forward and backward travelling waves has not been affected by the travelling waves refracted by the fault.

However, let us now consider the relaying location to be at terminal B. In order to determine the correct distance to fault, the time difference between the departure of u_{B2} and the arrival of u_{F3} needs to be determined. However, it can be seen from Fig 3.2, that the refracted wave, due to u_{F2}, reaches the relaying point first, which means that if the total travel time t_D was just calculated from the subsequent changes in the local voltage and current signals, the calculated travel time would be incorrect and of course the distance to fault given by (22) would also be incorrect.

It is apparent from the discussion above that the refracted waves affect the distance to fault calculation from terminal B but not from terminal A. The distance to fault calculation is affected at terminal B because the fault is closer to terminal A than it is to terminal B, thereby resulting in a refracted wave arriving at terminal B before the first reflected wave u_{f3}. It should be noted that if a fault is located at a distance greater than 50% of the line length from the relaying terminal, a refracted wave will arrive at the relaying point before the first reflected wave. Therefore, if the fault location is monitored from both ends, any fault on the transmission line, with a finite fault impedance, will result in one terminal, either A or B reporting an incorrect distance to fault.

The only case in which the above situation should not occur is when the fault is located exactly at the centre of the transmission line. This case is illustrated in Fig 3.3, in which a fault with non-zero impedance is located at the centre of the transmission line. In this case, we notice that both the reflected and refracted waves reach terminals A and B at the same time. The local signals will therefore change once, instantaneously, due to the arrival of both the reflected and refracted waves. The

magnitude of the change in the local signals will depend on the amplitude of the combined reflected and refracted waves. Let us consider how this affects the travel time calculation.

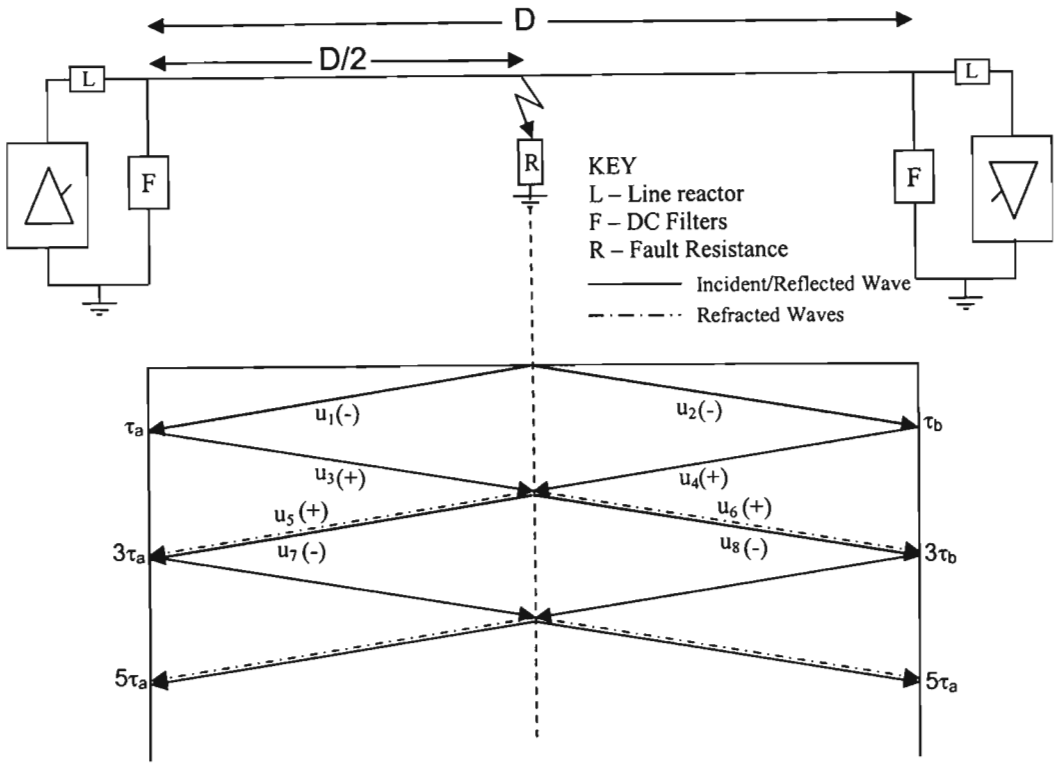

Fig 3.3. HVDC Transmission Line Fault with finite fault resistance located at the centre of the line.

From Fig 3.3, we know that the fault will initiate travelling waves, travelling towards both terminals *A* and *B*. Assuming the pole voltage to be positive, the polarity of these incident waves will be negative as shown in the Fig 3.3. On arrival at the relaying points, assuming an inductive termination impedance [37], these initial waves u_1 and u_2 will experience a negative reflection and travel towards the fault point as positive waves u_3 and u_4. Both waves will reach the fault point at the same time and experience both reflection and refraction at the fault point.

The reflection at the fault point will be negative while the refraction will be positive. The reflected wave u_7 and refracted wave u_5 travel towards terminal *A*, while reflected wave u_8 and refracted wave u_6 travel towards terminal *B*. As can be seen from Fig 3.3, the reflected and refracted waves travelling towards the relaying points have opposite polarities and thus have a cancelling effect on each another. Therefore, depending on

the reflection and refraction coefficients at the fault point, the changes seen in the local quantities at terminals *A* and *B* may be very small, thereby making them difficult to detect.

To prevent the problems discussed above with the identification of the reflected wave from the fault, a correlation method is required to uniquely identify the returning wave from the fault.

The cross-correlation method has been chosen for use in this research. The cross-correlation function has been chosen has a first pass because it is the most widely used theory in travelling wave protection [37], as well as, the availability of software applications that were capable of calculating the cross-correlation function at the time.

The next section briefly explains the cross-correlation function and describes how it will be used in order to fulfil our requirements.

3.2.2. Cross-Correlation

The cross-correlation function (CCF) is a measure of the similarities or shared properties between two signals [38]. The discrete cross-correlation function $\phi_{xy}(\tau)$, given in (38) below, is defined as a measure of the correlation between sections of the sampled signal x and the delayed signal y as a function of the delay τ [32], [36].

$$\Phi_{xy}(\tau) = \frac{1}{N}\sum_{k=1}^{N} x(k\Delta t + \tau) \cdot y(k\Delta t) \qquad (38)$$

Where
N is the number of sampling points in the correlation window.
Δt is the sampling interval.

So if the relaying signals S_F and S_B, as defined in (35) and (36), are correlated using (38), the time at which the returning wave from the fault due to reflection at the fault can be determined. However, "S_F and S_B have different mean values on which the

required travelling wave components are superimposed, so when the discrete cross-correlation function is applied to these signals, the different mean values may prevent a useful correlation between the relaying signals" [36]. "To avoid this problem, the correlation is performed between sections of S_B and the delayed S_F, from which the section mean values have been removed" [36]. The cross-correlation between sections of S_B and S_F with zero mean can be defined as [32], [36], [37], [39]:

$$\Phi(\tau)=\frac{1}{N}\sum_{k=1}^{N}\left[S_B(k\Delta t+\tau)-\overline{S_B}\right]\cdot\left[S_F(k\Delta t)-\overline{S_F}\right] \tag{39}$$

Where

$\overline{S_B}$ and $\overline{S_F}$ are the mean values of their respective sample groups as defined below:

$$\overline{S_B}=\frac{1}{N}\sum_{k=1}^{N}S_B(k\Delta t+\tau) \tag{40}$$

$$\overline{S_F}=\frac{1}{N}\sum_{k=1}^{N}S_F(k\Delta t) \tag{41}$$

The mean value removed correlation function $\phi(\tau)$ shows the similarity between the two relaying function S_F and S_B as a function of the time shift between them. The best match between the two waveforms is achieved when the correlation function is at its maximum. "The time delay when this occurs can be used in (22) to determine the distance to fault" [36].

Figure 3.4, extracted from [36], provides an example of the application of the mean value removed cross-correlation function. Fig 3.4(a) shows the relaying signals obtained for a particular fault on the transmission line. Fig 3.4(b) shows the relaying signals after they have been sampled and Fig 3.4(c) illustrates graphically how the magnitude of the cross-correlation is calculated.

(a). Relaying Signals

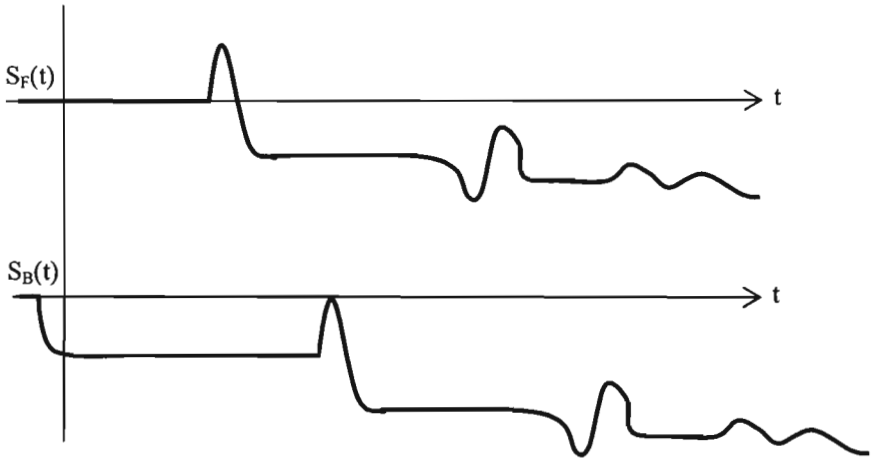

(b). Sampled Relaying Signals

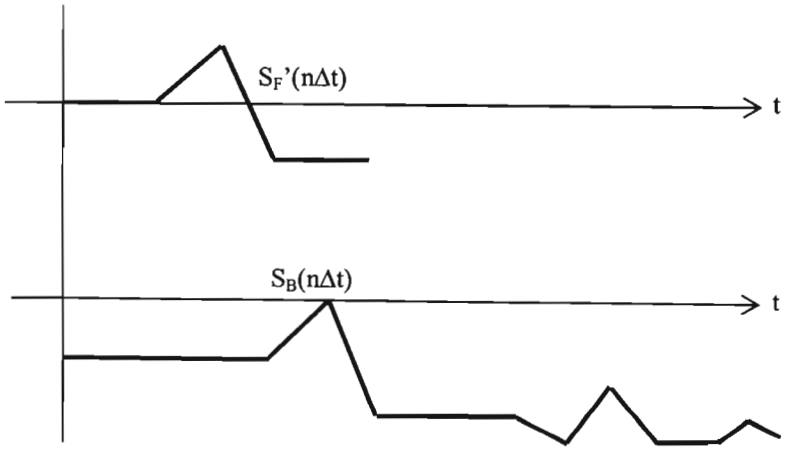

Where

$S_F'(n\Delta t) = S_F(t)$ *for* $t = n\Delta t$, $n = 1,2,3,\ldots N$

$S_B(n\Delta t) = S_B(t)$ *for* $t = n\Delta t$, $n = 1,2,3,\ldots \infty$

"Fig 3.4. Application example cross-correlation calculation" [36].

(c). Cross-correlation calculation

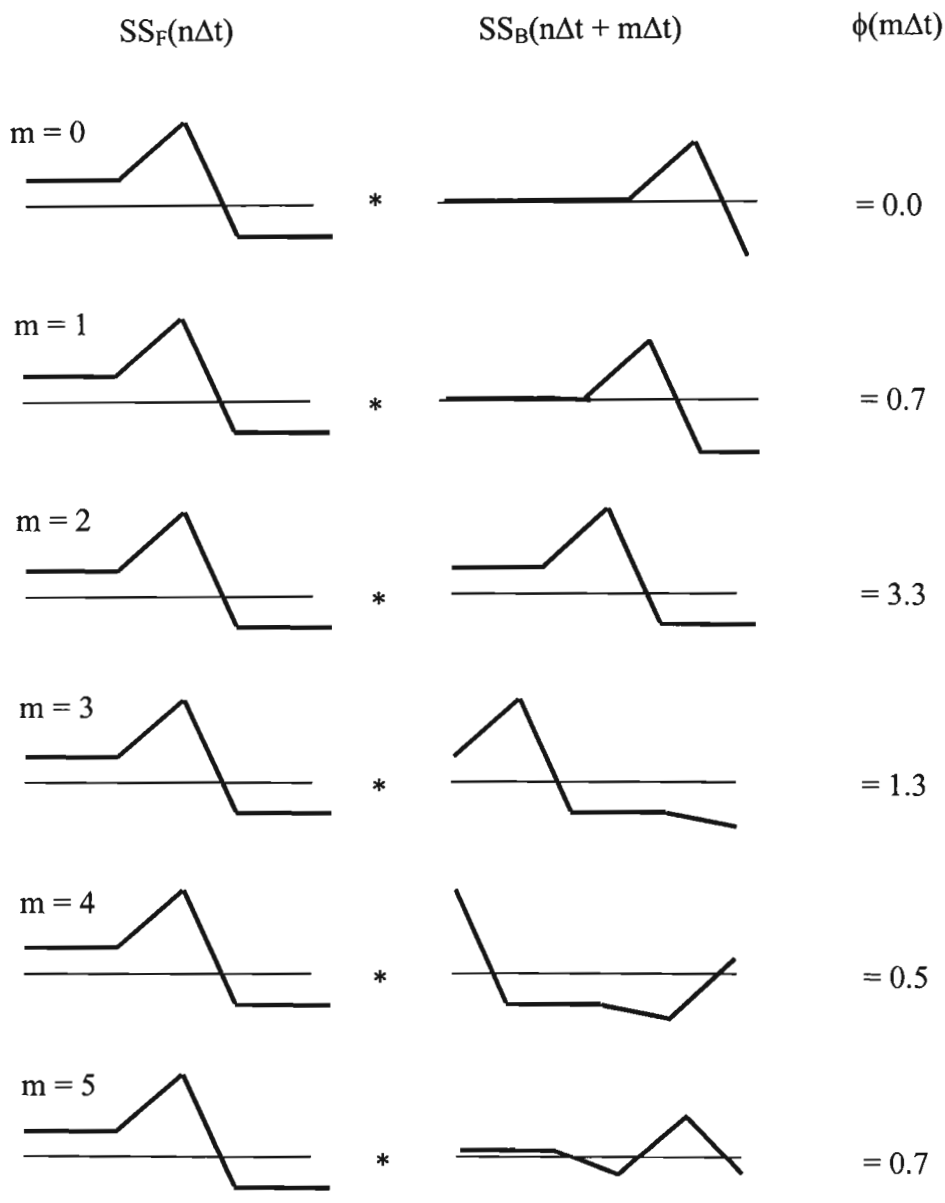

Where

$$SS_F(n\Delta t) = S_F{}'(n\Delta t) - \frac{1}{N}\sum_{k=1}^{N} S_F(k\Delta t)$$

$$SS_B(n\Delta t + m\Delta t) = S_B(n\Delta t + m\Delta t) - \frac{1}{N}\sum_{k=1}^{N} S_B(k\Delta t + m\Delta t) \quad m = 0,1,...,\infty$$

$$\Phi(\tau) = \frac{1}{N}\sum_{k=1}^{N} SS_F(n\Delta t) \cdot SS_B(n\Delta t + m\Delta t)$$

"Fig 3.4. Application example cross-correlation calculation" [36].

3.2.3. Protection Starter Requirements

The protection starter is required to detect the possible presence of a forward fault and activate the protection system. The purpose of the starter is to ensure that the protection relay or algorithm remains stable and does not cause any mal-operations during normal conditions. The protection starter will be activated once certain specific criteria are met. These criteria are discussed in 3.2.4. Once the protection starter is activated it will be latched in and remain active until the DC voltage returns to a certain percentage of the pre-fault voltage for a specified time. The above condition ensures that the protection starter will remain active as long as the fault condition exists. The protection system once activated by the protection starter can only be reset if a fault is detected and an instruction to de-energize the faulted pole is issued or the protection starter has been deactivated.

The need for a protection starter will be explained with the aid of Fig 3.5 and Fig 3.6 below. In Fig 3.5, a disturbance is located in the opposite converter station beyond the transmission line. This disturbance will cause a backward travelling wave S_{B1} to propagate through the transmission line and arrive at the relaying point at time τ_A. The magnitude of this wave will be small but, with the protection system always active, may cause enough change in the local quantities to start the correlation function.

The correlation function will use the reflected forward travelling wave S_F as a template and identify S_{B2} as the returning wave. The calculated distance to fault from this time should be equal to the line length. This will be the case for any fault beyond the transmission line as can be easily seen in Fig 3.5.

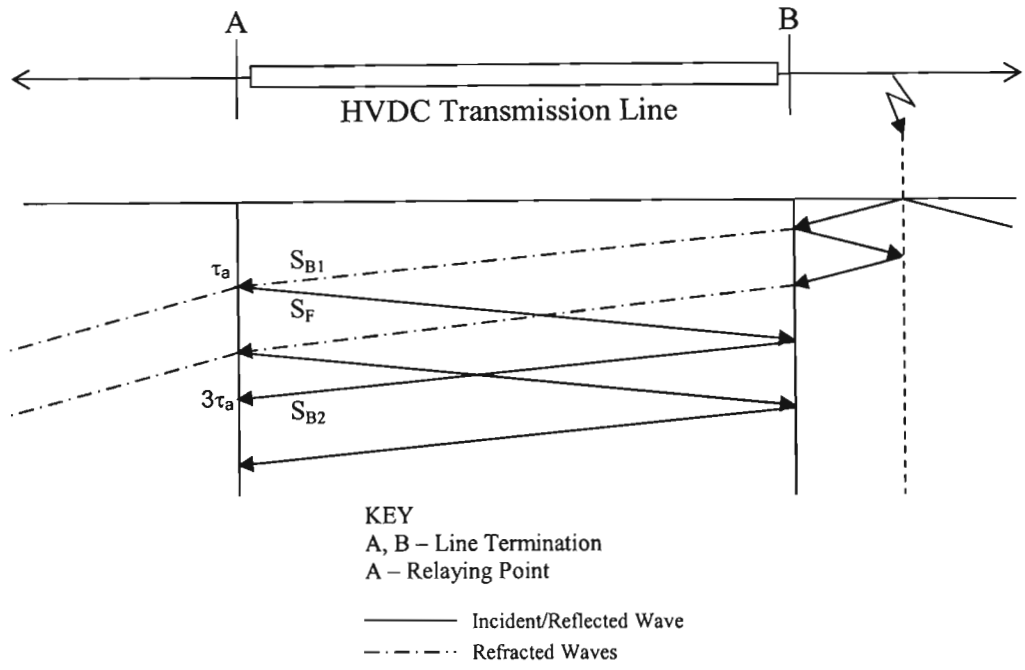

Fig 3.5. Fault located beyond the transmission line in front of the relay pointing.

In Fig 3.6, the disturbance is now located behind the relaying point. The figure shows how the travelling waves propagate through the transmission line and again if the protection system is always active, a distance to fault equal to the line length will be returned.

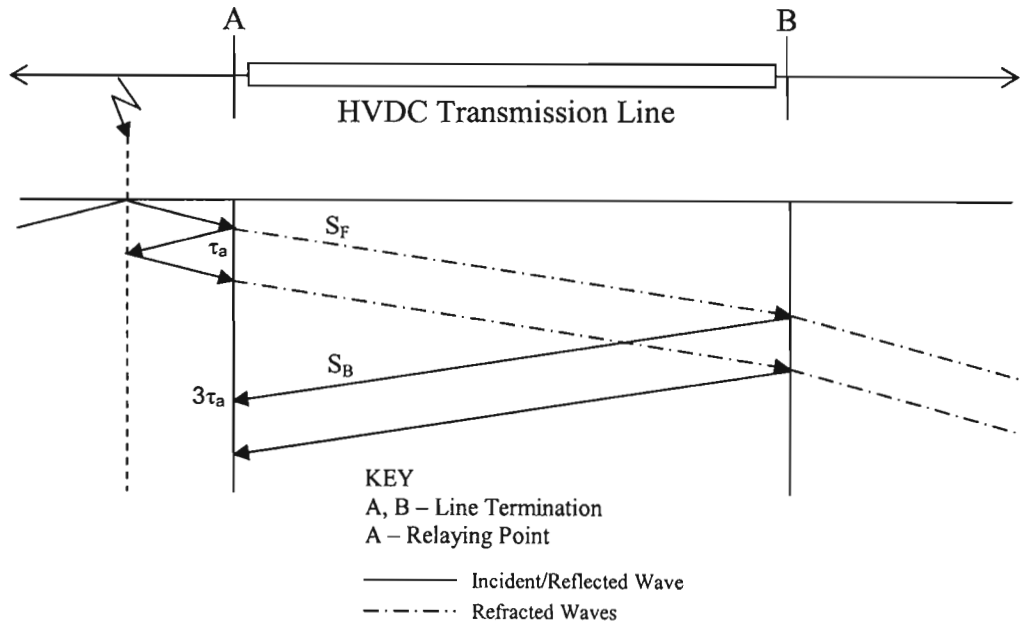

Fig 3.6. Fault located behind relaying point.

From the above two cases in Fig 3.5 and Fig 3.6, it should be apparent that it will not be possible for the protection system to be set to initiate fault clearance immediately for the entire line. So taking into account possible errors, due to the current and voltage transducers and depending on the sampling rate of the correlation function, the last 10 to 20 percent of the line will have to be cleared after a time delay. This time delay is required to ensure that the converter station protection is given a chance to clear the fault, should the fault not be located on the transmission line.

So for actual line faults on the last 10 to 20 percent of the line the fault clearance will be delayed, however this time delay can be eliminated when the telecommunication infrastructure is used to optimize the system, thereby only causing delayed fault clearance when the telecommunication infrastructure is unavailable and the fault is located in the last 10 to 20 percent of the line. This will be discussed in 3.3 to follow.

The fact that the HVDC transmission line is terminated through a line reactor may provide another possible method of eliminating the need for the time delay. In [34] and [37] it is pointed out that, an inductive termination introduces a decaying exponential component to the reflected travelling wave. So if we consider the two cases illustrated in Fig 3.5 and Fig 3.6, the returning wave to the relaying point would have been reflected by the inductive termination at the line end and contain an additional decaying exponential component. This will not be present in a wave returning from a fault. So if a method of determining this can be devised, this feature can be used to block tripping for the cases illustrated in Fig 3.5 and Fig 3.6 and thereby eliminate the need for delayed fault clearance. This feature was not investigated in this work and should be looked into as part of further work.

3.2.4. Possible Protection Starters

The protection starter needs to be based on information available at the relaying point. Table 3.1, illustrates the changes in local measured or calculated quantities at the relaying point.

Table 3.1. Changes in local quantities at the relaying location for various faults.

LOCAL QUANTITY CHANGES AT RELAYING POINT			
Case	ΔU, ΔI	U, I Gradients	Relaying Signals S_F and S_B
DC Line Fault Fig 3.1 – Fig 3.3	Change with opposite polarity	Change in opposite direction	Change Simultaneously
Fault beyond TL in front of Relay Fig 3.5	Change with opposite polarity	Change in opposite direction	Change Simultaneously
Fault Behind Relay Fig 3.6	Change with same polarity	Change in same direction	S_F changes before S_B

It can be seen that any one of the three local quantity changes given in Table 3.1. can be used to determine whether the fault is in front or behind the relay. However, as indicated in Table 3.1. these local quantity changes cannot be directly used to determine whether the fault is on the line or beyond the line. The starter will, therefore, be used to detect the presence of a forward fault and the calculated distance to fault will then be used to determine whether the fault is a line fault or not.

In accordance with Table 3.1, we have the following protection starter options:

Option 1. The voltage and current changes *ΔU* and *ΔI*

The voltage and current changes, *ΔU* and *ΔI*, can be multiplied together (i.e. *ΔU*×*ΔI*). During normal conditions and reverse faults, this product should be positive and during forward faults, the product will be negative. Small negative values may however appear during normal and starting conditions. These negative values appear because of the lag in voltage and current caused by the dc smoothing reactor between the converters and the dc line. The above condition must be taking into account when setting the starter threshold.

Faults can also be placed beyond terminal *B* in Fig 3.5 to determine a threshold setting that will block the starter for faults beyond the transmission line. The above will eliminate the need for the time delay in the last section of the line however the fault resistance coverage will be reduced.

Since ΔU and ΔI are already continuously calculated in order to determine S_F and S_B, the implementation of this option would only require that the product of the already determined ΔU and ΔI be calculated and compared to the starter threshold.

Option 2. The voltage and current gradient changes

The changes in voltage and current gradients can be multiplied together. A negative result will indicate a forward fault and a positive result will block the starter. Small negative values may also appear during normal and starting conditions. Again these negative values appear because of the lag in voltage and current caused by the dc smoothing reactor. The above condition must be taking into account when setting the starter thresholds.

The implementation of this option will be similar to that of option 1. The only difference in the implementation of this option is that the already calculated ΔU and ΔI would have to be divided by the sampling interval Δt to determine the gradients ($\Delta U/\Delta t$ and $\Delta I/\Delta t$). The product of these gradients ($\Delta U/\Delta t \times \Delta I/\Delta t$) would then have to be calculated and compared to the starter threshold. Note this option will provide very similar results to option 1 as the only difference between the two options is that ($\Delta U/\Delta t \times \Delta I/\Delta t$) is greater than ($\Delta U \times \Delta I$) by a constant factor of $1/\Delta t^2$.

Option 3. The changes in the S_F and S_B relaying signals

Since the relaying point is at the termination for the HVDC line, in the case of a forward fault both S_F and S_B experience a change simultaneously. However, in the case of a reverse fault, as shown in Fig 3.6, S_F will experience a change first and S_B will only experience a change after twice the line travel time.

Therefore, the changes in S_F and S_B can be monitored and the correlation function should only be started if there is both a change in S_F and S_B above the set threshold in quick succession. Note that due to the continuous switching operations of the converter valves, small changes in S_F and S_B are experienced

even under normal conditions. The starter threshold must be set higher, than these expected changes in relaying functions.

In order to implement this option the additional quantities ΔS_F and ΔS_B will have to be calculated. Both these quantities will then have to be compared to a magnitude threshold. If both ΔS_F and ΔS_B exceed this magnitude threshold, the time difference between ΔS_F and ΔS_B will then have to be determine and compared to a time threshold. If the time difference between ΔS_F and ΔS_B is less than the time threshold the starter will become active and activate the protection system.

From the discussions above, options 1 and 2 are much easier to implement as opposed to option 3. Therefore, the choice of option 3 will be eliminated for the time being. Both options 1 and 2 provide very similar results and, therefore, the choice of which option to use will be based on the ease of implementation. The final decision was to use option 1 has the protection starter. The protection system will, therefore, be activated when the product of ΔU and ΔI goes below the protection starter threshold setting P_s i.e. $(\Delta U \times \Delta I) < P_s$.

3.2.5. Bipolar System Considerations

As indicated in 2.2.6, majority of the HVDC systems are bipolar with the poles located within close vicinity between one and other. This results in mutual coupling between the poles, with surges on one pole inducing surges on the other. This is liable to cause errors in the correlation function if not correctly taken into account.

In 2.2.6, the concept of modal networks was introduced which allows the coupled network to be transformed into two balanced modal networks i.e. a positive sequence and zero sequence network. Fig 3.7, below provides an illustration of the positive and negative sequence networks.

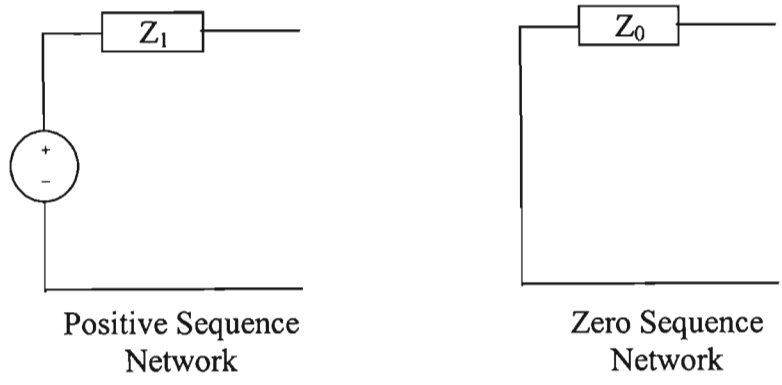

Fig 3.7. Illustration of the Modal/Sequence Networks.

The ground mode or zero sequence wave are only present when the fault involves a connection to earth, which in a HVDC system would account for the majority of the faults.

The propagation velocity and surge impedance of the ground mode is dependent on the fault resistance and is highly frequency dependent, whereas the pole or positive sequence waves have a substantially constant propagation velocity and surge impedance for frequencies above 20Hz [25].

Note that equation (22) used to calculate fault distance assumes a constant velocity, so if the local voltages and currents are used to develop the relaying signals S_F and S_B, errors will be introduced due to the frequency dependent propagation velocity of the ground mode wave. It is for this reason that the pole mode wave will be used in developing the relaying signals S_F and S_B, which will be used by the correlation function.

Now from 2.2.6, we know that the polarity of the ground mode wave on both poles will be the same and the polarity is dependent on which pole has faulted. The polarity of the ground mode wave will therefore be used to determine the faulted pole. This implies that both modes will be used in the protection systems, with the pole mode being used for fault location and the ground mode used for faulted pole identification.

3.2.6. Limitations of Standard Cross-Correlation Function

Inaccuracies in the standard cross-correlation function, as described in 3.2.2, have been reported in [36] and [37] when the fault resistance is high. The reason for this is given in [37] and can be best explained with reference to Fig 3.8.

The objective of the cross-correlation function (CCF) is to determine the time difference between *A1* and *A3*. In order to accomplish this, the CCF between the forward travelling wave *A1F1* and the subsequent backward travelling wave is calculated to detect the arrival of the desired signal *F3A3*. As the reflection coefficient at the fault point is negative, *A1F1* has the opposite polarity to *F3A3*, therefore, if – *A1F1* is taken as the template, the arrival of *F3A3* will generate a positive peak in CCF.

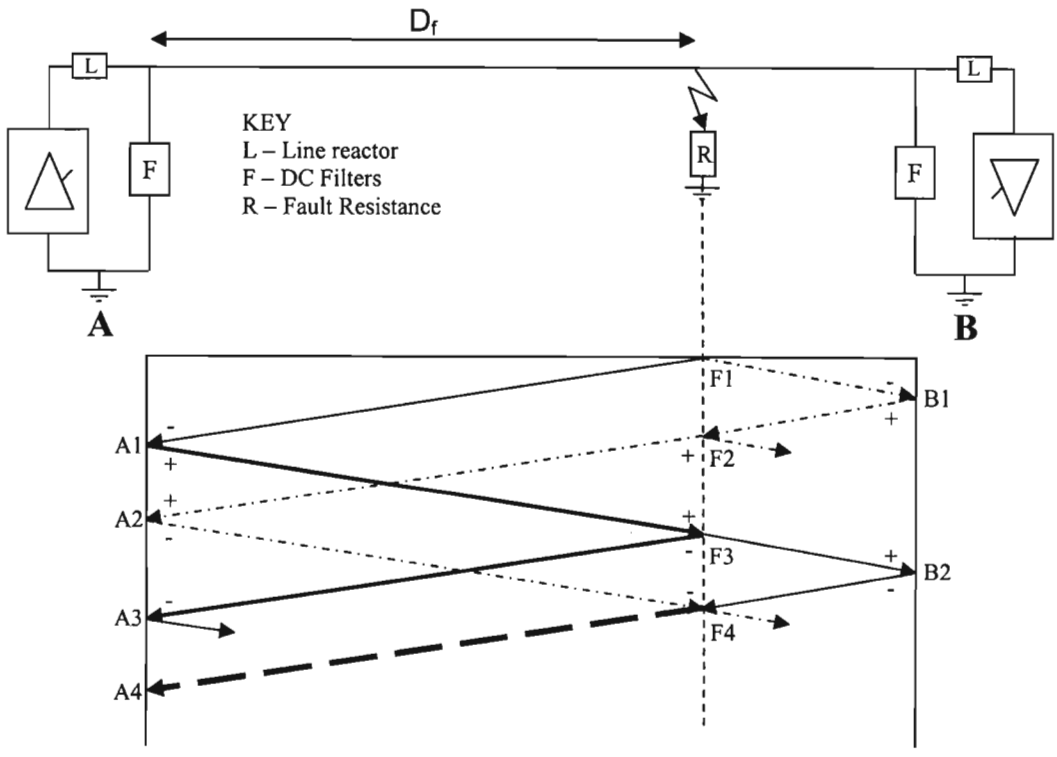

Fig 3.8. Bewley Lattice Diagram illustrating possible cause of inaccuracy in cross-correlation function.

Now in Fig 3.8, consider the transmitted wave *F3B2* which will be reflected by terminal *B* and transmitted through the fault point. Therefore, *F4A4* would arrive at the relaying point with the same polarity as *F3A3* and also generate a positive peak in

the correlation function. However, the backward travelling wave detected at *A4* also contains another part due to the reflection of the forward wave *A2F4*, which will have the opposite polarity. Therefore the polarity and amplitude of *F4A4* will be determined be the sum of the two signals.

So if the peak caused by *F4A4* is greater than the peak caused by *F3A3*, inaccuracy will result. The results obtained in [36] and [37] revealed that this inaccuracy resulted in a fault location estimation equal to the length of the line.

Since the reflection of *A2F4* is positive and the transmitted wave due to *B2F4* is negative, the magnitude of the peak caused by *F4A4* in the correlation function will increase as the amplitude of the transmitted wave due to *B2F4* increases. Therefore, we can deduce that, the larger the magnitude of the transmitted wave, the greater the chance of inaccuracy. The transmitted wave is based on the refraction coefficient, as defined in (2.2.2), which increases with fault resistance. Therefore, we can assume that there is a finite resistance, beyond which, inaccuracies will occur in the standard CCF.

This limitation is especially severe for earth faults on multi-conductor systems, as there is refraction present even for solid earth faults due to the coupling between the circuits. In order to explain this concept as applicable to a bipolar HVDC system, let us analyze a solid pole to ground fault on pole 1 of a bipolar HVDC system.

So, for a solid pole to ground fault on pole 1 we will have the following conditions:

$$u_{p1} = 0 \tag{42}$$

$$i_{p2} = 0 \tag{43}$$

Now substituting the above conditions into modal equations (25) and (28) respectively we obtain the following:

$$u_0 + u_1 = 0 \tag{44}$$

$$i_0 = i_1 \tag{45}$$

Equations (44) and (45) are satisfied by a series connection of the zero and positive sequence networks at the fault point as shown in Fig 3.9(a).

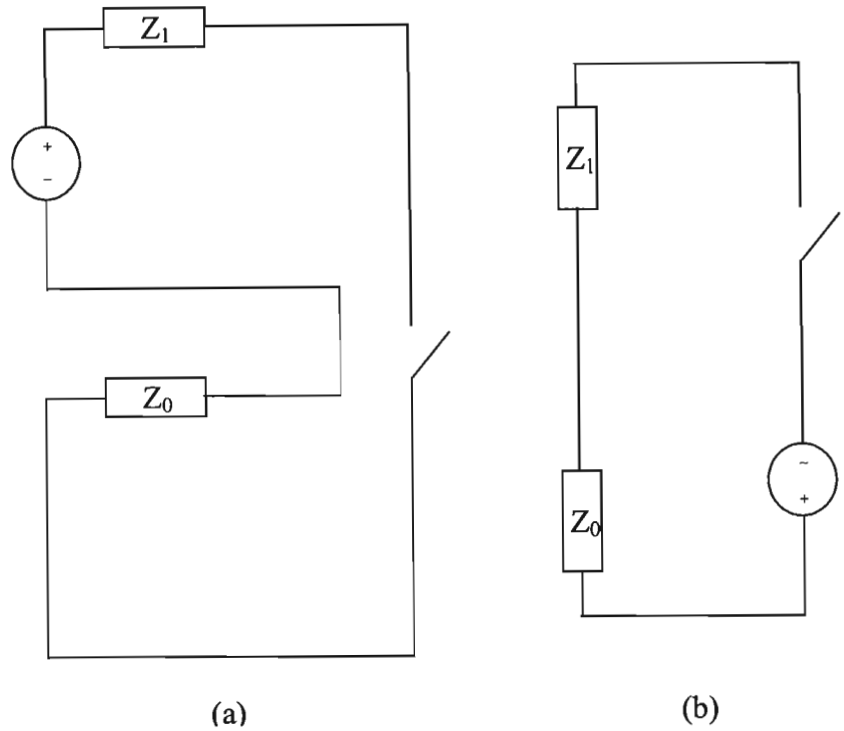

Fig 3.9. Connection of modal networks for pole to ground fault.

The circuit in Fig 3.9(a) can be modified in order to represent the transient components only by removing the EMF from the positive sequence network and applying it externally at the fault point [25] as shown in Fig 3.9(b). The most important fact that we can gather from Fig 3.9, is the fact that each mode is terminated in the surge impedance of the other mode. Now in general the surge impedance of the ground mode is larger than that of the pole mode and it is for this reason that, even for solid ground faults, there are significant refracted waves, which can cause inaccuracies in the standard CCF.

3.2.7. Auxiliary Cross-Correlation Function

In order to improve the performance of the correlation function, the authors in [37] have suggested the use of an auxiliary CCF to complement the existing standard CCF.

In order to explain the functioning of the auxiliary CCF, let us once again consider Fig 3.8. Now let us assume the fault impedance is large enough that *F4A4* causes a maximum in the standard CCF instead of *F3A3* (NB: there will still be a local maximum at *F3A3* but its magnitude will be smaller). This means, that the fault location provided by (22) would be incorrect. However if we take the time of this instant, to be t_1 and use *F4A4* as a template to calculate a second mean value removed CCF with respect to the forward waves, *A2F4* will be identified at time, t_2, by a maximum in this CCF, which is known as the auxiliary CCF.

Fig 3.8 also shows that the time difference between *A3* and *A1* is the same as the time difference between *A4* and *A2*. Therefore, the distance for this high impedance fault will be given by [37]:

$$D_{f2} = \frac{v(t_1 - t_2)}{2} \tag{46}$$

So now, we have two fault location estimates provided by (22) and (46). We know that fault location provided by (22) will be correct for low impedance faults, while (46) will provide a correct fault location for high impedance faults.

Obviously the protection system has no way of knowing whether a high impedance fault is present or not, therefore a strategy needs to be developed that the protection system will adopt in order to determine which of the fault location estimates is correct.

3.2.8. Cross-Correlation Fault Location Strategy

In order to develop the required strategy, the following should be noted:

- If the fault location given in (46) is correct, there will always be a local maximum in the standard CCF around the same distance, which will not be the case otherwise.

- Inaccuracy in the standard CCF reports a distance equal to the line length [36], [37]. The inaccuracy was verified by the extensive simulations conducted and reported in chapter 5. The significance of this is that, the use of the auxiliary CCF can be limited to instances, when the standard CCF reports a fault location of say, greater than 80 or 90 percent of the line length, depending on possible transducer errors as well as errors introduced due to the selected sampling rate. This is an important feature because the use of two correlation functions doubles the correlation time and we will obviously want to keep this to a minimum.

- The aim of the auxiliary CCF is to identify the refracted wave, which caused the inaccuracy in the standard CCF. Therefore, if time t_2 is greater than time t_1, the auxiliary CCF should be ignored, since it will not be possible for the maximum, in the standard CCF, to be caused by a refracted wave that occurred after the maximum in the standard CCF.

Bearing the above in mind the process in the flowchart below has been proposed for use in the protection system, in order to determine, which fault location estimate should be considered to be correct. The flowchart has been developed with reference to Fig 3.8 above.

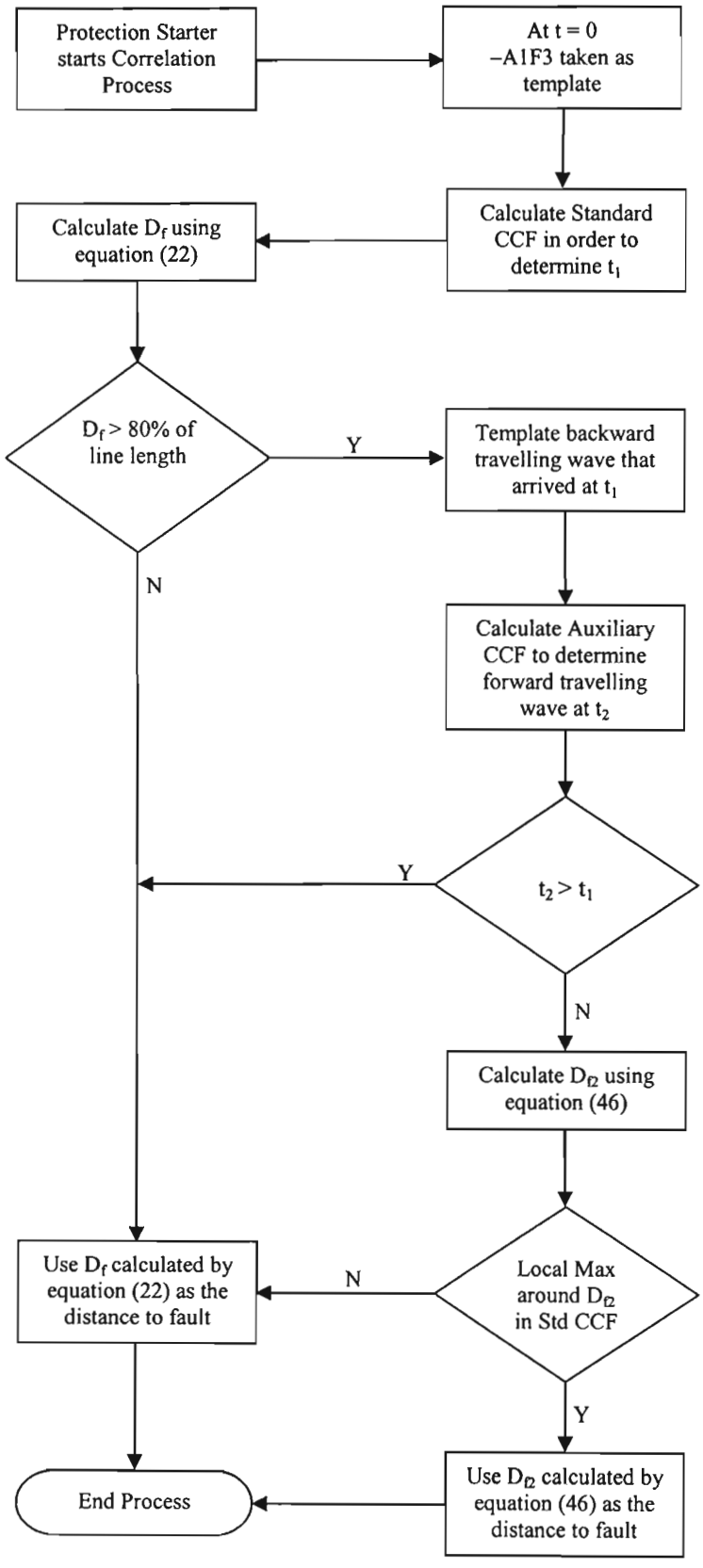

Fig 3.10. Flowchart of correlation process.

3.2.9. Functioning of Complete Local Detection Protection System

The local detection protection system is activated when the product of ΔU and ΔI are below the protection starter setting P_s. Once the starter is activated, it is latched until the DC voltage returns to a certain percent of the pre-fault voltage for a specified time.

Once the starter becomes active, the correlation process as shown in Fig 3.10 is started in order to determine the distance to fault D_f. This calculated distance to fault is then compared to a threshold setting D_s and if D_f is less than D_s a fault is detected immediately. If D_f is greater than D_s, a timer is started. If the starter is still active when the timer expires, a fault will also be detected otherwise the protection will be reset. The fault detection process is illustrated in Fig 3.11 below.

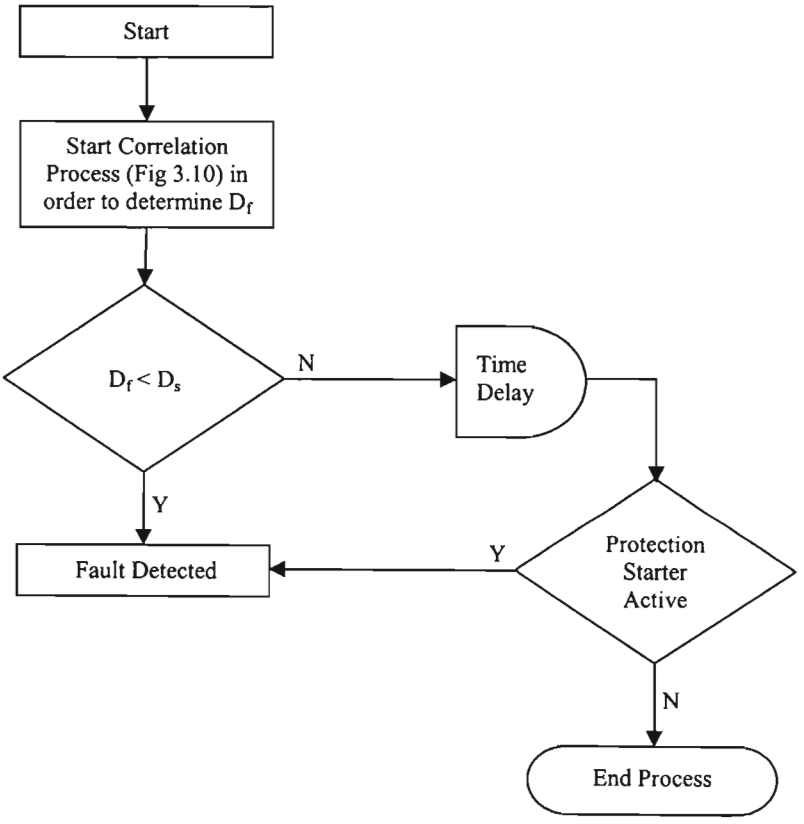

Fig 3.11. Flowchart of fault location and detection process.

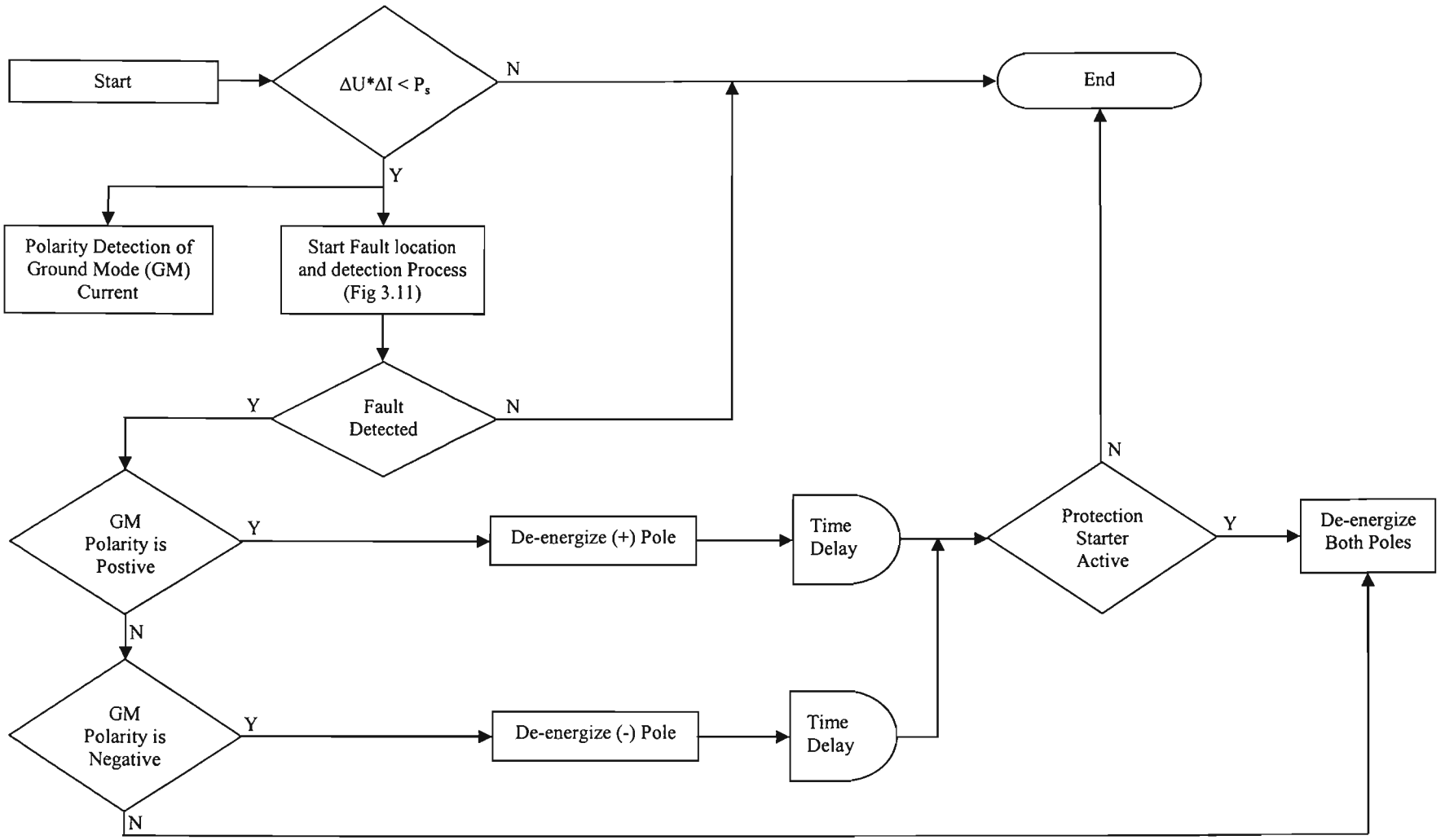

Fig 3.12 Flowchart of Complete Local Protection System.

Fig 3.12, above provides a flowchart of the entire local detection process. Note that at the same time the correlation process is started, a process to detect the polarity of the ground mode current is also started. The polarity of the ground mode is checked to determine which pole needs to be tripped to clear the fault as shown in the figure above.

When a fault is detected with no ground mode present, a bipole fault is assumed and both poles are tripped in order to clear the fault. Notice that when an instruction to trip a single pole is given a timer is started. If the protection starter is still active after the timer has expired, indicating that the fault is still present, an instruction to trip both poles will then be issued. This logic has been added to cater for the rare instance of an unbalanced pole to pole to ground fault.

3.3. Method of Using Telecommunications for Optimization.

All HVDC systems will have some sort of communication infrastructure between the converter stations for relaying control signals. Irrespective of the reliability of the telecommunications, if it is available, it should be used to try and optimize the response of the protection system, however, the correct operation of the protection system must in no way be reliant on the communication system. The protection system must be able to correctly detect faults in the absence of the communication system.

One simple method of enhancing the protection system is to have the local detection system described in the previous section installed at both line ends with fault detection information relayed from one end to the other using the telecommunication infrastructure. Assume that a fault develops on the transmission line and the distance from the rectifier terminal to the fault is greater than 90% of the line length. Under normal circumstances the above fault will only be cleared after a time delay by the local detection system installed at the rectifier end. However, if the protection system is installed at both ends, the rectifier end will register a fault located beyond 90% of the line length and the inverter will register a fault located within 10% of the line length from its terminals. Since both ends located the fault on the transmission line it stands to reason that the fault is definitely on the line. So if the fault location

information from the inverter end is sent through to the rectifier via the communication system, non delayed tripping could be initiated for this situation.

The above method requires that both ends need to detect the fault first using the process described in 3.2.8, and then only the information will be sent through to the other side. Note that each side with require a time equal to twice the travel time of the line upon arrival of the incident wave to register a distance to fault. Should the fault be a high impedance fault, this time will be further increased due to the auxiliary CCF.

The author therefore would like to propose another method of fault detection when the telecommunication infrastructure is available. Let us consider Figs 3.1 to 3.3, with synchronized clocks at both ends, the difference between τ_a and τ_b can be obtained by noting the time of arrival of the incident waves and transferring this information between both ends were the difference can be calculated. The distance to the fault can be calculated by using this information together with the length of the line ℓ in the equations below [31]:

$$D_A = \frac{\ell + v(\tau_a - \tau_b)}{2} \tag{47}$$

$$D_B = \frac{\ell - v(\tau_a - \tau_b)}{2} \tag{48}$$

Where
D_A and D_B are the distance to the fault from station A and B respectively.

We can now setup a distance measurement scheme for a HVDC system. Let us assume station A is the rectifier. We can then define D_{AB} as the distance to the fault from A as seen by B (inverter station) and this can be simply calculated using (49) below:

$$D_{AB} = \ell - D_B \tag{49}$$

Now if D_{AB} and D_A are within a specified tolerance ε, as given in (50) and D_A is less than a distance setting specified D_S, as given in (51), the protection system will detect a fault condition and issue an instruction to de-energize the faulted pole/s.

$$\left|\frac{D_{AB}}{D_A} - 1\right| \leq \varepsilon \tag{50}$$

$$D_A \leq D_s \tag{51}$$

The continuous switching operations by the converter valves will cause travelling waves to be setup even during normal HVDC system operation. These travelling waves are damped by the dc smoothing reactor and, therefore, have a much more gentle gradient as opposed to fault generated travelling waves. In order to ensure that only fault initiated incident waves are used by the protection system a starter will have to be adopted. The same protection starter ($\Delta U \times \Delta I$) as used by the local detection system can be adopted. Therefore, the time at which ($\Delta U \times \Delta I$) goes below the set threshold at terminals A and B marks the time of arrival of the fault initiated incident wave at terminals A and B respectively.

The advantage of this method is that the no complex signal processing is required. The time of arrival is simply tagged on detection of the protection starter at each end. This information is then send through to the rectifier were the simple calculations in (47) to (49) are performed and if the conditions given in (50) and (51) are met, a fault is detected. The faulted pole can again, be determined by the polarity of the ground mode current.

3.4. Proposed Complete DC Line Main Protection Scheme.

The purpose of this research is to develop a protection method for the protection of ultra long HVDC transmission lines based on locally available quantities. A method of accomplishing this has been proposed in 3.2. This method has been proposed as an enhancement, for use with the existing voltage derivative protection, which has a faster response to close in faults.

In section 3.3, the author went a step further in introducing a method of using the telecommunication infrastructure, when available, to optimize the response of the protection system. Fig 3.13, below shows the block diagram of the complete scheme with the proposed improvements.

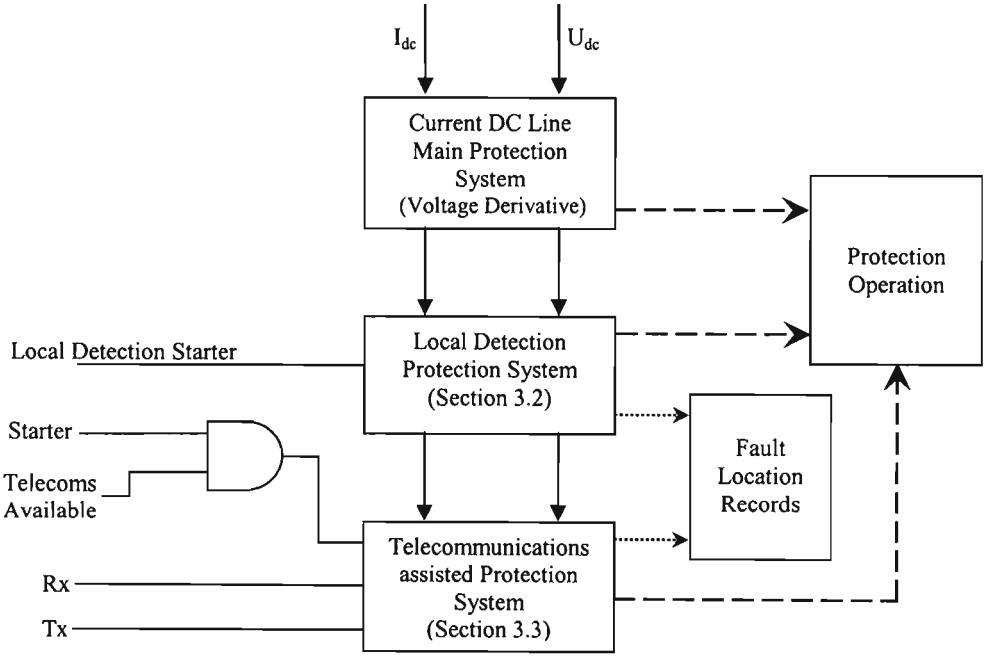

Fig 3.13. Block Diagram of Complete DC Line Main Protection Scheme.

Chapter 4: Research Design and Methodology

4.1. Introduction

The objective of this chapter is to describe the methodology used in evaluating the HVDC line main protection scheme proposed in chapter 3.

The evaluation of the protection system was accomplished with the aid of computer simulations. The computer simulation software package PSCAD/EMTDC was chosen for this evaluation task. In order to accomplish this, a working EMTDC model of an HVDC system had be to acquired, on which the protection system could be evaluated.

The HVDC transmission line, DC filters and all other quantities required by the protection system were modelled using EMTDC. The above data was then exported into Matlab, where the protection system was modelled in order to determine the performance of the protection system. The results of these simulations were used in the final evaluation of the proposed protection system.

4.2. PSCAD/EMTDC

EMTDC™ (Electromagnetic Transients including DC) is a time domain transient simulation program which can duplicate the response of the power system at all frequencies [40]. This feature is important when studying the response caused by travelling waves which have a wide frequency spectrum.

PSCAD® (Power Systems CAD) is the user interface to the EMTDC solution engine. It allows the user to schematically construct a circuit, run a simulation, analyze the results, and manage the data in a integrated, graphical environment [41].

4.3. HVDC System Model

The author made every effort possible to obtain an EMTDC model of an existing HVDC system on which the protection system could be evaluated. However, this was not possible at the time of this research. The author then opted to use a bipole model of the famous Cigre Benchmark Model. The bipole model was formulated from the original monopole Cigre Model by the Manitoba HVDC Research Centre in Canada [42]. Fig 4.1 shows the schematic diagram of the electrical HVDC system model [42]. The schematic diagram of the rectifier and inverter controls models are given in Fig 4.2 and Fig 4.3 respectively [42]. All details and information regarding these models are provided in [43]

The specifications for the HVDC system under study are given in Table 4.1 below.

Table 4.1. Specification of Bipole HVDC System under Study.

HVDC SYSTEM SPECIFICATIONS	
Configuration	Bipole (12 pulse)
Pole Voltage	± 500kV
Pole Current	1000A
System Power	1000MW
Pole Power	500MW
Rectifier Short Circuit Ratio (SCR)	2.5
Inverter Short Circuit Ratio (SCR)	2.5
Rectifier AC Voltage	345kV
Rectifier - AC Frequency	50Hz
Inverter AC Voltage	230kV
Inverter – AC Frequency	50Hz
Reactive Power Compensation	Fixed Capacitors
AC Filters	Damped Filters
DC Filters	No DC Filters

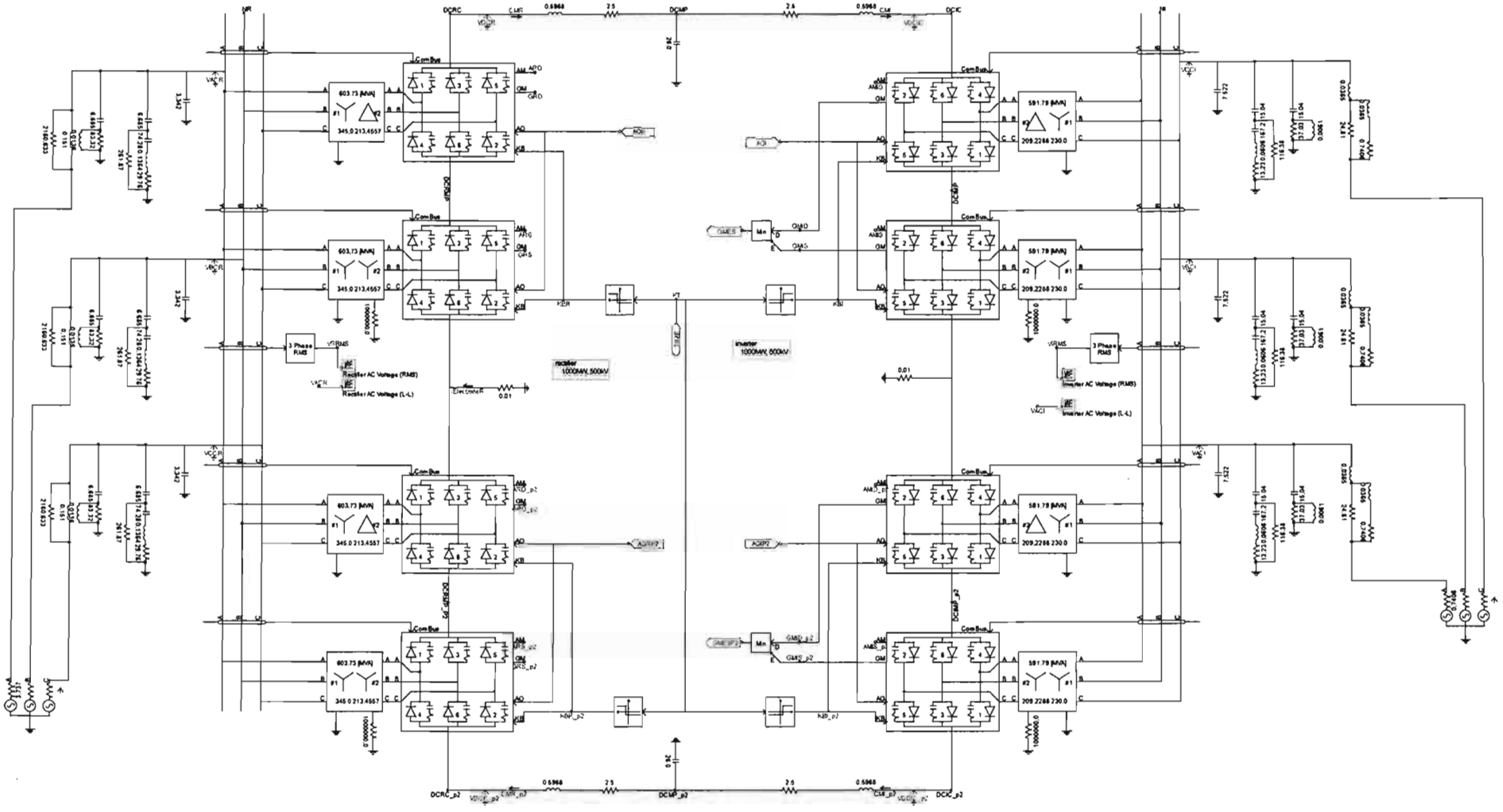

Fig 4.1. Schematic Diagram of the Electrical System Model [42].

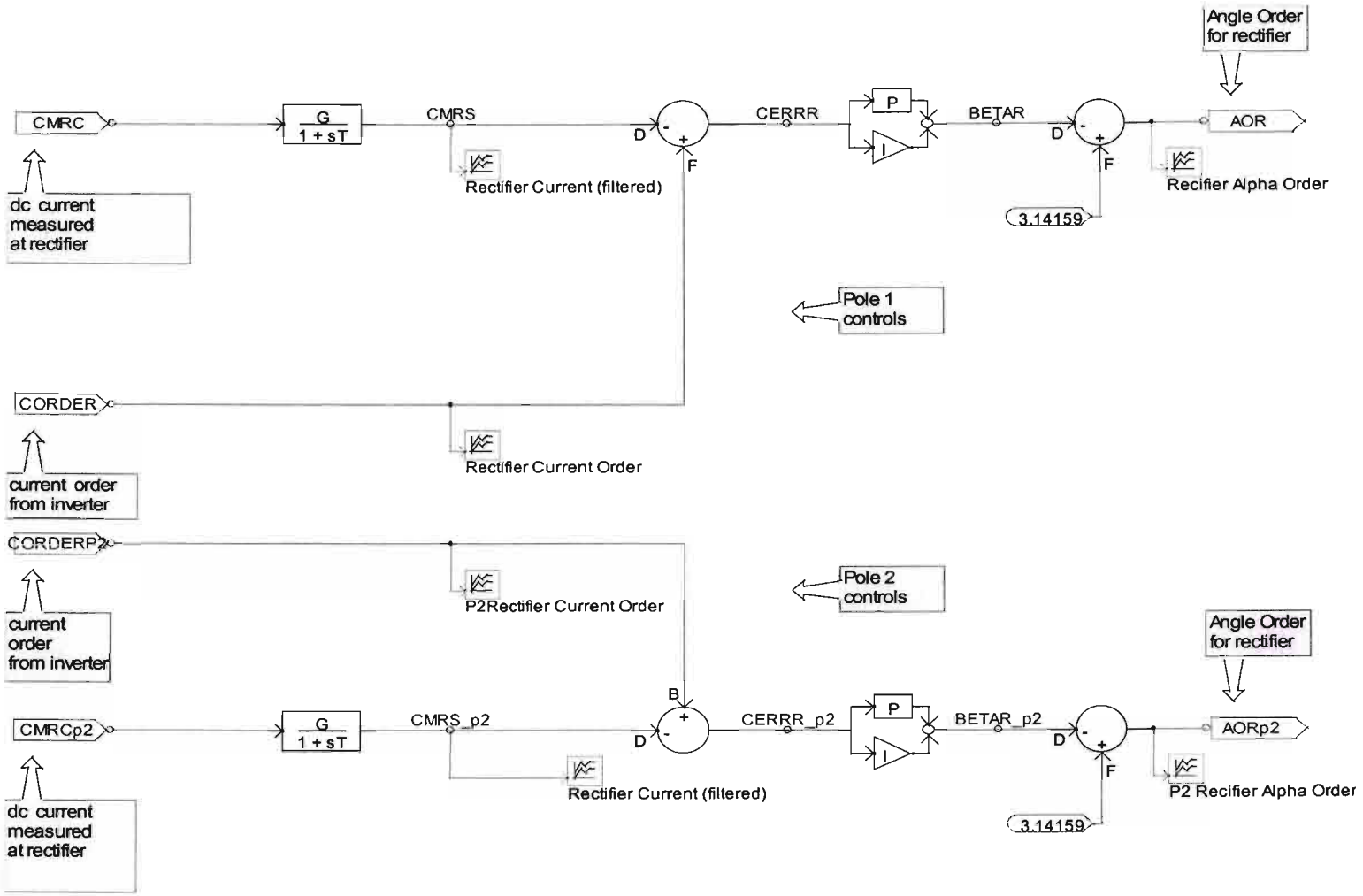

Fig 4.2. Schematic Diagram of the Rectifier Control System Model [42].

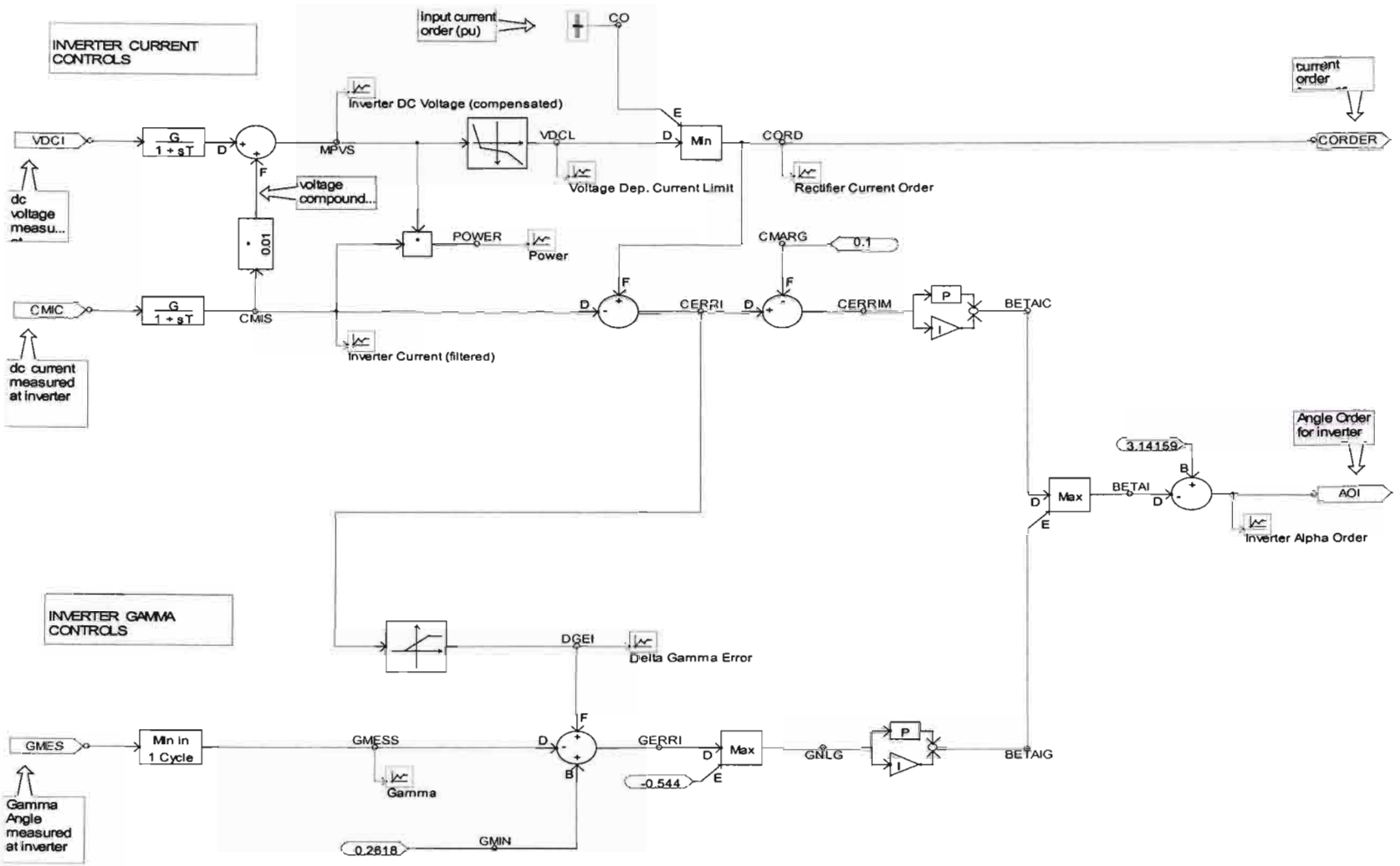

Fig 4.3. Schematic Diagram of the Pole Inverter Control System Model [42].

4.4. HVDC Transmission Line Model

The DC line protection system proposed in the previous chapter is based on the travelling waves arriving at the relaying location. Therefore, in order to accurately assess the suitability of this proposed protection system, the transmission line model used must be able to accurately represent the physical transmission line under these transient conditions. This is only possible with the use of a travelling wave line model.

Fig 4.1 indicates that the dc transmission line in this system is modelled by a simple T network. This is clearly shown in Fig 4.4 below, where *DCRC* and *DCIC* indicate the connection point to converter at the rectifier and inverter ends respectively on pole 1.

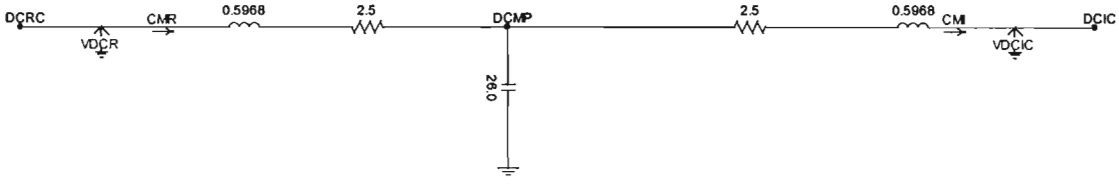

Fig 4.4. Currently used line model in HVDC System.

This line model will not exhibit the same response during transient conditions as the physical transmission line and, therefore, cannot be used to represent the HVDC transmission line.

EMTDC has three travelling wave line models available for use. These three models are the bergeron model, the frequency dependent (mode) model and the frequency dependent (phase) model [40].

The bergeron model, is a single frequency model and will, therefore, only provide an accurate response for the chosen frequency [40]. The fault initiated travelling waves have a wide frequency spectrum. Therefore, since the frequency dependence of all parameters need to be examined the bergeron model will not be suitable for the given application.

The frequency dependent (mode) model and the frequency dependent (phase) model both incorporate the frequency dependence of all parameters [40]. For non transposed transmission lines the frequency dependent (phase) model should be used in order to produce accurate results [40]. However, for transmission lines that are transposed both models produce exactly the same results [40]. So in a bipole HVDC transmission line both the above line models will produce the same results.

The author has decided to use the frequency dependent (phase) model for the modelling of the HVDC transmission line. Details of the theory on which the above line models are based can be found in references [40-41].

4.4.1. Transmission Line Details

The protection system has been developed with the aim of protecting long HVDC transmission lines, therefore, a line length of 3500km, around the same length as the proposed Westcor HVDC line, has been chosen.

The Westcor HVDC system is expected to have a final voltage of 800kV [11]. It was not possible at this stage to consider a 800kV HVDC system case study because this technology is still under development [8] and, therefore, no suitably validated models exist. The 800kV voltage will only be introduced in the second phase of the project when each bipole system will be required to transmit more than 2GW [11]. The second phase is due for completion in 2020 [11]. The first phase will make use of a 500kV HVDC system voltage. The feasibility of this option has already been established and according to [11] the "500kV HVDC technology was the optimum transmission technology" for the first phase.

So the 500kV HVDC system under study here will be directly applicable to the first phase of the project. Since the HVDC system under consideration is a 500kV system, the standard 500kV bipole HVDC line tower used by ABB has been adopted. The transmission line conductors and configuration was then chosen to minimise power losses and voltage drops across the dc line.

The line configuration and tower dimensions are shown in Fig 4.5, where *C1* and *C2* represent the conductor on pole 1 and 2 respectively and *G1* and *G2* represent the two ground conductors. The line data for the pole and ground conductors is provided in Table 4.2.

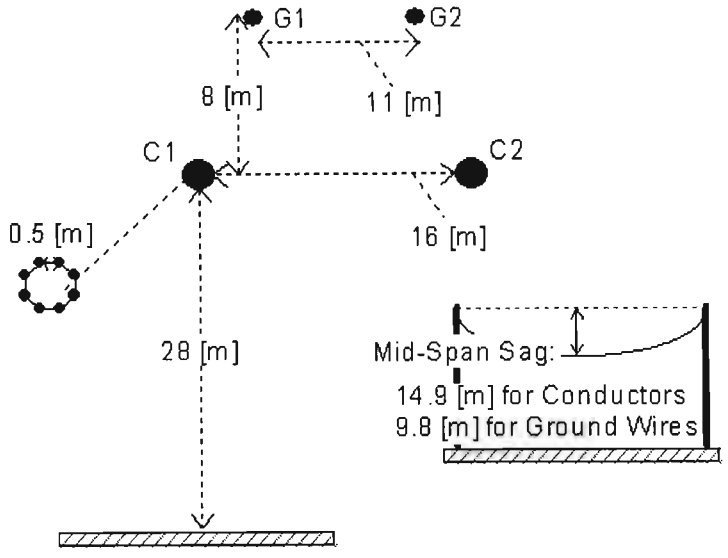

Fig 4.5. HVDC Transmission Line and Tower Configuration.

Table 4.2. HVDC Transmission Line Information

HVDC TRANSMISSION LINE INFORMATION		
	POLE	GROUND
Conductor Name	Joree	7/16 Steel
Conductor Radius	0.0239m	0.0057m
Conductor DC Resistance	0.0226Ω/km	3.34Ω/m
Conductor Sag	14.9m	9.8m
No of Conductors in a Bundle	8	N/A
Bundle Spacing	0.5m	N/A
Height Above Ground	28m	N/A
Height Pole Conductor	N/A	8m
Horizontal Distance between Conductors	16m	11m
Ground Resistivity Assumed	100 Ω.m	
Transmission Line Length	3500kms	
Line Operating Frequency	DC System therefore 0Hz	

4.4.2. PSCAD/EMTDC Modelling of a Transmission Line

Any transmission line adopting one of the travelling wave models available in EMTDC is represented in PSCAD with two components viz. a transmission line configuration component and a transmission line interface component. An illustration of this is shown in Fig 4.6.

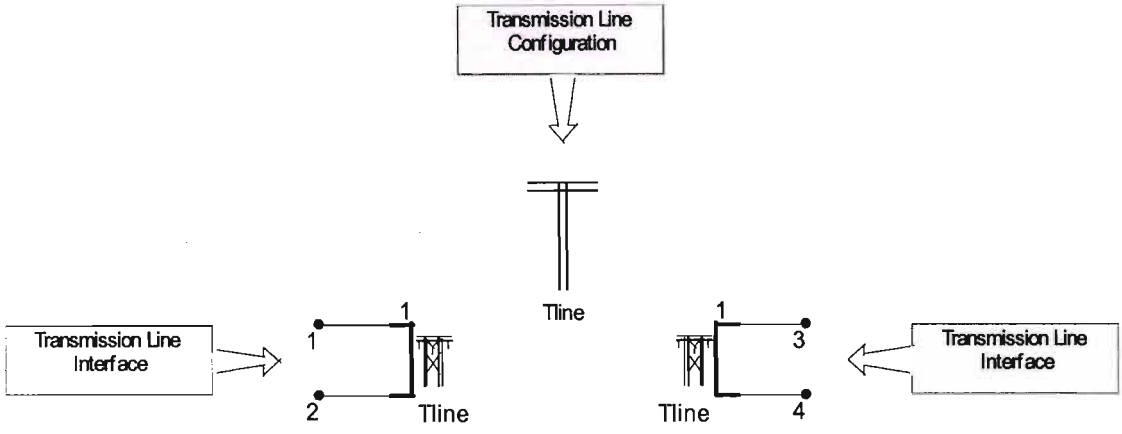

Fig 4.6. HVDC Transmission Line Modelling in PSCAD.

The transmission line configuration component represents the transmission line, this is where the transmission line is physically modelled using the data in Table 4.2 and one of the three line models described earlier. The transmission line interface provides the point of connection between the transmission line and the external components.

The Frequency Dependent (Phase) Line Model utilizes curve fitting to approximate the impedance and admittance at the various frequencies. Therefore, in order to model the line in EMTDC using the frequency dependent (Phase) model, the following parameters, as given in Table 4.3, need to be defined in addition to the information provided in Table 4.2.

Table 4.3. Frequency Dependent Model Parameters.

Frequency Dependent (Phase) Model Options	
Travel Time Interpolation:	On
Curve Fitting Starting Frequency:	0.5 [Hz]
Curve Fitting End Frequency:	1e6 [Hz]
Maximum Order of Fitting for YSurge:	20
Maximum Order of Fitting for Prop. Func.:	20
Maximum Fitting Error for YSurge:	0.2 [%]
Maximum Fitting Error for Prop. Func.:	0.2 [%]

A brief description of each of the above parameters and its significance is given below [40-41].

- ***Travel Time Interpolation*** – the calculated travel time of the line will not be an exact integer multiple of the time step. Not interpolating the travel time can introduce errors by artificially increasing or decreasing the effective line length. Interpolating the travel time will give the correct effective length and should be used especially if the line is short.

- ***Curve Fitting Starting Frequency*** – This parameter sets the starting frequency for curve fitting. The starting frequency affects the shunt conductance of the line and must be chosen carefully [40]. It should be noted that the choice of starting frequency will also affect the accuracy of the curve fitting of the surge impedance. The accuracy is affected because "the maximum error is specified as a percentage of the maximum, and the surge impedance will get larger as the starting frequency is lowered" [40].

- ***Curve Fitting End Frequency*** – Selects the end frequency for curve fitting. This frequency may be beyond the highest frequency, which can be represented with the chosen time step as the program will truncate the curve fitting data to preserve efficiency.

- ***Maximum Order of Fitting Settings*** – This parameter sets the maximum number of poles to be used for determining the surge admittance (YSurge) and propagation function (Prop.Func). Normally the Transmission Line Constants program will iterate and continuously increase the order of the curve-fitted waveforms until the error is below the Maximum Fitting Error (see below). This setting is only applicable in real-time applications where, there may only be enough time to calculate a lower-order approximation.

- ***Maximum Fitting Error for YSurge*** – This parameter sets the maximum fitting error for the surge impedance.

- ***Maximum Fitting Error for Prop.Func*** – This parameter sets the maximum fitting error for the propagation function.

The accuracy of the line model will depend on the choice of the above parameters. ABB has used field test measurements made on existing HVDC systems to determine the best values for the above curve fitting parameters [12]. The curve fitting parameter values as suggested in [12] for the standard 500kV configuration is given in Table 4.3. The author has, therefore, opted to use the parameter values as suggested in [12].

EMTDC creates a log file which shows any warnings and errors produced by the line constants program, and also indicates the final accuracy of the curve fitting process. The user can inspect this file in order to ensure that the required level of accuracy has been achieved. Upon inspection of this file for the various simulations performed, it was found that the number of poles for curve fitting of the surge impedance and propagation function never exceeded 9 and 15 respectively. Also the maximum curve fitting error for both the surge impedance and propagation function as calculated by the line constants program was always below the specified error of 0.2%, indicating that the required curve fitting accuracy was achieved.

4.4.3. Modelling the Proposed HVDC Transmission Line in PSCAD

This section describes how the proposed line in 4.4.1 was modelled in PSCAD. Firstly note that we are required to place faults along the transmission line. In order to achieve this, the transmission line was modelled as two sections. This allowed faults to be simulated anywhere on the line by simply varying the line lengths of the two sections.

Fig 4.7 shows the complete line model together with all the auxiliary components required for simulating fault conditions. In Fig 4.7, the two transmission line sections are connected to each other externally via the transmission line interface component. This external connection provided the necessary points (*SCBP1* and *SCBP2*) for the various faults to be applied. The distance to this external connection is simply varied by varying the line lengths of the two sections as explained earlier.

Pole to ground faults were simulated by the use of single phase fault components *FAULTP1* and *FAULTP2* in series with a variable dc fault resistance component *Rfltx*. The DC fault resistance was controlled via the *DC Fault Resistance* control shown at the bottom of Fig 4.7. *FAULTP1* and *FAULTP2* are controlled by a *Timed Fault Logic* control. The above control allowed the user to specify the time that the specific fault should be applied as well as the duration of the fault. When *FAULTP1* is activated, node *SCBP1* is connected to ground via the fault resistance. This resulted in a pole 1 (positive pole) to ground fault. Similarly when *FAULTP2* is activated a pole 2 (negative pole) to ground fault resulted.

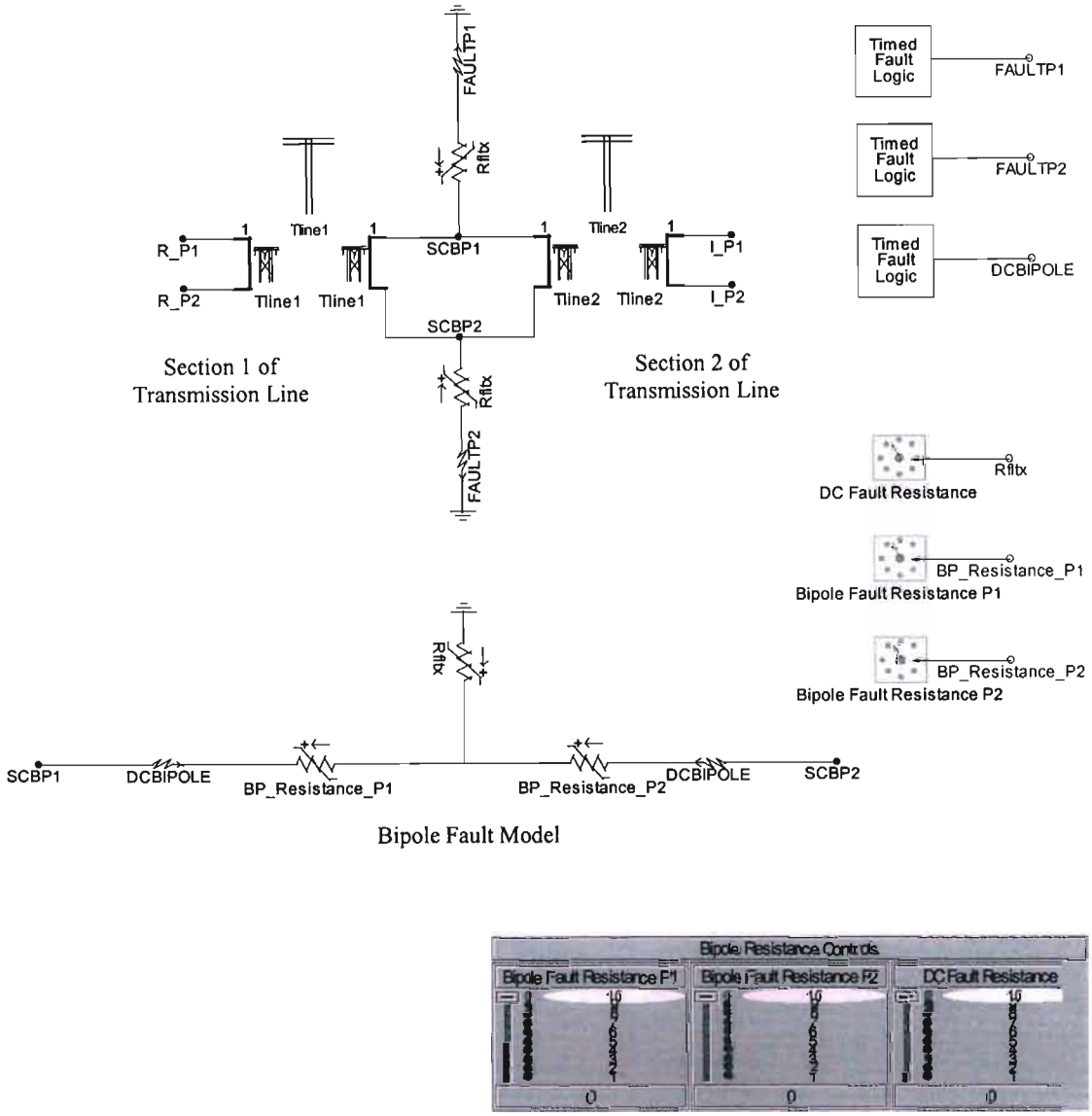

Bipole Fault Model

Fig 4.7. Complete Line Model with Auxiliary Components Required for Fault Simulation.

The model used to simulate bipole faults is also shown in Fig 4.7. Note that in PSCAD, two or more nodes can be connected to each other without any physical connection by giving all the nodes to be connected together the same name. Therefore, note that the bipole model is actually connected across the transmission line interface component through nodes *SCBP1* and *SCBP2*.

A bipole fault is simulated by activating the single phase fault component *DCBIPOLE*, which is also controlled by a *Timed Fault Logic* component. The fault resistances between the poles are varied by the *Bipole Fault Resistance P1* and *Bipole*

Fault Resistance P2 controls and the pole to ground fault resistance is again controlled by the *DC Fault Resistance* control. This model also allows unbalanced pole to pole to ground faults to be modelled by using different fault resistance values for the two poles.

4.4.4. Incorporating the Line Model into HVDC System Model

In Fig 4.7 the nodes *R_P1* and *R_P2* indicate the points to be connected to the rectifier station on poles 1 and 2 respectively. Similarly nodes *I_P1* and *I_P2* indicate the points to be connected to inverter station on poles 1 and 2 respectively.

The line model described above can therefore be easily incorporated into the HVDC system by first, simply removing the existing T network model of the line shown in Fig 4.4 and then renaming the open points caused by the removal of this T network models with the appropriate node name viz. *R_P1*, *R_P2*, *I_P1* or *I_P2* to signify an electrical connection. This is illustrated in Fig 4.8.

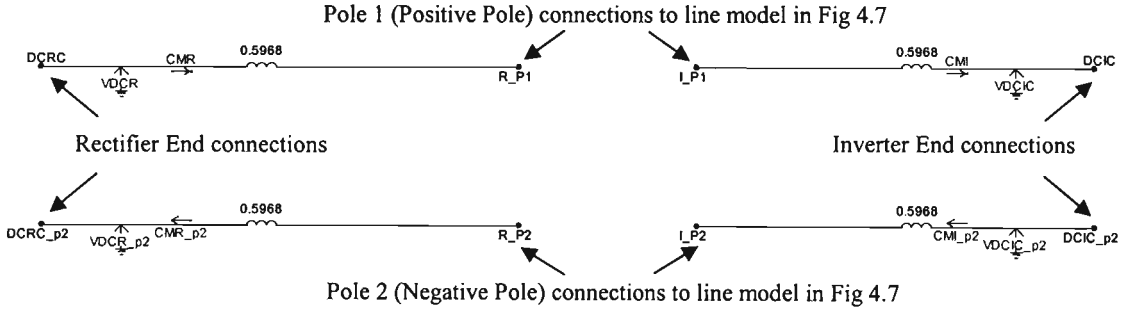

Fig 4.8. Incorporating the Proposed Line Model into the HVDC System Model.

In Fig 4.8 the nodes *DCRC* and *DCRC_p2* are connected to the rectifier terminals on poles 1 and 2 respectively. Nodes *DCIC* and *DCIC_p2* are connected to the inverter terminals on poles 1 and 2 respectively. Fig 4.8 indicates that the line model in Fig 4.7 is now physically connected to HVDC system model on poles 1 and 2 to the rectifier and inverter station via the line reactors at either end, with nodes with the same names been connected.

The HVDC system operating states were then checked to ensure that the system is operating within acceptable limits with the inclusion of the new line model representing the 3500km transmission line.

Table 4.4. Comparison of Steady State Operating Conditions.

HVDC SYSTEM STEADY STATE OPERATING CONDITIONS		
	Initial System	Modified System
Average DC Voltage	1.03 pu	1.025 pu
Operating Alpha Angle	20.1 degrees	19.2 degrees
Operating Gamma Angle	29.8 degrees	29.8 degrees
DC Current/Pole	1000A	1000A
Power Transfer/Pole	500MW	500MW

Table 4.4 indicates that both the initial and modified systems operate with very similar steady state conditions. The results in Table 4.4, therefore, confirm that the modified system with the new line model is operating within acceptable voltage and firing angle (alpha and gamma) limits.

4.5. DC Side Filters

DC side filter are used to filter out the harmonics caused be AC/DC conversion process. These harmonics do not affect the HVDC system significantly in anyway, however, when in the vicinity of telecommunication lines, the harmonic coupling with the telecommunication causes interference in these telecommunication lines.

DC Filters are therefore normally designed to ensure that the interference caused by the harmonic currents on the telecommunication line is minimal. In order to include the effects of harmonic filtering on the protection system, the author implemented a 12^{th} harmonic and a high pass filter in the HVDC System. Details of these filters are given in Fig 4.9.

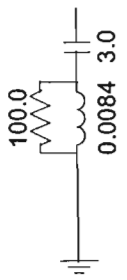

High Pass Filter with R = 100Ω,
C = 3uF and L = 0.0084H

12th Harmonic Filter with R = 6Ω,
C = 6uF and L = 0.1675H

Fig 4.9. High Pass and 12th Harmonic DC Filters.

The DC Filter implementation for the positive pole is shown in Fig 4.10. The implementation in the negative pole was exactly the same.

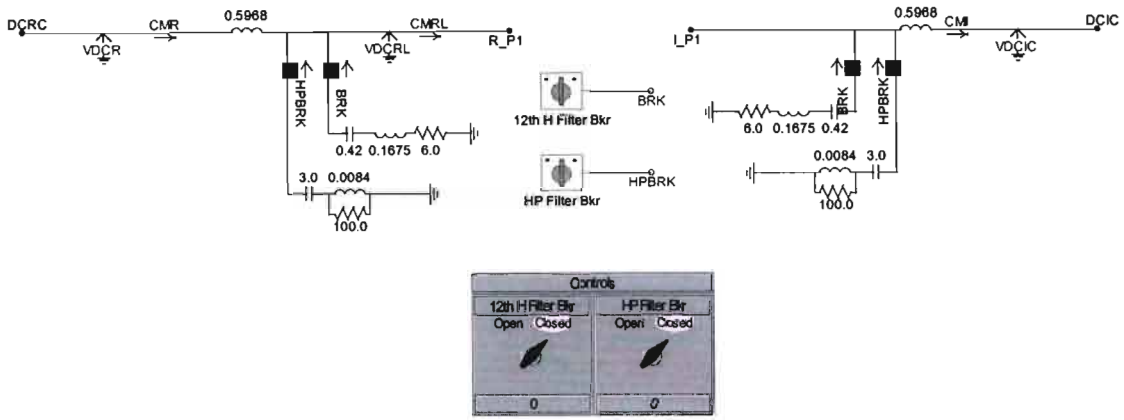

Fig 4.10. Implementation of DC Filters on the Positive Pole.

Note that the DC Filters have been connected through circuit breakers *BRK* and *HPBRK* representing the 12th harmonic filter breaker and high pass filter breaker respectively. Circuit breakers have been used so that the filters can be switched in and out at any time to evaluate the response of the protection system with and without DC filters. The circuit breakers are controlled by the controls *12 H Filter Bkr* and *HP Filter Bkr* shown at the bottom of Fig 4.10.

A voltage measuring component *VDCRL* and a current measuring component *CMRL* has also been added to measure the positive pole dc line voltage and current respectively. The voltage measuring component *VDCRL_p2* and a current measuring component *CMRL_p2* have also been included on the negative pole to measure the

negative dc line voltage and current respectively. These measurements are required in order to calculate the modal quantities, as defined in 2.2.6, that are required for calculating the relaying signals.

4.6. Protection Modelling

The purpose of this section is to detail how the quantities required by the protection system were calculated from the measured quantities using EMTDC.

4.6.1. Calculation of Modal Voltages and Currents

The modal quantities are calculated from the actual quantities using equations (29) to (32). The implementation of these equations in PSCAD was accomplished by the use of summing junctions and divider blocks as shown in Fig 4.11.

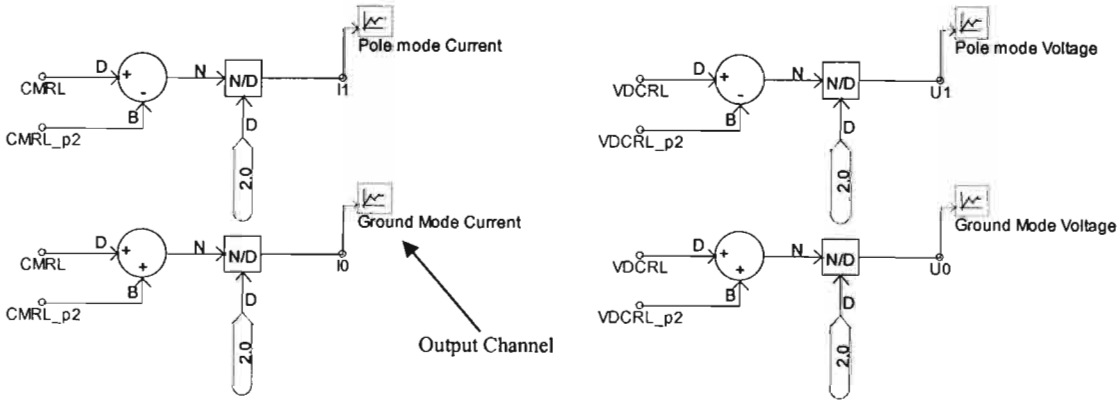

Fig 4.11. Calculation of Modal Voltages and Currents.

The signals *CMRL*, *CMRL_p2*, *VDCRL* and *VDCRL_p2* are the measured dc line currents and voltages as defined in 4.4 above. The calculated modal quantities I_1, I_0, U_1 and U_0 are then sent through an output channel to be plotted for analysis as shown in Fig 4.11.

4.6.2. Protection Starter Modelling

In order to model the protection starter as well as calculate the relay signals, the change in the pole mode current ΔI_l and the change in pole mode voltage ΔU_l need to be first determined. In order to determine ΔI_l and ΔU_l the pole mode voltage and currents need to be shifted by at least 1 sampling interval. Fig 4.12 indicates how this was accomplished using the delay function in PSCAD.

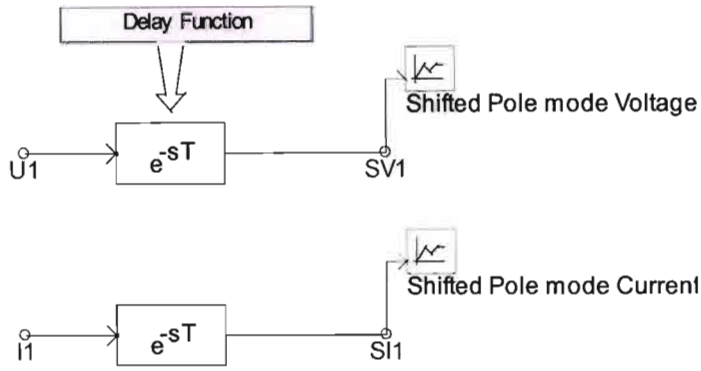

Fig 4.12. Time Shifting of Modal Voltages and Currents.

The delay function was set to one sample interval and, therefore, output signals *SV1* and *SI1* represented the pole mode voltage and pole mode current, shifted by one time step, respectively. Now ΔI_l was determined by subtracting *SI1* from *I1* and similarly ΔU_l was determined by subtracting *SV1* from *U1*. Once ΔI_l and ΔU_l were calculated, they were then multiplied together to form the protection starter as shown in Fig 4.13.

The starter values were normalized based on the dc voltage level and dc current. Here the normalizing value is fixed and represented by *normalize* in Fig 4.13. However, if the HVDC system can be operated at different voltage and power levels, the normalizing value should be obtained from the measured voltages and currents. Note that the normalizing value is made negative. The above has been done in order to invert the calculated starter values so that the setting comparator can be set using positive values instead of negative values.

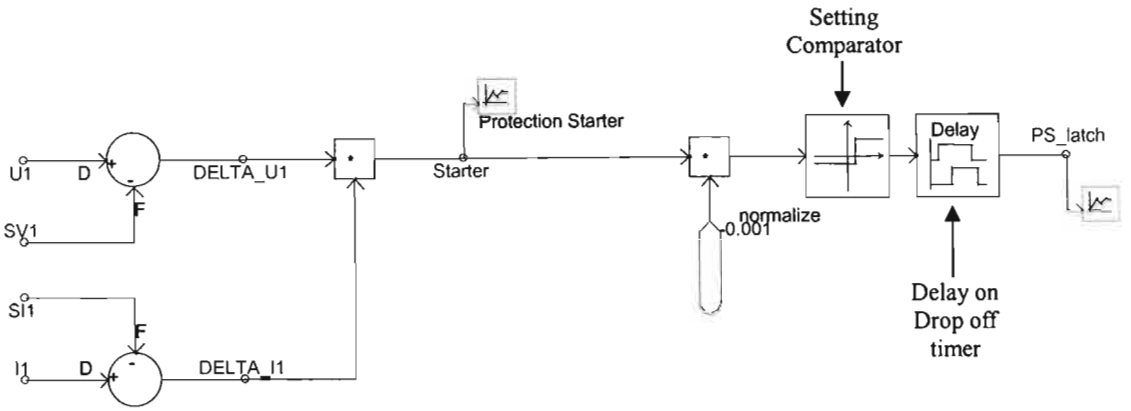

Fig 4.13. Protection Starter Implementation.

Once the normalized starter value exceeds the setting comparator value the protection is activated and the starter is latched in by a delay on drop off timer. This timer is set equal to the duration of the fault, ensuring that the starter remains activated for the complete duration of the fault.

The timer is only used for simulation purposes. In practice the starter will be latched and reset only when the dc voltage returns to a certain percentage of the prefault voltage for a predefined period of time, signifying that the fault has been cleared.

4.6.3. Calculation of Relaying Signals

The relaying signals were used by the cross-correlation function to determine the distance to fault. In order to calculate the relaying signals the surge impedance of the pole mode needed to be calculated. The line constants program in EMTDC was used to calculate this surge impedance as well as the other line parameters for the proposed line in 4.4.1.

The line constants program computed the values of the above parameters for a single frequency. Since, as explained in 3.2.5, the pole mode surge impedance and propagation velocity is almost constant, for frequencies above 20Hz, the AC system frequency of 50Hz was used in the line constants program. Fig 4.14 shows the output of the line constants program. The line constants program calculates both the pole and

ground mode quantities. The ground mode quantities are reflected on the left hand side while the pole mode quantities are reflected on the right hand side.

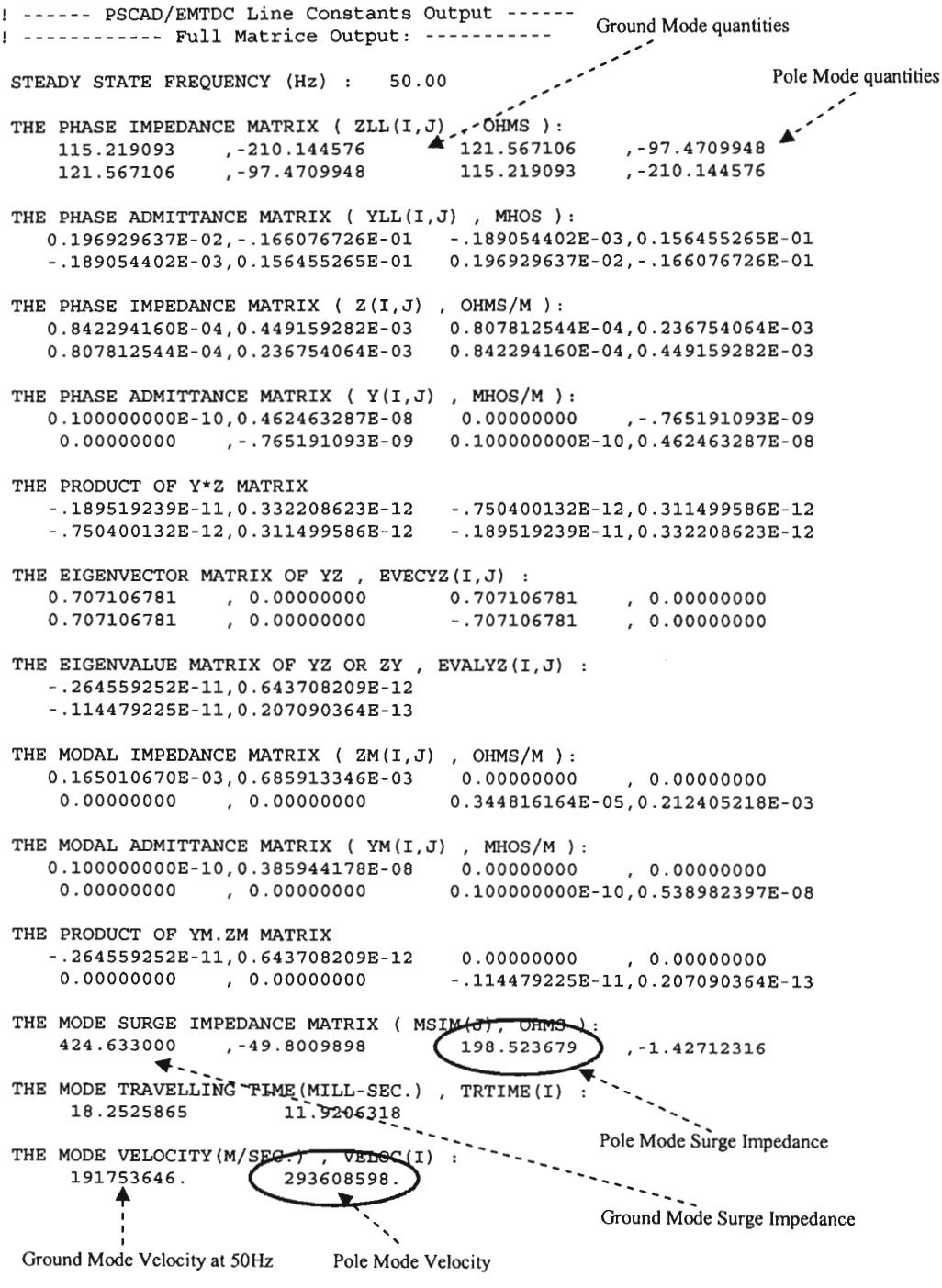

Fig 4.14. Output of Line Constants Program.

The calculated pole velocity of 293.61km/ms was used to calculate the distance to fault. The calculated pole surge impedance of 198.52Ω returned by the line constants program was used in the calculation of the relaying signals.

Note that the relaying signals were calculated from instantaneous changes in the voltage and current quantities. Fig 4.15 indicates how the per unit instantaneous changes in the pole mode voltage *DELTA_U1_pu* and the current *DELTA_I1_pu* were calculated.

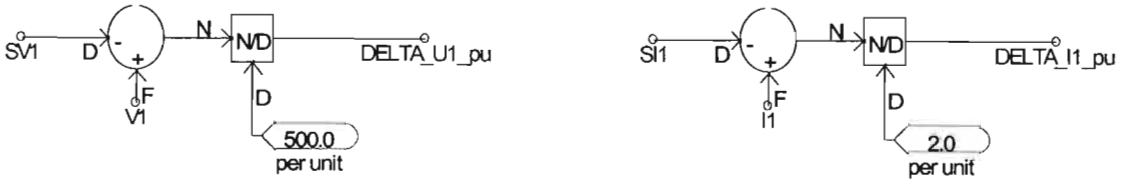

Fig 4.15. Calculation of DELTA_U1_pu and DELTA_I1_pu.

Now using *DELTA_U1_pu* and *DELTA_I1_pu* calculated above, the instantaneous value of the relaying signals S_F and S_B can be calculated using (35) and (36) respectively. The PSCAD implementation of these equations is shown in Fig 4.16 below.

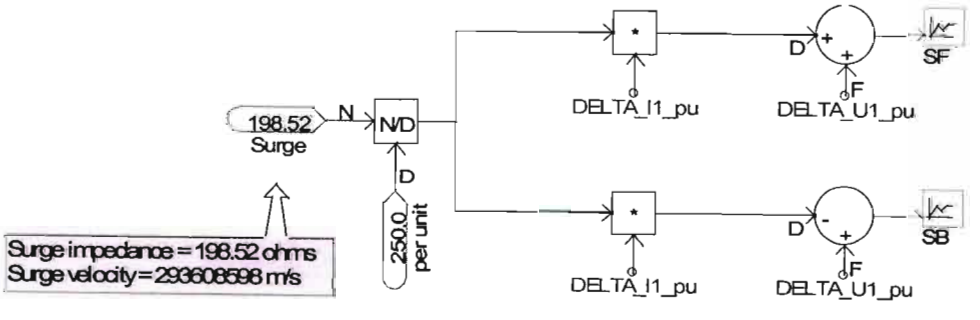

Fig 4.16. Calculation of Relaying Signals S_F and S_B.

Note that the surge impedance must also be in per unit as the signals, *DELTA_U1_pu* and *DELTA_I1_pu* are per unit values, therefore, the surge impedance is divided by 250Ω in Fig 4.16. This base value is calculated by simply dividing the square of the dc voltage by the rated power. The relaying signals were then sent to output channels so that they could be plotted and the data exported into Matlab.

4.6.4. Protection System Algorithm

The previous sections up to now have illustrated how the various quantities required by the protection system were determined using EMTDC. The protection system itself, however, has been implemented in Matlab with the aid of M files.

Matlab is a powerful high-performance technical computing program that can be used, among a multitude of other functions, to calculate or write M files to calculate a host of mathematical functions. M files are similar to normal programs written with languages like C++ or any other programming language. These M files can be written in any text editor and contain sets of instructions that Matlab must execute.

The protection system algorithm has been coded by the author in an M file called "protectionsystem.m". The code for the above M file can be found in Appendix A. The protection system requires various input parameters. Some of these parameters are the quantities determined during the EMTDC simulation.

The quantities required from the EMTDC simulation are the protection starter latch signal, *PS_latch* as shown in Fig 4.13. and the relaying signals S_F and S_B. The *PS_latch* signal is required to determine when and if the protection starter was activated. The *PS_latch* signal will be logic 0 under normal circumstances and only changes to logic 1 when the protection starter has been activated. The relaying signals are required to calculate the standard and auxiliary cross-correlation functions. Therefore, the above three signals have to be exported from EMTDC and imported into Matlab. The above mentioned import and export process is the only manual process involved. All other processes are automated and require no human intervention.

The other input parameters required by the protection system are general setting parameters that will vary based on the application. These parameters are listed below and must be specified by the user for the given application.

- *numlags* – number of time lags for which the correlation process must be calculated. This is the correlation process duration setting as given in 5.2. (1400lags = 28ms).
- *v* – propagation velocity in m/s. (293608598m/s). Determined by the line constants program in Fig 4.14.
- *ds* – distance protection setting in km for up to which instantaneous tripping is allowed. (80% of 3500km = 2800km) – See Fig 3.11.
- *pre* – number of prefault samples required. (25samples = 0.5ms). See 5.2 for details.
- *post* – number of postfault samples required. (150 samples = 3ms). See 5.2 for details.

The value in brackets represent the parameter values that have been used for the case under study in this work. The significance of the above parameters as well as why the above values have been chosen are discussed in chapters 3 through to 5.

The M file "protectionsystem.m" calls other M files, all of which have been written by the author, in order to perform specific tasks. Once the M file "protectionsystem.m" has been run, it calls the M file "datainput.m". The purpose of the M file "datainput.m" is to firstly determine whether the protection starter has been activated or not. If the protection starter has not been activated the program will report this fact and break the program as the protection system cannot be activated unless the protection starter has been activated. If on the other hand the protection starter has been activated, the M file "datainput.m" will determine the section of S_F to be used as the template based on the input parameters *pre* and *post*. The above mentioned M file will then also use the input parameters *pre*, *post* and *numlags* to determine the sections of S_B and S_F that will be used to calculate the standard and auxiliary cross-correlation functions respectively.

Once the above process is complete the protection system calls another M file "comcorr.m" in order to calculate and plot the cross-correlation functions. Once the cross-correlation functions have been calculated, the M file "protectionsystem.m" is then able to determine were the maximum peak occurs in the cross-correlation

functions. Note the protection algorithm looks for the maximum peak value in the correlation functions and not the global maximum. The above is done because the global maximum in the standard cross-correlation function will always occur at zero time lags.

In order to explain why the above occurs, note that the first section of S_F following the activation of the protection starter is inverted and taken as the template. Also note that S_F is due to the reflection of S_B at the relaying point. Since the discontinuity is at the relaying point, S_F and S_B change simultaneously and have opposite polarities. Therefore, the template and S_B at zero time lags will have a very similar shape and only differ in magnitude due to the scaling caused by the reflection coefficient at the discontinuity. The returning wave from the fault on the other hand will suffer attenuation and distortion as it propagates along the line and will be further scaled by the reflection coefficient at the fault. The reflection coefficient at the fault as already discussed previously can be low even for solid ground faults. Therefore, the correlation between the template and S_B at zero time lags is greater than the correlation between the template and the returning fault initiated travelling wave. It is for the above mentioned reason that the global maximum occurs at zero time lags.

In order to ensure that the maximum peak in the correlation function is located and not the global maximum, the protection algorithm checks the following before declaring a maximum peak value :

1. Is the value immediately before the selected value less than the selected value.
2. Is the value immediately after the selected value less than the selected value.
3. Is the selected value greater than all previous peak values.

Only if all 3 of the above conditions are true will the system consider the selected value to be the maximum peak value.

The M file "protectionsystem.m" then uses the results from the cross-correlation functions to determine the fault location. Once the fault location or locations have been determined, the M file "protectionsystem.m" will run through a list of various conditions (see M file for these conditions) and report the following:

1. Whether a fault was detected or not.
2. Fault location.
3. Whether the fault was cleared instantaneously or not.
4. Whether the fault was a high resistance fault.

All the M files written by the author in order to implement the protection system in Matlab are included in Appendix A.

4.7. External Fault Modelling

External faults are faults that occur outside the transmission line either behind the relaying point or beyond the transmission line. These faults can occur on the DC side or AC side of the system.

The faults on the DC side of the system were modelled using the single phase fault component in a similar manner as shown in Fig 4.7. AC side faults were modelled using the three phase fault model shown in Fig 4.17 below. The points A, B and C are connected to the respective phases at the location to be faulted.

The type of fault (e.g. B-C phase fault) and the fault resistances are inputted directly into the fault model. The time of fault application and duration of the fault is controlled by the *Timed Fault Logic* component.

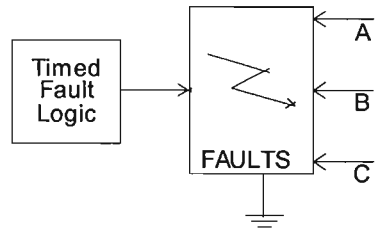

Fig 4.17. AC System Fault Modelling.

The complete model of the modified HVDC system including all fault modelling and well as the model of all the protection elements can be found in Appendix B.

4.8. Simulation Procedure

The simulation procedure was as follows:

- Internal or External faults were applied in EMTDC at some time *t*.
- The signals *PS_latch*, S_F and S_B were then exported from EMTDC and imported into Matlab.
- In Matlab, the M file "protectionsystem.m" was run using relevant input parameters.

The main aim of the above simulations was to assess the accuracy of the protection algorithm for the various scenarios. The final assessment was based on the simulation results.

Chapter 5: Simulation Results and Discussion

The objective of this chapter is to present and discuss the results obtained from the simulations conducted in order to evaluate the performance of the proposed protection system.

5.1. Startup and Steady State Operating Conditions

The startup and steady state operating condition of the modified Bipolar HVDC system is presented in this section. Fig 5.1 shows the DC voltages and currents from startup to steady state for both poles 1 and 2.

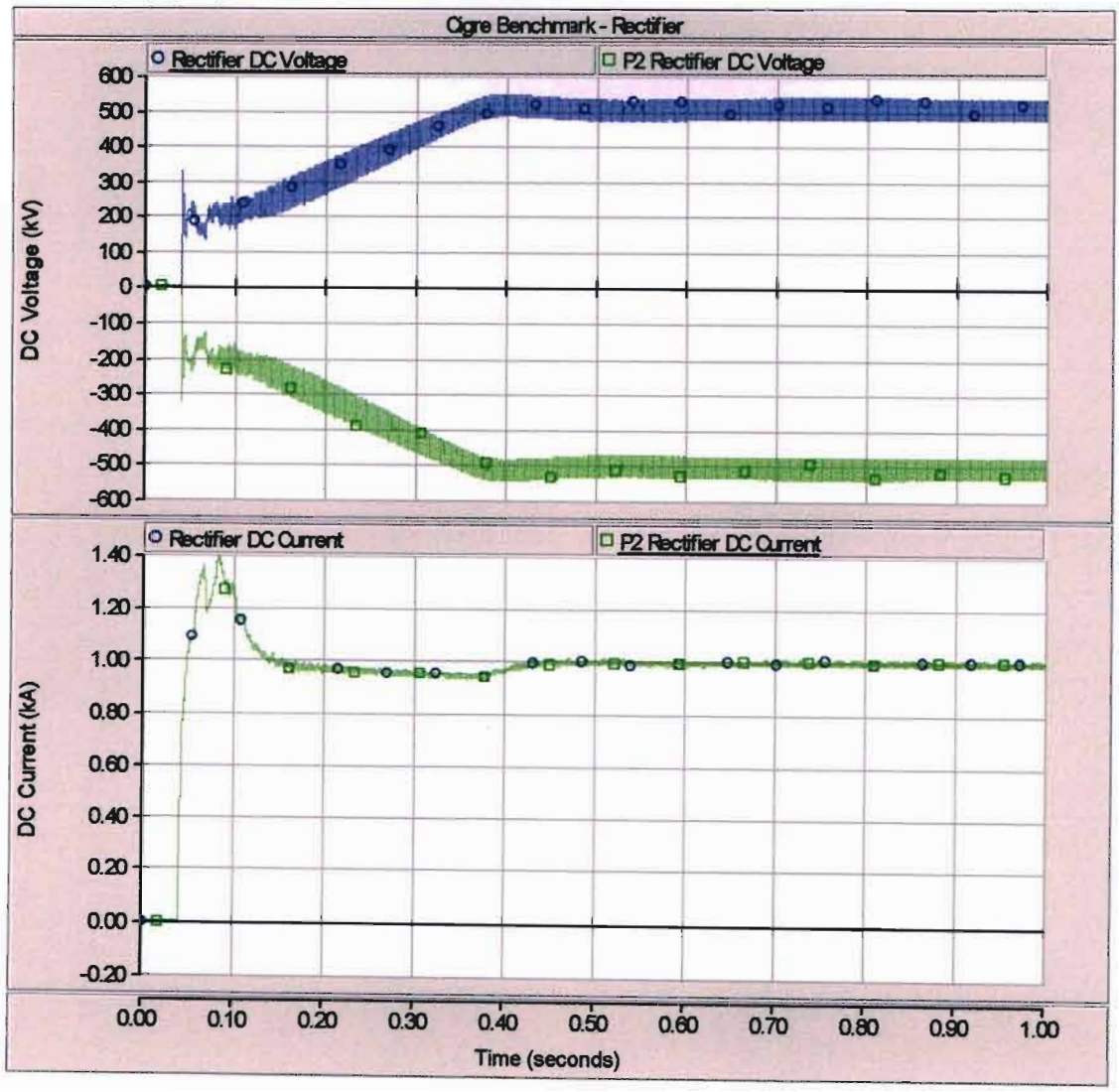

Fig 5.1. Startup and Steady State Operating DC Voltage and Current.

With reference to Fig 5.1, one can consider the system to be in steady state from 0.5s onwards. Averaging the DC voltage from 0.5s onwards reveals an average steady operating DC Pole voltage of ± 512.5kV or ± 1.025pu. The steady state dc current is 1000A or 0.5pu (assuming a 2kA base current) which gives a power transfer per pole of 500MW or 0.5pu (assuming a 1000MW base power) as shown in Fig 5.2.

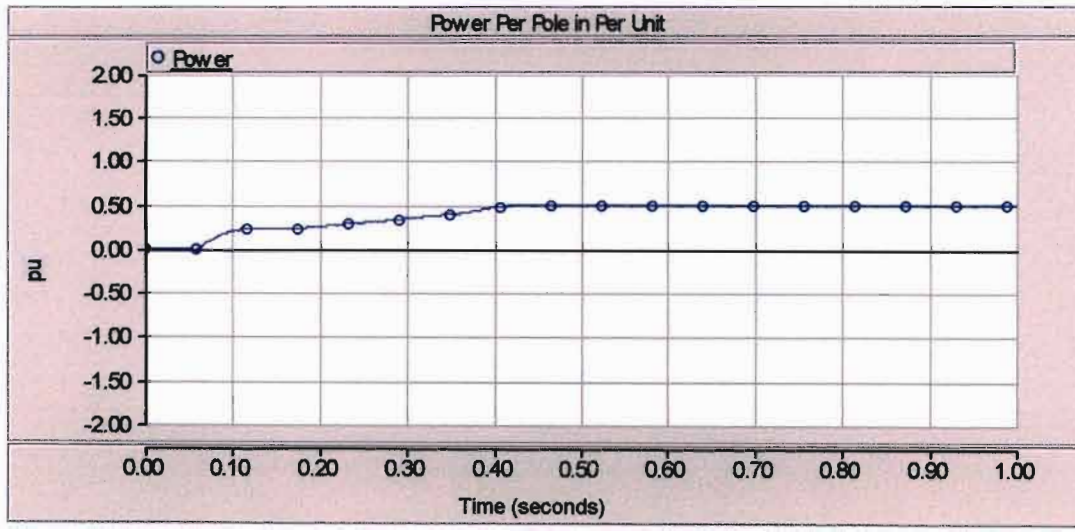

Fig 5.2. Power Transfer per Pole in pu.

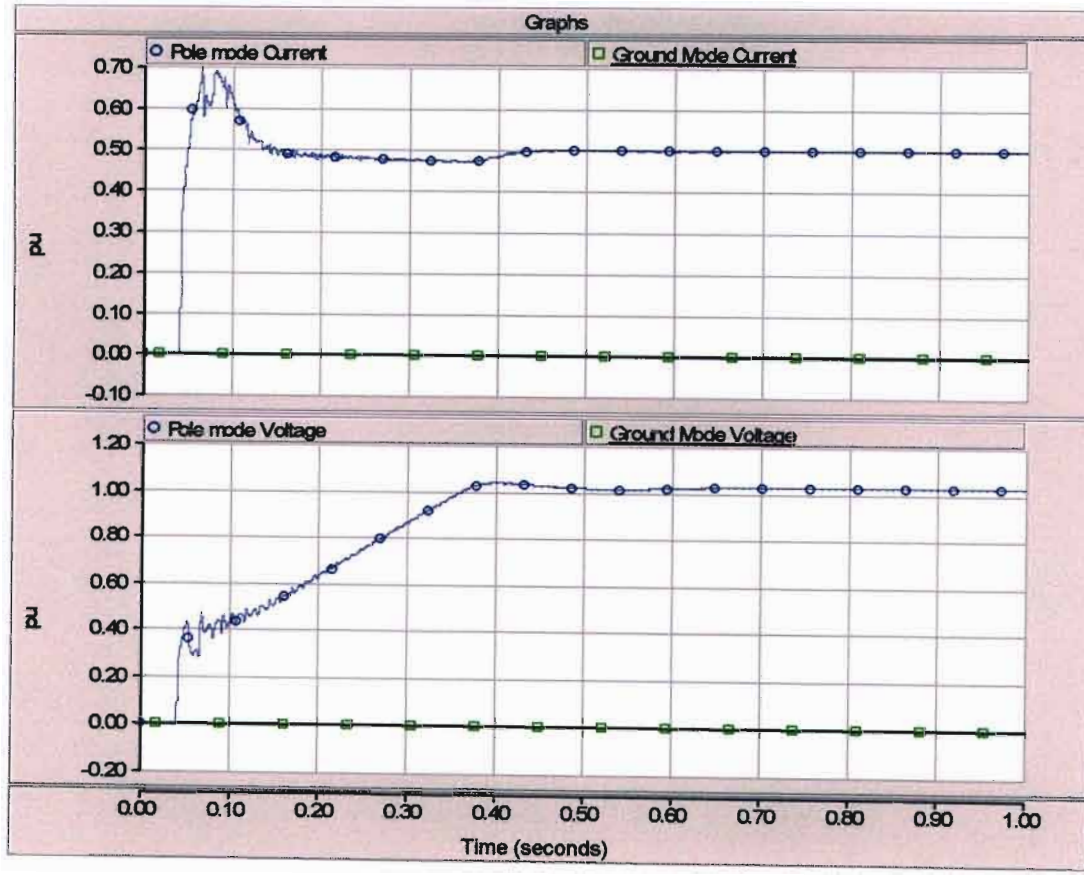

Fig 5.3. Modal Line Voltages and Currents.

Fig 5.3 shows the calculated modal line voltages and currents. As expected, there are no ground mode quantities present as the system is balanced and, therefore, the pole mode quantities are equal to the actual dc line quantities. When there is current flow in the ground due to a fault, the polarity of the ground mode wave will be used to determine the faulted pole while the pole mode quantities will be used to develop the relaying signals that are used to determine the distance to fault.

Fig 5.4 shows the calculated relaying signals from the positive mode line quantities. During startup the relaying signals have very small magnitudes that approach almost zero as the steady state operating condition is approached. The relaying signals can never be exactly zero because of the continuous switching operations of the converters.

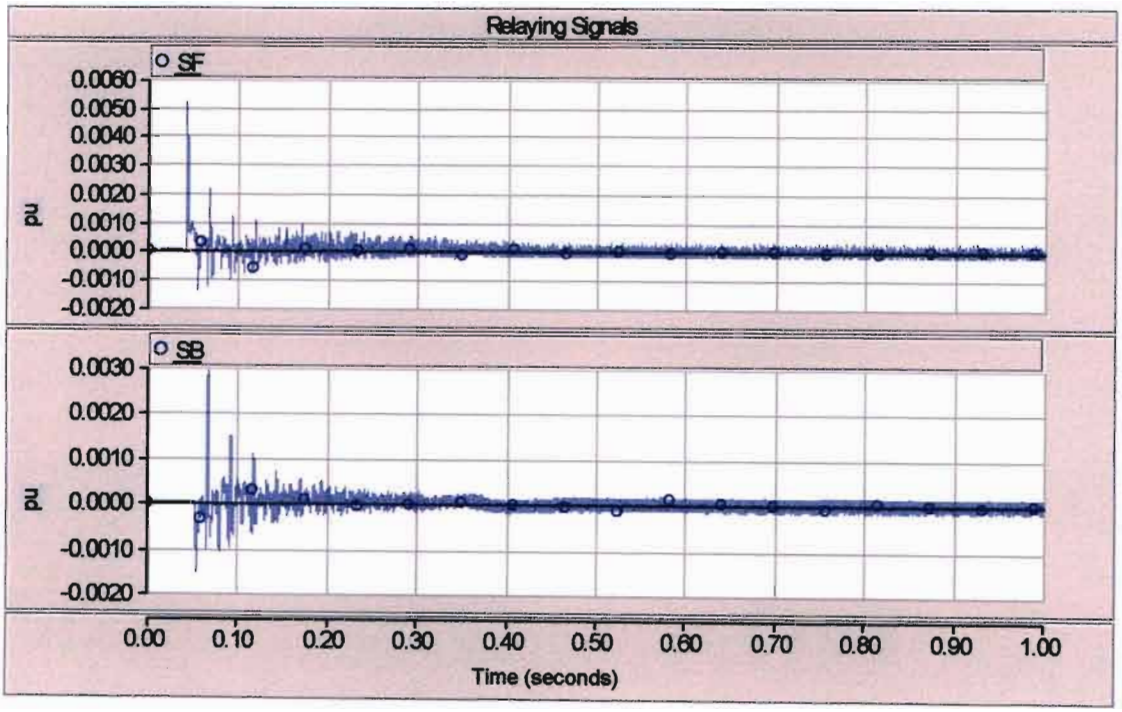

Fig 5.4. Relaying Signal from Startup to Steady State.

Fig 5.5 shows the calculated normalized protection starter values from startup through to steady state. It can be seen from Fig 5.5 that small negative values appear during startup. The reason for these negative values has been explained in 3.2.4 and the protection starter threshold must, therefore, be set so that the protection system is not started for these negative values. The advantage of using the dc line voltage and

current to normalize the starter values is that similar results as those shown in Fig 5.5 can be obtained for all the different possible operating conditions.

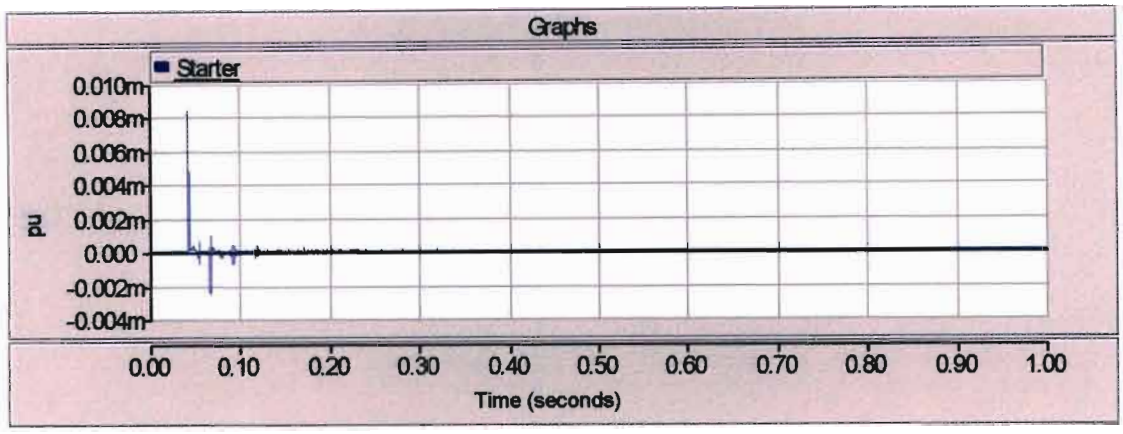

Fig 5.5. Protection Starter Values from Startup to Steady State.

5.2. Protection Starter and Correlation Settings

In Fig 5.5, the minimum recorded value during startup was -0.0025E-3 pu. In order to ensure that the protection system will not be activated for startup conditions a safety margin must be allowed between the recorded minimum value and the starter threshold setting. As a first pass a safety margin of 10 times the minimum recorded value was used. Noting that the starter value is inverted when it is normalized a threshold setting of 0.025E-3 pu was thus adopted.

In terms of the cross-correlation settings, both the duration of the CCF and the template length must be determined. In order to determine the duration we need to calculate the time required for the pole mode wave to travel the length of the line. This time was calculated to be 11.92ms in Fig 4.14 by the line constants program. Note that the travelling wave will only return to the relay after a time equal to twice the fault distance. Thus for the case with the fault at the end of the line, the travelling wave will only return after a 23.84ms (2*11.92ms).

The duration of the CCF must be set to this time plus some safety margin to allow for possible errors. These errors include possible transducer errors as well as errors introduced by the sampling process. Note the CCF duration directly influences the

protection operating time and must, therefore, be chosen carefully to provide the required safety margin without unduly increasing the operating time. A duration setting of 28ms which allows for a 17.5% error in the correlation function has been adopted.

As the length of the template S_F is increased, the correlation function's ability to distinguish between reflections from the fault and reflection from a remote discontinuity reduces. On the other hand reducing the size of the template increases the risk of maloperation due to non fault transients and noise [32]. It is mentioned in [32] that a good first estimate for the template size would be the time required for the travelling wave to travel 1/4 the distance of the line. The author has therefore decided to adopt a template length of 3.5ms. This template will contain 0.5ms of data prior to the fault to ensure that the entire wave is captured. Therefore, the template contains 0.5ms of prefault data and 3ms of postfault data.

5.3. Sampling Interval

The relaying signals are continuously sampled. This information will be used by the CCF in determining the distance to fault when the protection starter threshold is exceeded. The higher this sampling rate the more accurate the calculated distance to fault.

On the other hand the hardware requirements increase with increasing sampling rates. The higher the sampling rate, the greater the number of samples and hence the greater the number of calculations that must be performed. This means that the processing time is also increased. The author has decided to adopt a sampling frequency of 50 kHz for this work. The sampling frequency of 50kHz was chosen because it was the largest sampling rate that could be utilized based on the processing power and storage capacity of the computer on which the simulations were run.

5.4. Fault Simulations

5.4.1. Pole to Ground Faults

Consider a positive pole to ground fault (PP-G) at time t equal to 0.85s, located 350kms (10% of line length) from the relaying point. Fig 5.6 shows the modal voltages and currents.

Notice that both the pole and the ground mode current have the same polarity with the initial changes being positive. Therefore, the fault is clearly located on the positive pole. Fig 5.7 indicates that the value of the calculated starter (0.0359) exceeds the starter threshold setting. The starter will, therefore, be latched as shown in Fig 5.8, for the duration of the fault and the CCF will be initiated in order to determine the distance to fault.

Fig 5.8 also shows the initial values of the relaying signals. The relaying signal data and the starter latch signal data was then exported from EMTDC and imported into Matlab. The M file, "protectionsystem.m", written by the author was then run to determine the protection system's response to the above fault. The output of the standard CCF (SCCF) is shown in Fig 5.9.

Note that in Fig 5.9. the global maximum occurs at zero time lags. The reason for the above has been explained in 4.6.4. Also as explained in 4.6.4. the protection system looks for the maximum peak value in the correlation function and not the global maximum. Therefore, when we talk of a "maximum" in the CCF we are referring to the maximum peak value and not the global maximum.

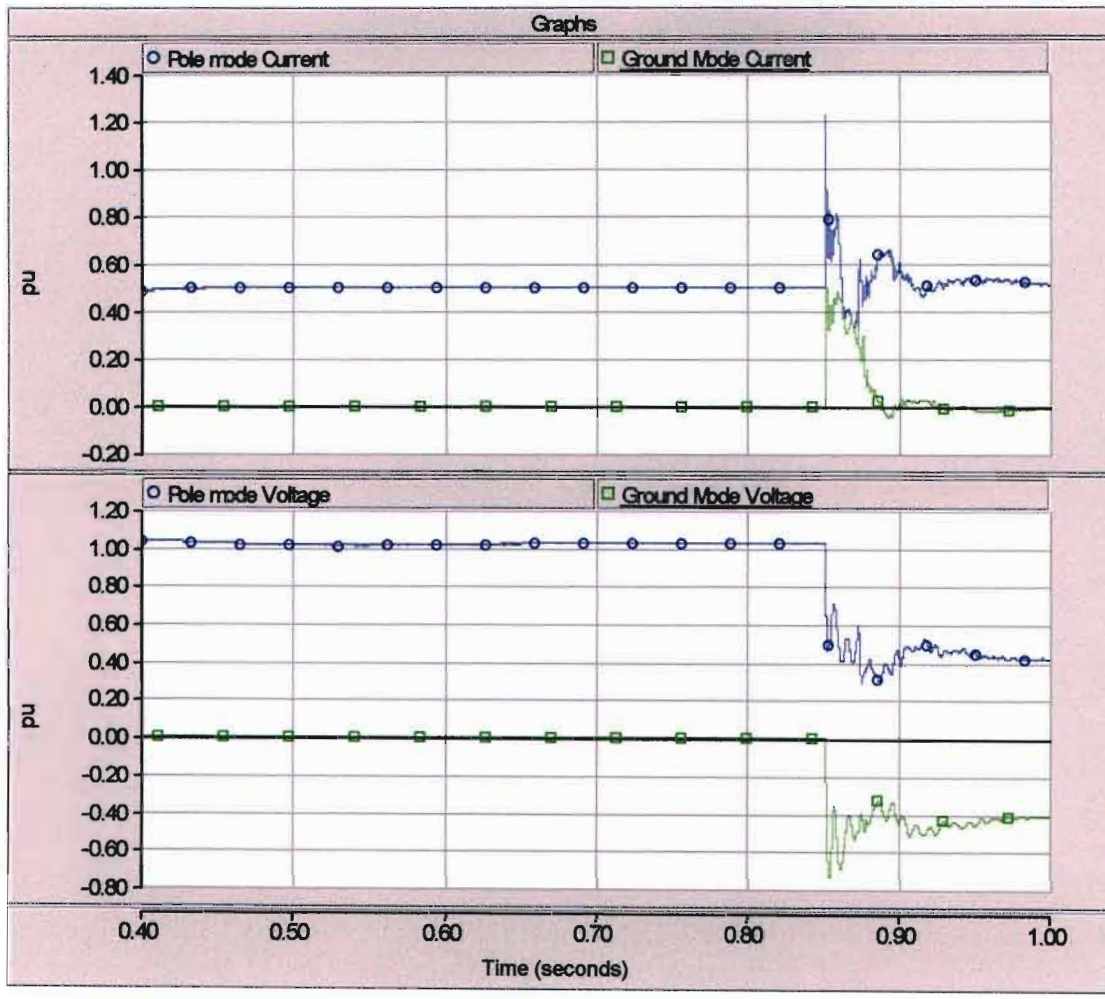

Fig 5.6. Modal Voltages and Currents for PP-G Fault Located 350kms from Relaying Point.

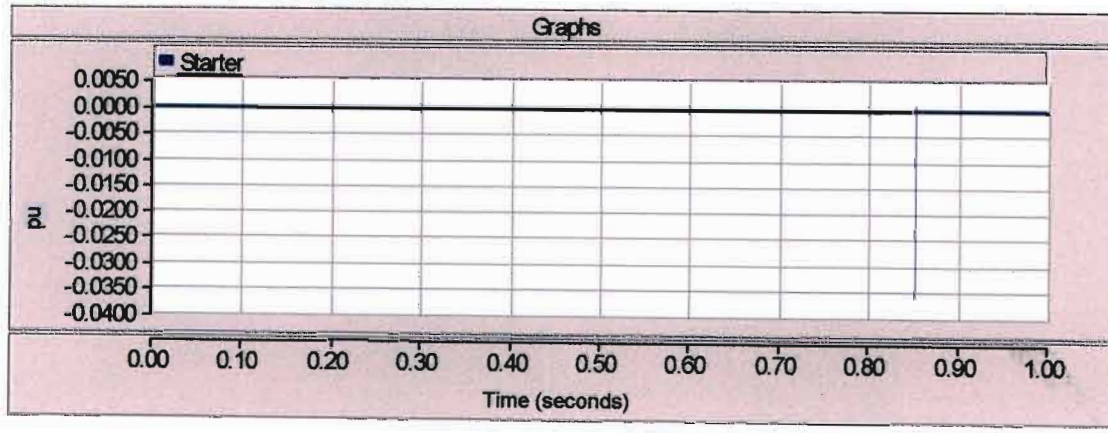

Fig 5.7. Calculated Starter values for PP-G Fault at 10% of Line Length

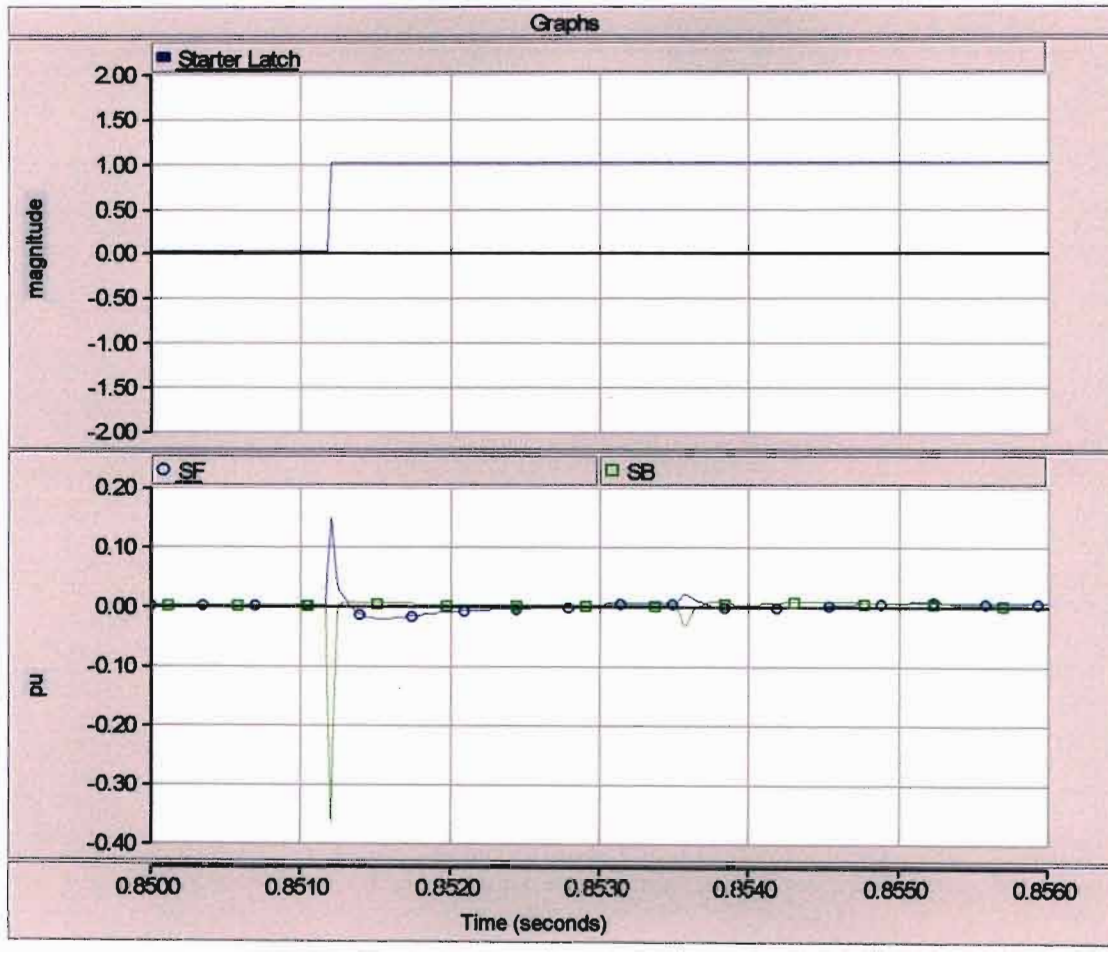

Fig 5.8. Relaying Signals for PP-G Fault Located 350kms from Relaying Point.

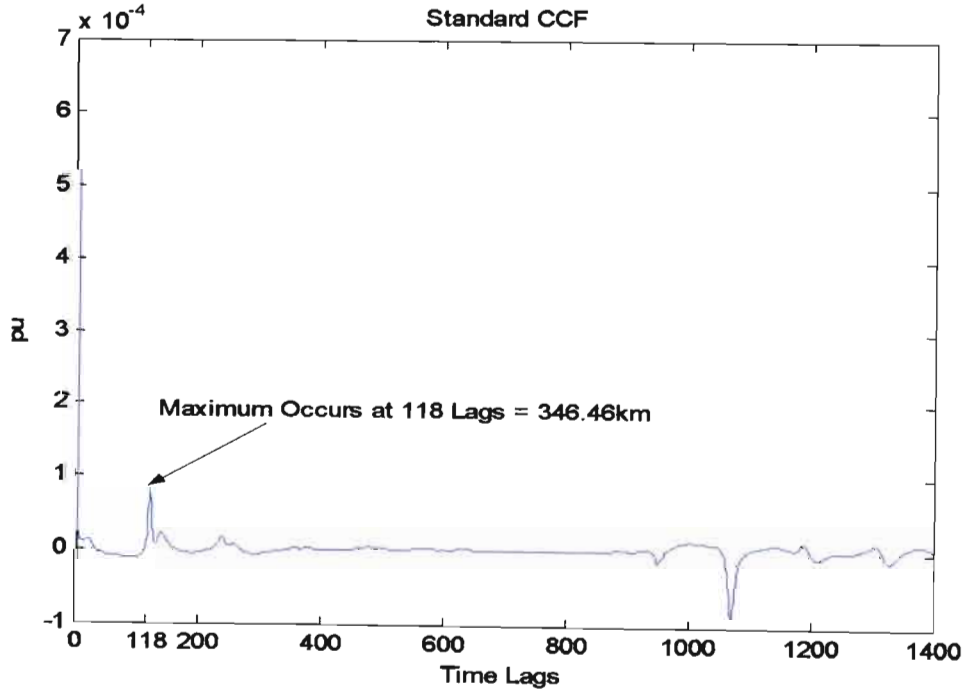

Fig 5.9. SCCF output for PP-G fault located at 350kms.

From Fig 5.9, it can be seen that the maximum occurs after 118 time lags where 1 time lag is equal to 20μs. The time travel can, therefore, be calculated from the sample frequency using the following equation:

$$t = \frac{\textbf{Number of Time Lags}}{\textbf{Sampling Frequency}} = \frac{118}{50 \times 10^3} = 2.36ms$$

The distance to fault can then be calculated from (22) as follows:

$$D_{f1} = \frac{vt}{2} = \frac{293608598 \times 2.36 \times 10^{-3}}{2} = 346.46km$$

The percentage error is given by:

$$\%_{Error} = \frac{346.46 - 350}{350} \times 100\% = -1.01\%$$

Clearly the fault has been detected with a high level of accuracy. There is no need for the auxiliary CCF in this case as the fault is located within the first 80% of the line. Note that the M file, "protectionsystem.m" automatically performs all the necessary processing and calculations to detect and locate the fault. All the manual calculations shown are just for illustrative purposes.

Note the outputs of the standard CCF have very small magnitudes. The small magnitudes are due to the reflection coefficient at the fault being small because of the high refraction coefficient caused by mutual coupling between the poles. The above should, however, not be a problem as the CCF calculation and detection will be accomplished using software algorithms and not hardware. If detection should become a problem, the output of the CCF can be normalized by using the autocorrelation of the template as the normalizing factor. The standard CCF with the output normalized is shown in Fig 5.10.

The author realizes that the above discussion assumes that the signals to be correlated contain no noise. However, in practice both the template and the relaying signal to be

correlated will contain some noise. This noise will be superimposed on the signals to be correlated and will, therefore, influence the similarities between the two signals. As indicated above the CCF can be normalized by using the autocorrelation of the template. "In a lossless system with complete reflection from the fault the CCF peak will have this value" [32]. The value of this normalized peak will be 1 and the peak value will occur twice in the CCF of a lossless system with complete reflection at both the fault point and the relaying location. The peak value will first appear at time $t = 0$ when the template is being compared with itself and will again occur when the returning wave from the fault is identified.

However, in our study case there is a low reflection coefficient at the fault point even for solid faults. The low reflection coefficient results in the returning wave from the fault producing smaller peaks in the CCF as shown in Fig 5.10. The CCF itself is an effective noise filter [32], [38]. However, as the fault resistance increases, the values of ΔU and ΔI at the relaying point become smaller. The increased fault resistance also causes the reflection coefficient at the fault to be further reduced resulting in even smaller peaks in the CCF.

Note that a very noisy signal will also produce very small peaks in the CCF because white noise is uncorrelated [32]. Therefore, "in the event of the CCF output being low then either the travelling wave levels are low or the noise levels are high" [32]. So the problem lies in determining whether the peaks in the CCF were caused by low magnitude travelling waves or by high noise levels. One solution to the problem is to filter out the noise from the physical voltage and current signals before the relaying signals are calculated. In this way both the signals to be correlated will be noise filtered and the CCF will, therefore, be unaffected by noise. So in the above situation the low peaks in the CCF can only be caused by low magnitude travelling waves.

The authors in [39] have shown that it is possible to design such a filter that will effectively filter out the noise without degrading the travelling wave information in the physical voltage and current signals. Other methods of recovering signals with small signal to noise ratios are discussed in [38]. One method of signal recovery discussed in [38] first involves a special autocorrelation of the individual signals (i.e.

the template and relaying signal to be correlated) in order to filter out noise before the CCF is calculated.

The above discussion indicates that it is possible to filter out the noise before calculating the CCF, thereby providing the CCF with immunity from noise. Since the purpose of this research is mainly on the development of a protection method rather that the implementation, the author has assumed that for this work the signals to be correlated can be effectively filtered to remove noise before the CCF is performed. Under the above assumption, the CCF will be shielded from the effects of noise. The exact method of filtering out this noise will be considered as part of further work.

Noting the above assumption that the signals to be correlated have been effectively filtered to remove noise, let us now consider a negative pole to ground (NP-G) fault located 350kms away from the relaying point (10% of the line length).

Fig 5.11 shows the modal voltages and currents for the NP-G fault. Clearly both the pole and ground mode current waves have the opposite polarity with the initial ground mode polarity being negative. Clearly the fault is located on the negative pole.

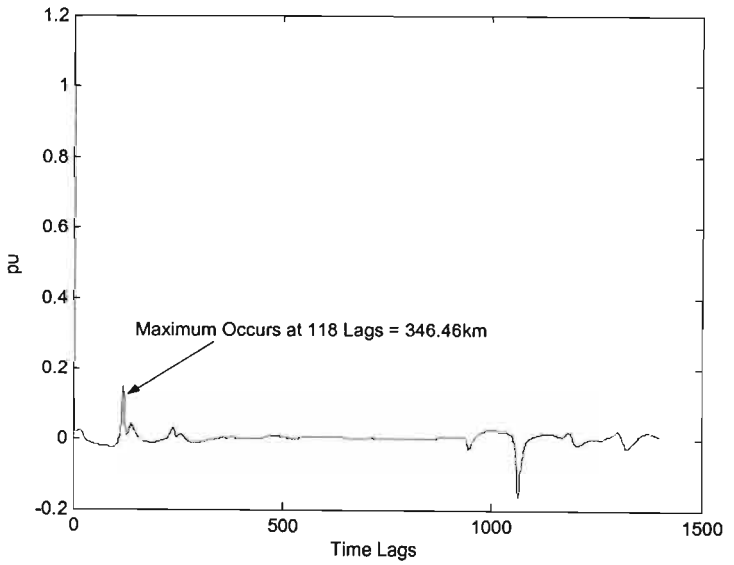

Fig 5.10. Normalized SCCF output for a PP-G Fault located at 350kms.

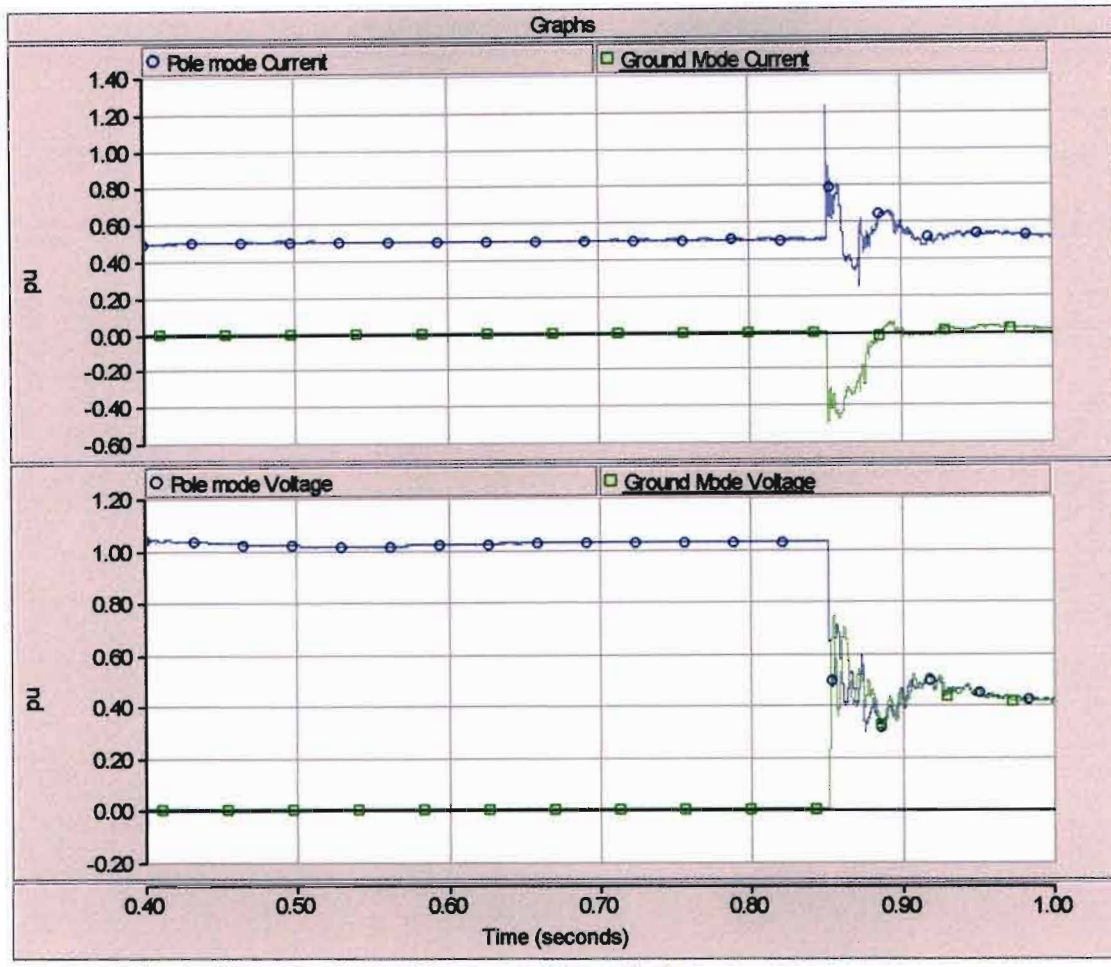

Fig 5.11. Modal Voltages and Currents for NP-G Fault Located 350kms from Relaying Point.

Fig 5.12 and Fig 5.13 show the plots of the calculated starter and relaying signal values. As expected these graphs are similar to Fig 5.7 and Fig 5.8 as the modal components have been used to calculate these quantities.

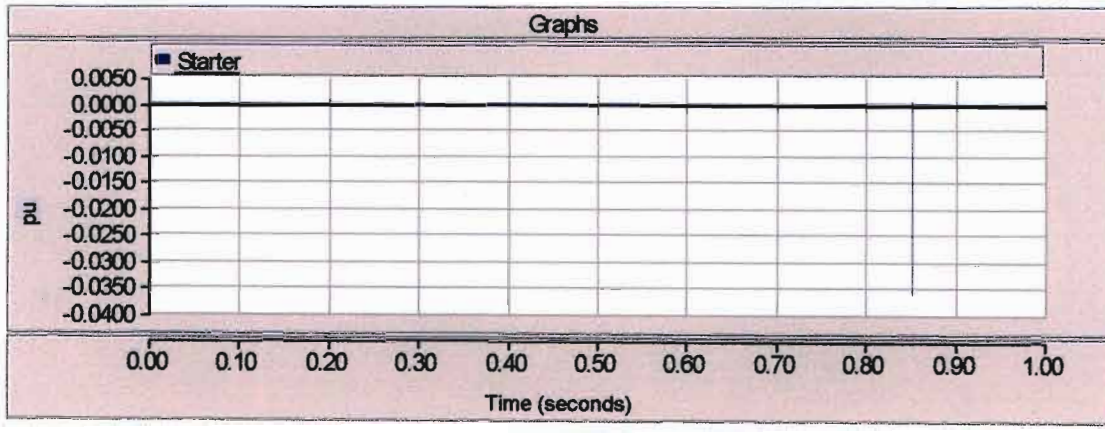

Fig 5.12. Calculated Starter values for NP-G Fault at 10% of Line Length.

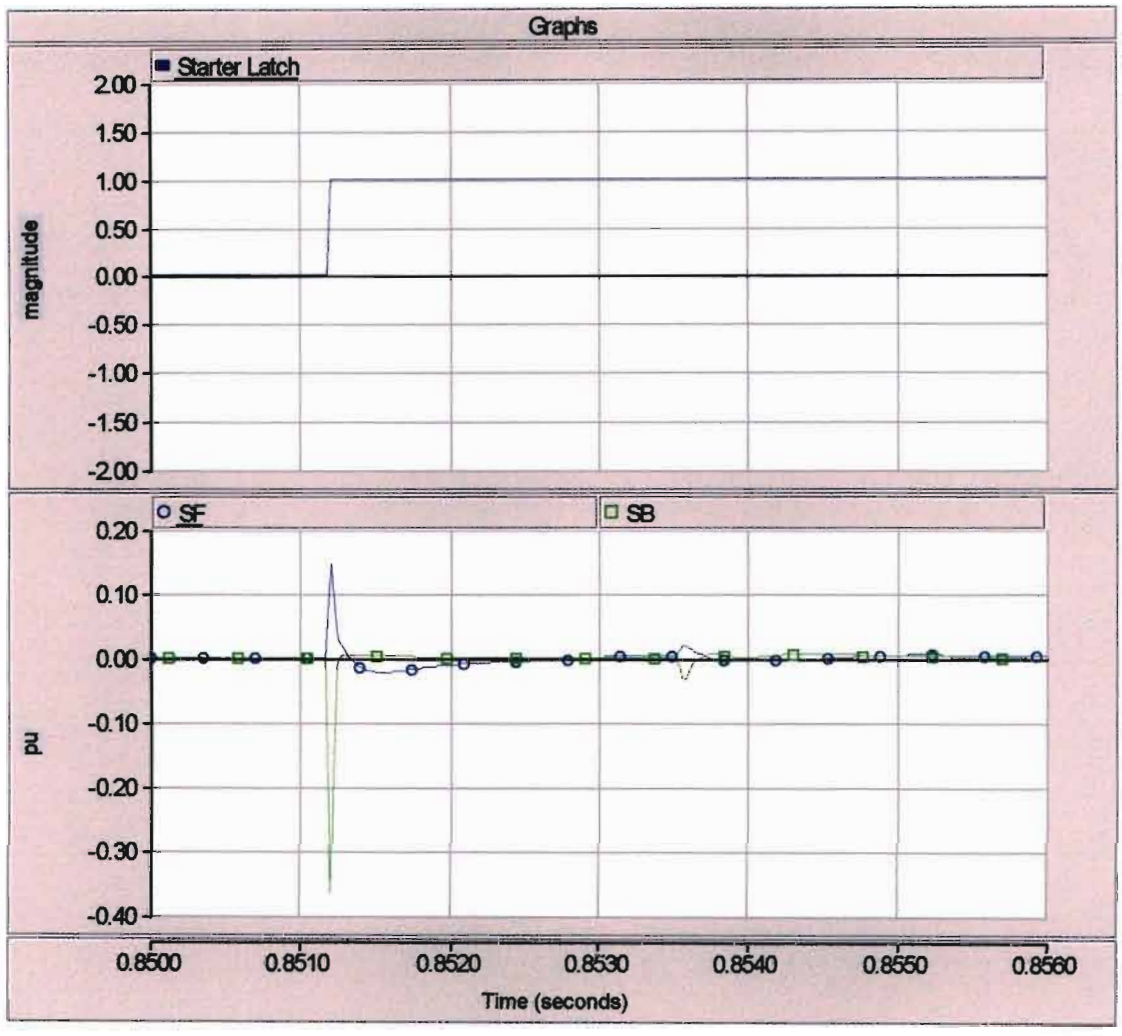

Fig 5.13. Relaying Signals for NP-G Fault Located 350kms from Relaying Point.

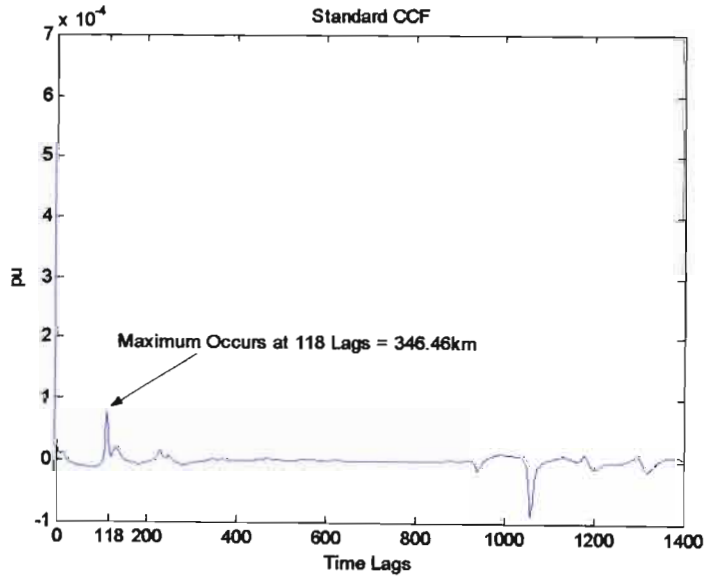

Fig 5.14. SCCF output for a NP-G Fault located at 350kms.

Fig 5.14 above illustrates the standard CCF output for the NP-G fault and indicates the NP-G fault distance is calculated with the same level accuracy as the PP-G fault distance.

Let us once again consider a PP-G fault located at 10% of the line length (350km) but this time with a finite fault resistance. In this research study fault resistances of 50Ω, 100Ω, 200Ω and 400Ω which are approximately equal to 25%, 50%, 100% and 200% of the surge impedance have been used.

Note the fault resistance for a pole to ground fault includes both the arc resistance and the ground contact resistance [44]. The ground contact resistance (GCR) is the resistance seen by the fault at the ground entry point and this resistance varies based on the soil resistivity [44]. The GCR can, therefore, be very high for rocky and dry conditions [44-46]. Utilities will try to reduce the GCR to acceptable values, which for a 500kV line will be 50Ω or less [44]. However, the reduction of the GCR to acceptable values is not always possible. In these cases the utilities normally increase the line insulation levels to limit the possibility of flashovers in the areas with high GCR [46]. Therefore, it stands to reason that faults occurring in areas with high GCR will have a significant fault resistance component. In Eskom, the South African Utility, during the period October 2000 to October 2004 the highest fault resistance recorded on their Transmission Network was 244Ω which occurred on a 275kV line on the 30th April 2004 [47]. Note that on a point to point dc transmission line no load is connected on the dc line. Therefore, any connection between the dc line and ground irrespective of the impedance will constitute a line fault. The author's choice of maximum resistance was, therefore, chosen to illustrate the protection coverage provided by the proposed protection system. The author does not mean to imply that of fault resistance of 400Ω will occur in practise.

Note that for the PP-G fault with the fault resistances given above the protection starter values exceeded the setting threshold for all resistances values indicating a fault and starting the correlation process. Also the polarity of the ground mode current for all fault resistance values was positive indicating the fault was on the positive pole.

Fig 5.15 shows the results obtained when a 50Ω fault resistance was assumed. The standard CCF clearly shows a maximum at 346.46km, therefore the fault is accurately located. As would be expected, the magnitude of the CCF is smaller than that of the solid ground fault.

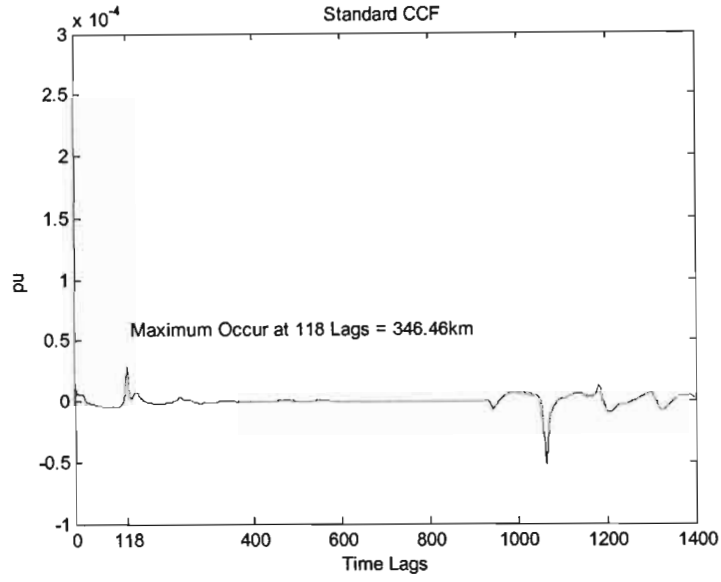

Fig 5.15. SCCF output for a PP-G Fault located at 350kms with a 50Ω Fault Resistance.

Fig 5.16 shows the results obtained when a 100Ω fault resistance is assumed. The standard CCF again shows a maximum at 346.46km and therefore the fault is accurately located. Notice that the magnitude of the output at 1184 lags is increasing due to the increase in refraction coefficient caused by the increase in fault resistance.

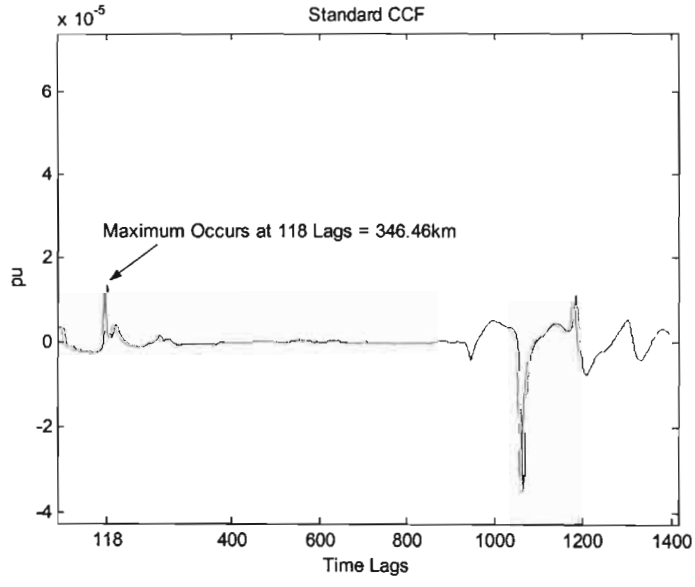

Fig 5.16. SCCF output for a PP-G Fault located at 350kms with a 100Ω Fault Resistance.

Fig 5.17 shows the results obtained when a 200Ω fault resistance is assumed. This time the standard CCF records a maximum at 1184 lags or 3476.33km which is almost equal to the line length (LL). Also note that there is a local maximum at 118 lags or 346.46km were the fault is actually located.

Now since the fault location exceeds 80 percent of the line length, the auxiliary CCF (ACCF) is initiated. The output of the auxiliary CCF is shown in Fig 5.18 with a maximum output at 1066 lags or 3129.87km.

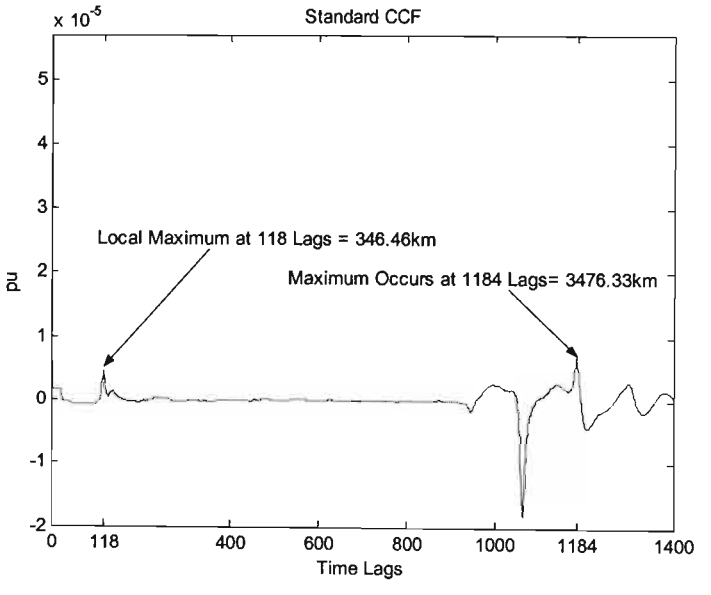

Fig 5.17. SCCF output for a PP-G Fault located at 350kms with a 200Ω Fault Resistance.

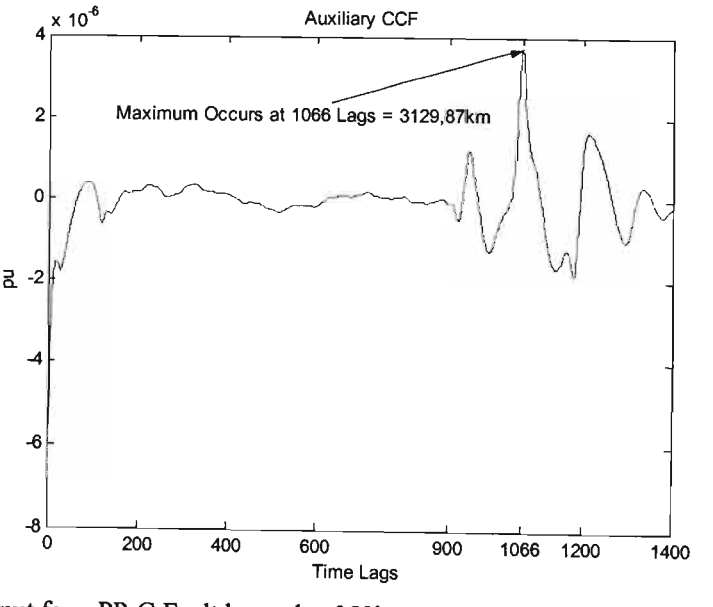

Fig 5.18. ACCF output for a PP-G Fault located at 350kms with a 200Ω Fault Resistance.

The protection system will now calculate a second fault location estimate using (46) as follows:

$$D_{f2} = \frac{v(t_1 - t_2)}{2} = \frac{293608598 \times \left(\frac{1184 - 1066}{50 \times 10^3}\right)}{2} = 346.46km$$

So now we have two fault location estimates with the fault location provided by (22) being 3376.33km and the fault location provided by (46) being 346.46km. However, since there is a local maximum at 346.46km in the standard CCF, the fault location of 346.46km provided by (46) is taken as the final fault location. As already indicated the M file "protectionsystem.m" automatically makes all the above decisions and outputs the relevant information as indicated in 4.6.4.

Note the use of the auxiliary function has doubled the correlation duration from 28ms to 56ms. This effectively means that the protection operating time as also doubled as majority of the operating time is due to the correlation process.

Fig 5.19 shows the results obtained when a 400Ω fault resistance is assumed. Again the standard CCF records a maximum at 1184 lags or 3476.33km which is almost the line length and again there is a local maximum at 118 lags or 346.46km were the fault is actually located.

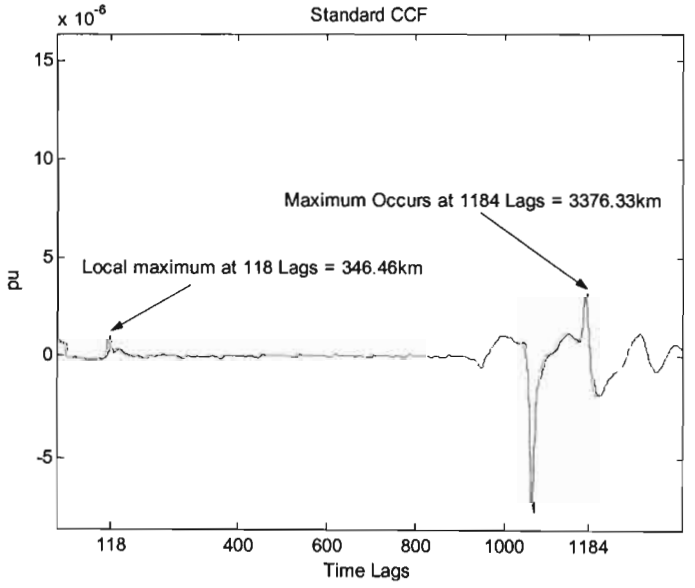

Fig 5.19. SCCF output for a PP-G Fault located at 350kms with a 400Ω Fault Resistance.

Since the fault location exceeds 80 percent of the line length, the auxiliary CCF is initiated. The output of the auxiliary CCF is shown in Fig 5.20 and again like Fig 5.18 has a maximum output at 1066 lags or 3129.87km.

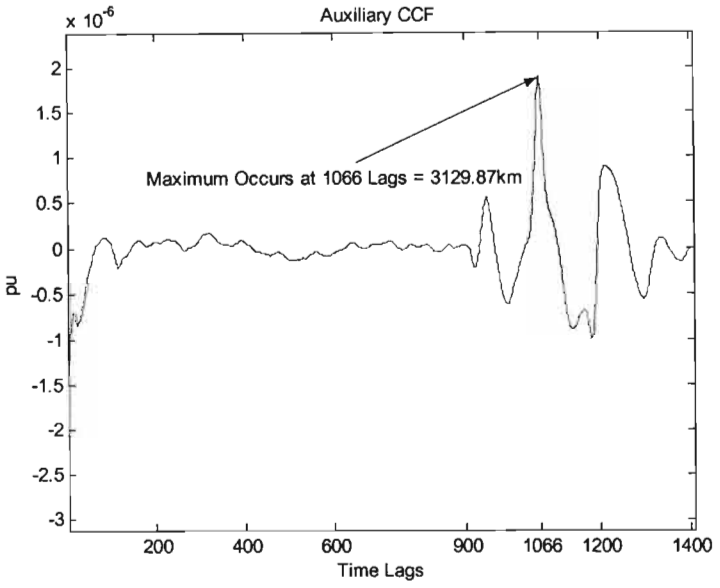

Fig 5.20. ACCF output for a PP-G Fault located at 350kms with a 400Ω Fault Resistance.

Therefore D_{f2} calculated using (46) will again be equal to 346.46km and since there is a local maximum at 346.46km in the standard CCF, the result of (46), 346.46kms, will be taken as the final fault location.

Negative pole to ground faults at 10% of the line length with the various resistances were also simulated, the results of which are given in Table 5.1. The results obtained are identical to those of the positive pole to ground faults except for the polarity of the ground mode wave which was negative in these cases indicating that the fault was located on the negative pole.

Further simulations were conducted with pole to ground faults located at 20%, 40%, 60%, 80%, 90% and 100% of the line length. The results obtained for these simulations are given in Tables 5.2 – 5.7. Note that the protection starter threshold was exceeded in every case, thereby releasing the protection and indicating the possible presence of a fault on the dc transmission line.

Table 5.1. Fault Location Results for a NP-G Fault located at 350kms.

NEGATIVE POLE TO GROUND FAULT AT 350KM (10% OF LL)				
Fault Resistance	Fault location Using Standard CCF Equation (22)	Fault location Using Auxiliary CCF Equation (46)	Final Fault Location	Percentage Error
50Ω	346.46km	N/A	346.46km	-1.01%
100Ω	346.46km	N/A	346.46km	-1.01%
200Ω	3476.33km	346.46km	346.46km	-1.01%
400Ω	3476.33km	346.46km	346.46km	-1.01%

Table 5.2. Fault Location Results for a Pole to Ground Fault located at 700kms.

POLE TO GROUND FAULTS AT 700KM (20% OF LL)					
Faulted Pole	Fault Resistance	Fault Location Using Standard CCF Equation (22)	Fault Location Using Auxiliary CCF Equation (46)	Final Fault Location	Percentage Error
Positive	0Ω	692.92km	N/A	692.92km	-1.01%
Negative	0Ω	692.92km	N/A	692.92km	-1.01%
Positive	50Ω	692.92km	N/A	692.92km	-1.01%
Negative	50Ω	692.92km	N/A	692.92km	-1.01%
Positive	100Ω	692.92km	N/A	692.92km	-1.01%
Negative	100Ω	692.92km	N/A	692.92km	-1.01%
Positive	200Ω	3476.33km	692.92km	692.92km	-1.01%
Negative	200Ω	3476.33km	692.92km	692.92km	-1.01%
Positive	400Ω	3476.33km	692.92km	692.92km	-1.01%
Negative	400Ω	3476.33km	692.92km	692.92km	-1.01%

Table 5.3. Fault Location Results for a Pole to Ground Fault located at 1400kms.

POLE TO GROUND FAULTS AT 1400KM (40% OF LL)					
Faulted Pole	Fault Resistance	Fault Location Using Standard CCF Equation (22)	Fault Location Using Auxiliary CCF Equation (46)	Final Fault Location	Percentage Error
Positive	0Ω	1388.77km	N/A	1388.77km	-0.80%
Negative	0Ω	1388.77km	N/A	1388.77km	-0.80%
Positive	50Ω	1388.77km	N/A	1388.77km	-0.80%
Negative	50Ω	1388.77km	N/A	1388.77km	-0.80%
Positive	100Ω	1388.77km	N/A	1388.77km	-0.80%
Negative	100Ω	1388.77km	N/A	1388.77km	-0.80%
Positive	200Ω	3476.33km	1388.77km	1388.77km	-0.80%
Negative	200Ω	3476.33km	1388.77km	1388.77km	-0.80%
Positive	400Ω	3476.33km	1388.77km	1388.77km	-0.80%
Negative	400Ω	3476.33km	1388.77km	1388.77km	-0.80%

Table 5.4. Fault Location Results for a Pole to Ground Fault located at 2100kms.

POLE TO GROUND FAULTS AT 2100KM (60% OF LL)					
Faulted Pole	Fault Resistance	Fault Location Using Standard CCF Equation (22)	Fault Location Using Auxiliary CCF Equation (46)	Final Fault Location	Percentage Error
Positive	0Ω	2084.62km	N/A	2084.62km	-0.73%
Negative	0Ω	2084.62km	N/A	2084.62km	-0.73%
Positive	50Ω	2084.62km	N/A	2084.62km	-0.73%
Negative	50Ω	2084.62km	N/A	2084.62km	-0.73%
Positive	100Ω	2084.62km	N/A	2084.62km	-0.73%
Negative	100Ω	2084.62km	N/A	2084.62km	-0.73%
Positive	200Ω	3476.33km	2084.62km	2084.62km	-0.73%
Negative	200Ω	3476.33km	2084.62km	2084.62km	-0.73%
Positive	400Ω	3476.33km	2084.62km	2084.62km	-0.73%
Negative	400Ω	3476.33km	2084.62km	2084.62km	-0.73%

Table 5.5. Fault Location Results for a Pole to Ground Fault located at 2800kms.

POLE TO GROUND FAULTS AT 2800KM (80% OF LL)					
Faulted Pole	Fault Resistance	Fault Location Using Standard CCF Equation (22)	Fault Location Using Auxiliary CCF Equation (46)	Final Fault Location	Percentage Error
Positive	0Ω	2780.47km	N/A	2780.47km	-0.69%
Negative	0Ω	2780.47km	N/A	2780.47km	-0.69%
Positive	50Ω	2780.47km	N/A	2780.47km	-0.69%
Negative	50Ω	2780.47km	N/A	2780.47km	-0.69%
Positive	100Ω	3476.33km	2780.47km	2780.47km	-0.69%
Negative	100Ω	3476.33km	2780.47km	2780.47km	-0.69%
Positive	200Ω	3476.33km	2780.47km	2780.47km	-0.69%
Negative	200Ω	3476.33km	2780.47km	2780.47km	-0.69%
Positive	400Ω	3476.33km	2780.47km	2780.47km	-0.69%
Negative	400Ω	3476.33km	2780.47km	2780.47km	-0.69%

Table 5.6. Fault Location Results for a Pole to Ground Fault located at 3150kms.

POLE TO GROUND FAULTS AT 3150KM (90% OF LL)					
Faulted Pole	Fault Resistance	Fault Location Using Standard CCF Equation (22)	Fault Location Using Auxiliary CCF Equation (46)	Final Fault Location	Percentage Error
Positive	0Ω	3129.87km	2780.47km	3129.87km	-0.64%
Negative	0Ω	3129.87km	2780.47km	3129.87km	-0.64%
Positive	50Ω	3129.87km	2780.47km	3129.87km	-0.64%
Negative	50Ω	3129.87km	2780.47km	3129.87km	-0.64%
Positive	100Ω	3476.33km	3129.87km	3129.87km	-0.64%
Negative	100Ω	3476.33km	3129.87km	3129.87km	-0.64%
Positive	200Ω	3476.33km	3129.87km	3129.87km	-0.64%
Negative	200Ω	3476.33km	3129.87km	3129.87km	-0.64%
Positive	400Ω	3476.33km	3129.87km	3129.87km	-0.64%
Negative	400Ω	3476.33km	3129.87km	3129.87km	-0.64%

Table 5.7. Fault Location Results for a Pole to Ground Fault located at 3500kms.

POLE TO GROUND FAULTS AT 3500KM (100% OF LL)					
Faulted Pole	Fault Resistance	Fault Location Using Standard CCF Equation (22)	Fault Location Using Auxiliary CCF Equation (46)	Final Fault Location	Percentage Error
Positive	0Ω	3476.33km	-79.27km	3476.33km	-0.67%
Negative	0Ω	3476.33km	-79.27km	3476.33km	-0.67%
Positive	50Ω	3476.33km	-129.19km	3476.33km	-0.67%
Negative	50Ω	3476.33km	-129.19km	3476.33km	-0.67%
Positive	100Ω	3476.33km	-129.19km	3476.33km	-0.67%
Negative	100Ω	3476.33km	-129.19km	3476.33km	-0.67%
Positive	200Ω	3476.33km	-132.12km	3476.33km	-0.67%
Negative	200Ω	3476.33km	-132.12km	3476.33km	-0.67%
Positive	400Ω	3476.33km	-132.12km	3476.33km	-0.67%
Negative	400Ω	3476.33km	-132.12km	3476.33km	-0.67%

Notice that in Table 5.6 and 5.7 the auxiliary function is calculated even for zero resistance faults. This occurs because the fault location estimates, although correct, given by the standard CCF exceed 80% of the line length and therefore need to be verified.

In Table 5.6, the zero and 50Ω resistance faults cause a maximum in the auxiliary CCF at 2780.47km but since no local maximum occurs near this value in the standard CCF, the standard CCF estimate of 3129.87kms is taken as the final fault location.

In Table 5.7 all the auxiliary CCF fault location estimates are negative. These negative values occur because the refracted wave is occurring after the reflected wave and, therefore, as explained in 3.2.7 these negative values can be ignored. The final fault location is then 3476.33kms as given by the standard CCF.

Clearly, all the faults simulated so far have posed no problem and have been correctly located with a high degree of accuracy. The CCF outputs of these can be found in Appendix C.

Let us now consider a solid positive pole to ground fault located exactly in the centre of the line (1750km). The output of the standard CCF is shown in Fig 5.21, which indicates a maximum at 3476.33km according to (22). This is greater than 80% of the line length, therefore, the auxiliary CCF will be initiated. The output of the auxiliary CCF is shown in Fig 5.22.

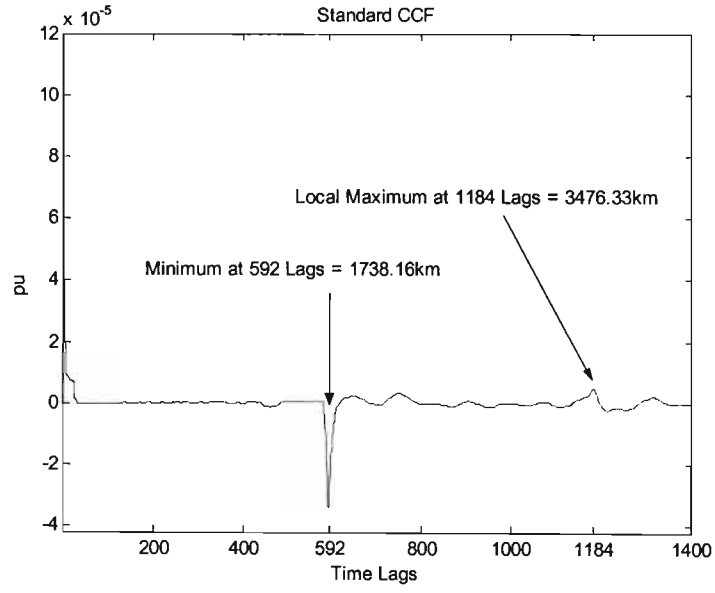

Fig 5.21. SCCF output for a PP-G Fault located at 1750kms.

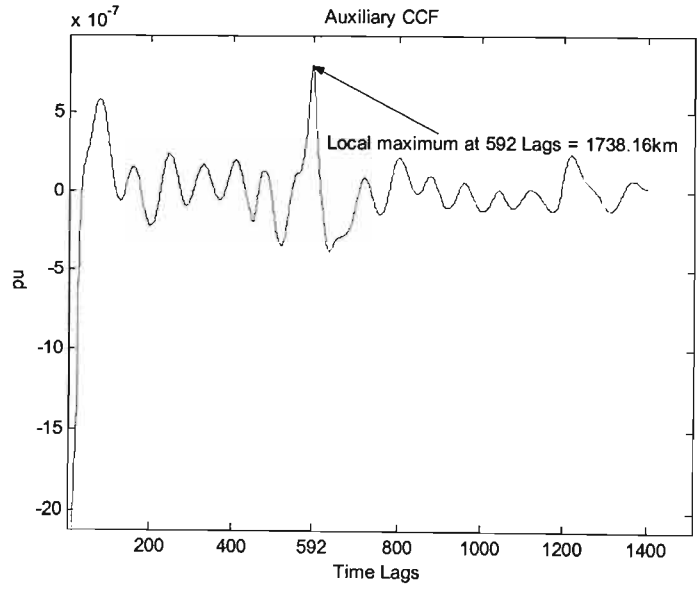

Fig 5.22. ACCF output for a PP-G Fault located at 1750kms.

Now using (46) the second fault location estimate will be calculated as follows:

$$D_{f2} = \frac{v(t_1 - t_2)}{2} = \frac{293608598 \times \left(\frac{1184 - 592}{50 \times 10^3}\right)}{2} = 1738.16km$$

In the standard CCF there is no local maximum around 1738.16km. In fact there is a minimum peak at this exact point. The protection system will, therefore, assume the fault location provided by (22) to be correct and return a fault location of 3476.33km. This fault location is obviously incorrect because we already know that the fault is located at the centre of the line (1750km).

Now apart from the fault location being incorrect, the protection operating time has doubled due to the use of the auxiliary CCF and added to this, the fault clearing process will also be delayed because the fault has been located in the last 20% of the line.

The reason for this inaccuracy is due to the refracted and reflected wave reaching the relaying point at the same time. As explained in 3.2.6, when a pole to ground fault occurs on a bipolar system, the pole mode surge impedance is terminated through the ground mode surge impedance at the fault point. Since the ground mode surge impedance is larger that the pole mode surge impedance the refraction coefficient is larger than the reflection coefficient.

The above implies that if both the reflected and refracted waves arrive at the relaying point at the same time the resultant wave would be negative. This explains the minimum at the fault location in the standard CCF. The fact that the refracted wave arrives at the same time as the reflected wave is further verified by the auxiliary CCF, as it indicates that the refracted wave arrived at 592 lags which is the same time as the minimum peak in the standard CCF.

The above problem exists irrespective of the faulted pole or fault resistance. In fact the peaks in the CCF become more defined as the fault resistance is increased. This

can be seen in Fig 5.23 and 5.24 were a NP-G fault was applied at the centre of the line with a 400Ω fault resistance.

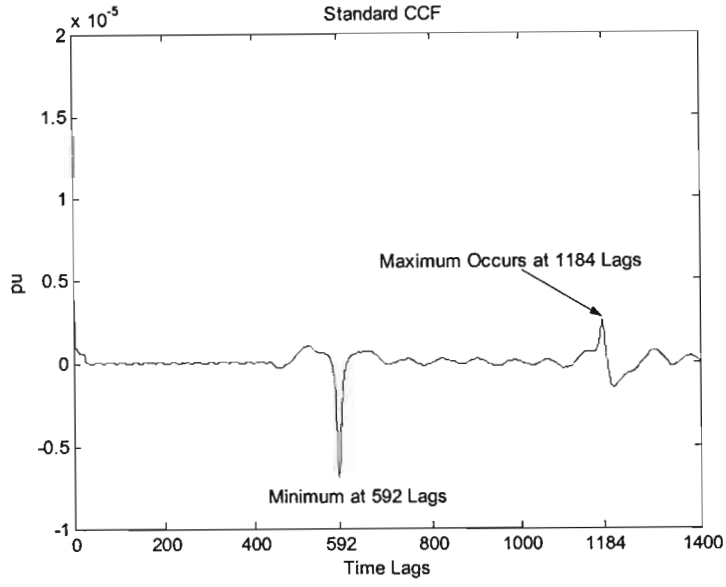

Fig 5.23. SCCF output for a NP-G Fault with 400Ω Fault Resistance located at 1750kms.

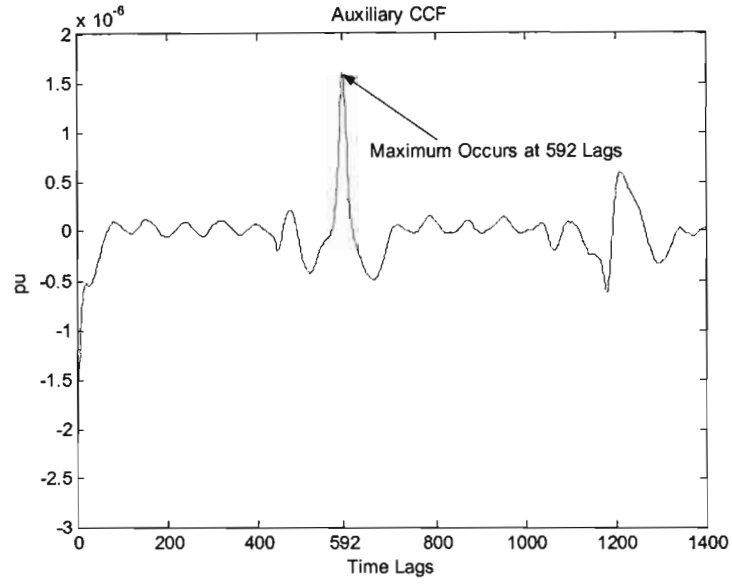

Fig 5.24. ACCF output for a NP-G Fault with 400Ω Fault Resistance located at 1750kms.

One way of solving this problem would be to add, to the protection algorithm an instruction, to assume the fault to be at the centre of the line, if the minimum peak value in the standard CCF occurs around the centre of the line. The advantage of this method is that both solid and non-zero resistance faults will be detected without the use of the auxiliary CCF.

The only time the minimum peak should appear at the centre of the line is when the fault is at the centre of the line and the refracted wave is greater than the reflected wave. The above, however, cannot be guaranteed as noise and transducer errors could cause the minimum peak to occur around the centre of the line and in this case, mal-operation may occur.

Therefore, the use of the above method is not recommended. The author would, however, suggest that once the second fault location estimate is calculated using (46) and there is no local maximum in the standard CCF, before assuming the fault location calculated by (22) to be correct, the calculated value in (46) should be compared with the maximum in the auxiliary CCF. If the distance represented by the maximum in the ACCF corresponds to the distance calculated in (46), within a specified error range, the fault location calculated by (46) should be used. The only time the above two values will correspond is when the reflected and refracted waves reach the relaying point at the same time i.e. the fault is located at the centre of the line. So adding this to the flowchart given in Fig 3.10 will allow a fault at the centre of the line to be correctly detected. The modified correlation process which includes the additional check is shown in Fig 5.25. The additional check has already been incorporated in the M file "protectionsystem.m" to ensure that midpoint faults are correctly detected.

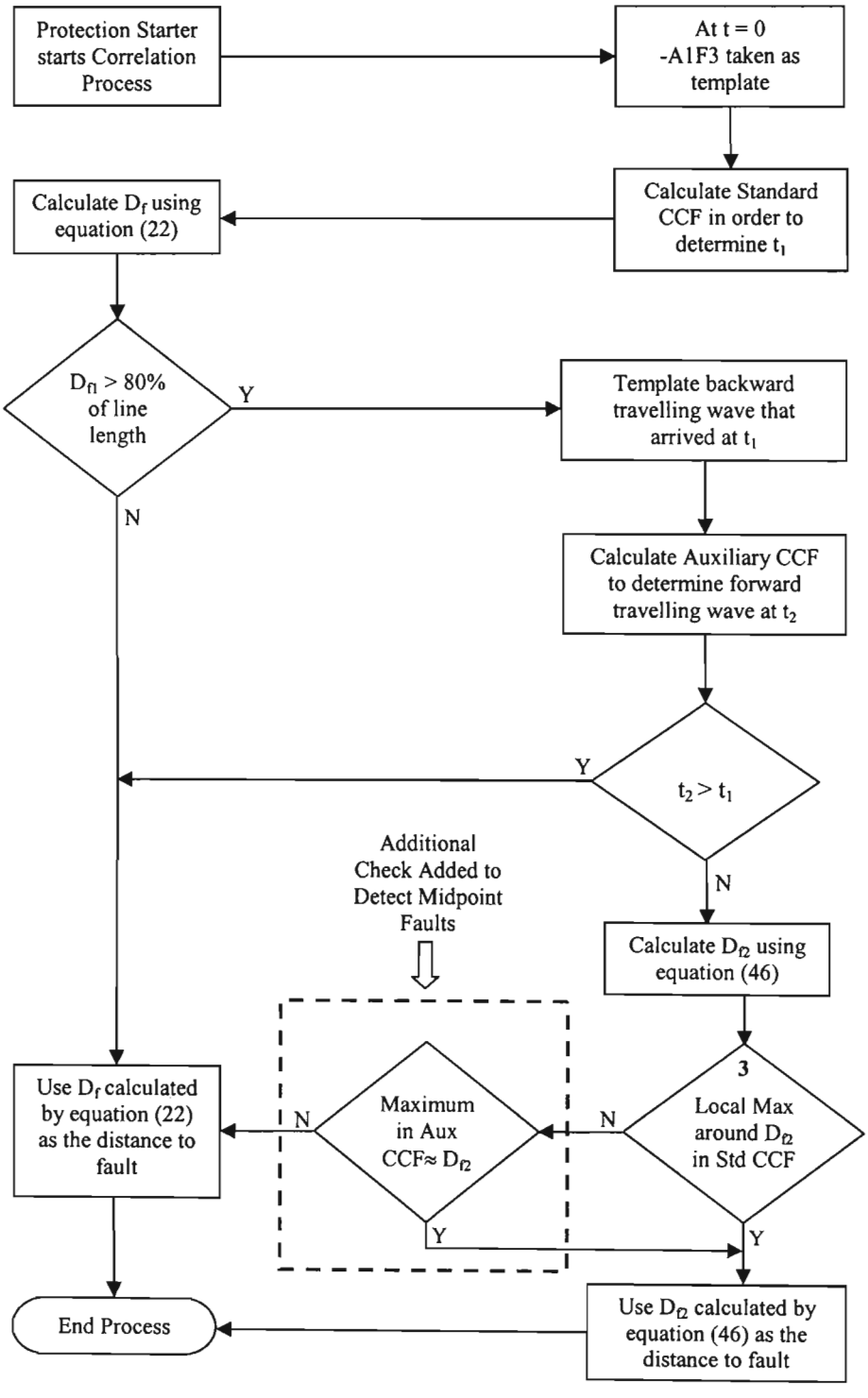

Fig 5.25. Correlation Process with Additional Check added to detect midpoint faults.

As indicated previously the problem associated with detecting midpoint faults using the existing process in Fig 3.10. is due both the refracted and reflected waves arriving at the same time. The range for which the CCF will experience the above problem is dependent on the sampling rate. The possible error in the CCF due to a sampling rate of 50 kHz is around ± 6km. Faults were then applied at 1740kms (49.7% of LL) and 1760kms (50.3% of LL) to illustrate this point. The results are shown in Fig 5.26 and Fig 5.27 which indicate that there is no problem locating these faults.

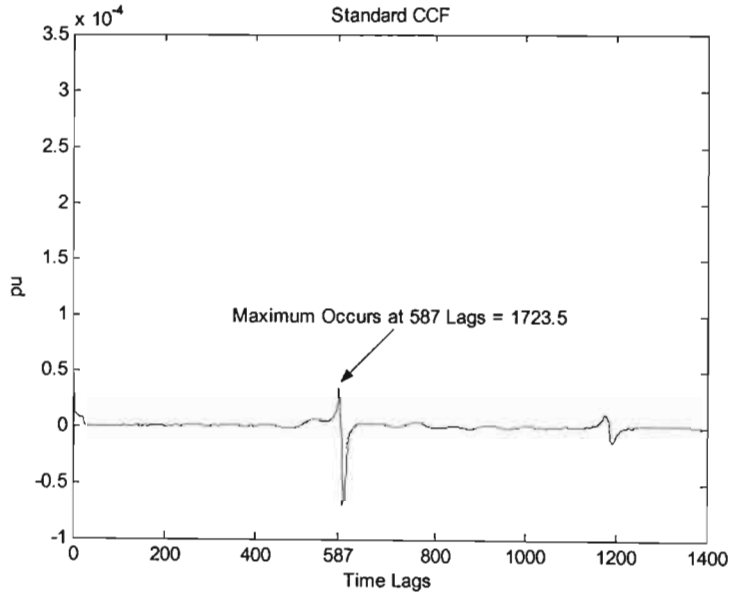

Fig 5.26. SCCF output for a P-G Fault Located at 1740kms.

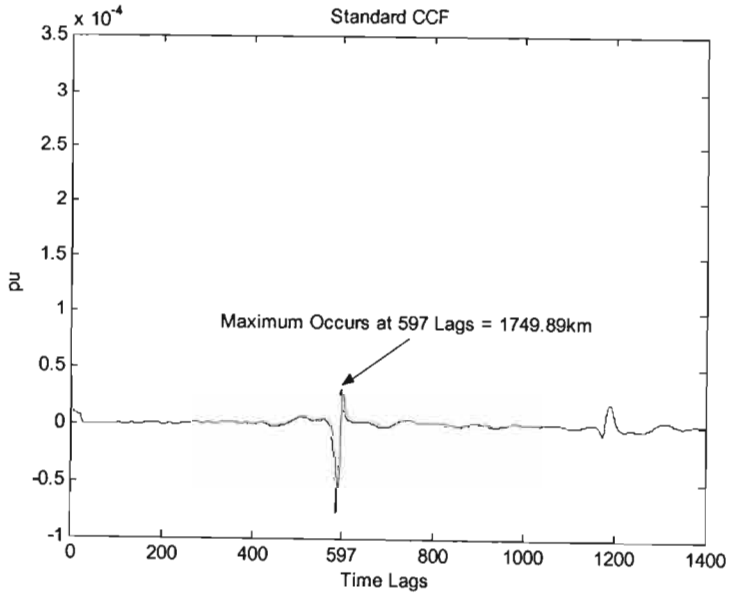

Fig 5.27. SCCF output for a P-G Fault Located at 1760kms.

5.4.2. Bipole Faults

Let us now analyse the protection system's response to bipole (P-P) faults. Let us first consider a bipole fault occurring in the middle of the line at time t equal to 0.85s. The modal quantities are shown in Fig 5.28 and as expected there are no ground mode quantities present as there will be no current flow through the ground conductors.

Note that in the case of P-G faults located at the centre of the line the SCCF reported an incorrect distance to fault. However, Fig 5.29 which shows the SCCF output for the above bipole fault clearly indicates that this bipole fault has been correctly located at the centre of the line. The above condition is to be expected as in this case there are no ground mode quantities present to cause the refraction coefficient to exceed the reflection coefficient. However as the fault resistance between the poles increases, so will the refraction coefficient leading to similar problems as experienced by P-G faults when the fault resistance is high.

The above condition is illustrated in Fig 5.30 where the same bipole fault as above is applied except this time there is a 400Ω fault resistance between the poles. The author realizes the possibility of a 400Ω fault resistance occurring between the poles is very low. Again the high fault resistance has been used to illustrate the protective coverage of the protection system. There is a minimum peak at 592 lags were the fault should be located. The simulation results obtained using the M file "protectionsystem.m" has indicated that the solution applied to the protection algorithm for midpoint P-G faults also works in the case of bipole faults.

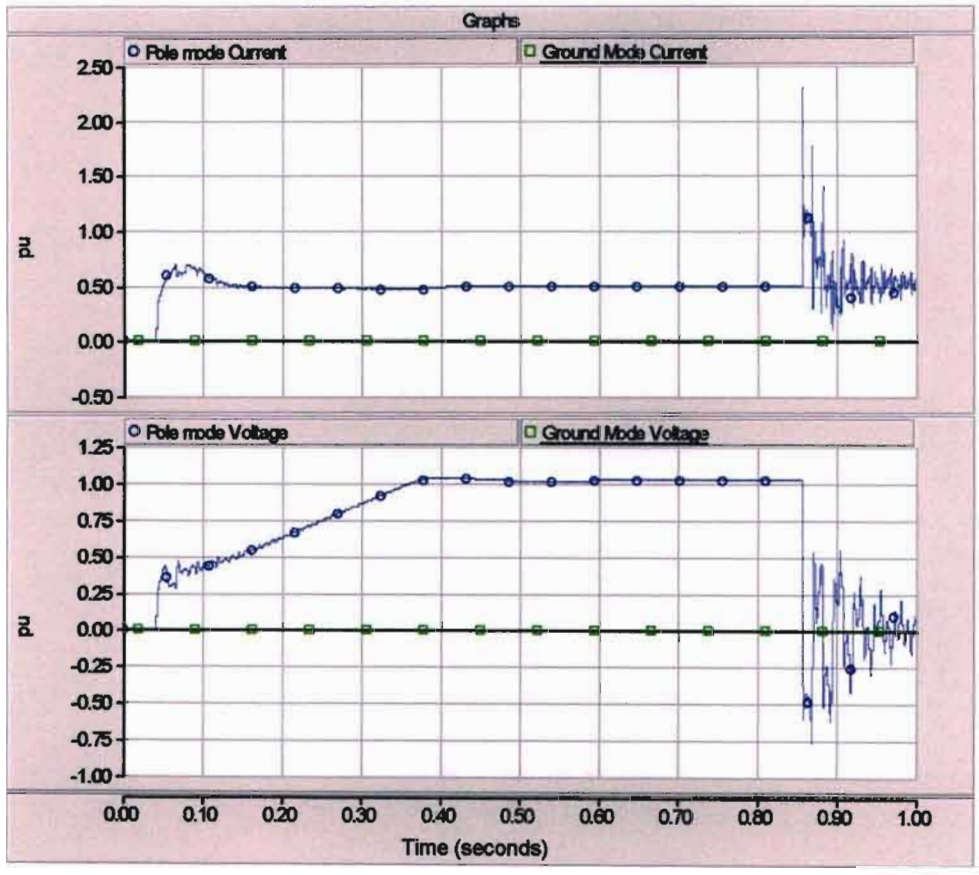

Fig 5.28. Modal Quantities for a Bipole Fault at 0.85s located at 1750kms

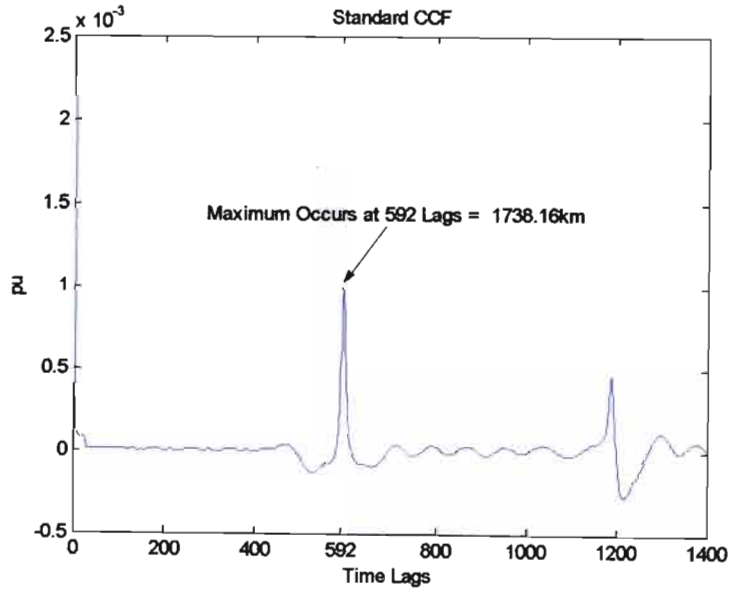

Fig 5.29. SCCF Output for a Bipole Fault at 1750kms

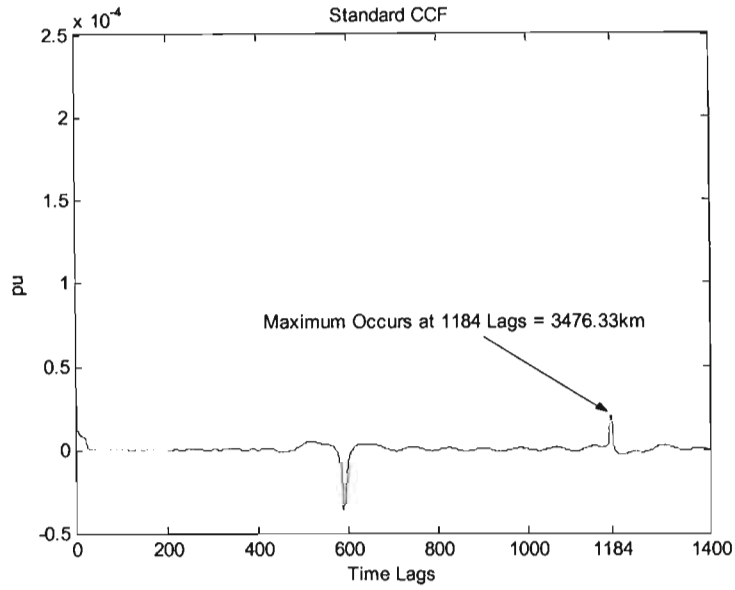

Fig 5.30. SCCF Output for a P-P Fault with 400Ω Bipole Fault Resistance at 1750kms

Note that a balanced pole to pole to ground (P-P-G) fault at the centre of the line will also provide the exact same results has given in Fig 5.28 and Fig 5.29. The results will be the same because just as in the case of a P-P fault, a balanced P-P-G fault will also cause no current to flow in the ground conductors. Therefore the value of the ground fault resistance has no effect in a balanced system since there is no ground current.

Let us now consider unbalanced faults at the centre of the line. An unbalanced P-P-G fault may develop from a P-G fault that has caused the surrounding air to ionize, leading to a breakdown of the air around the poles resulting in the P-G fault becoming a P-P-G fault. A schematic illustration of a P-P-G fault is shown in Fig 5.31.

The bipole fault resistance between Pole 1 and 2 is what causes the unbalance and allows current to flow through the ground. When the bipole resistances, *BP_Resistance_P1* and *BP_Resistance_P2* in Fig 4.7. are different, a residual voltage to ground will develop at the connection point between the two pole resistances. In Fig 4.7, at the pole resistance connection point there is also a connection to ground through a resistance component *Rfltx*. So if *Rfltx* is made a finite value, ground current will flow because of the residual voltage setup by the different fault resistances between the poles. The above discussion explains the method used for simulating unbalanced P-P-G faults.

Therefore, for unbalanced P-P-G faults, ground quantities will be present. The ground mode current polarity would indicate a fault on the pole with the least resistance to ground and in Fig 5.31 this would be Pole 2. The method of insuring that both poles are tripped for this fault has been explained in 3.2.8.

Let us now consider a P-P-G fault with a fault resistance of 400Ω between the poles and a 0Ω fault resistance between the negative pole and ground. Fig 5.32 shows the calculated modal quantities for this fault.

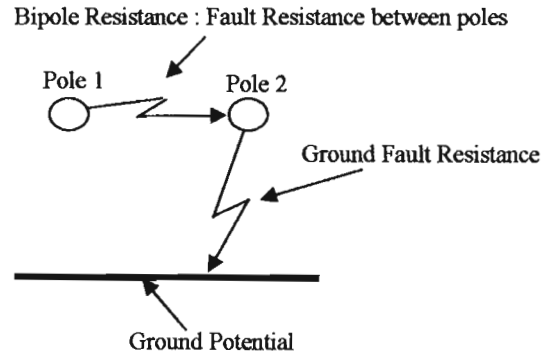

Fig 5.31. Schematic of P-P-G Fault Illustrating the Fault Resistances Present.

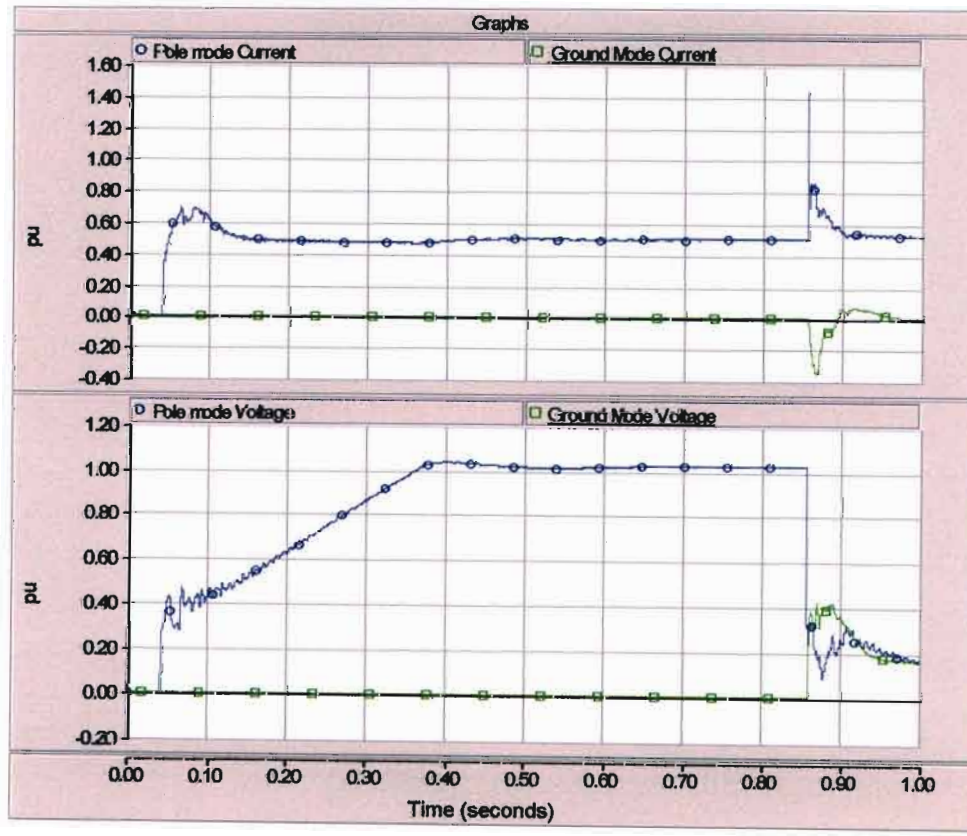

Fig 5.32. Modal Quantities for unbalanced fault at 1750kms.

Fig 5.32 indicates that, as expected, the initial polarity of the ground mode current wave is negative for this case. Fig 5.33 shows the standard CCF output for the above case. Notice that in this case the fault at the centre of the line is clearly located as opposed to the case in Fig 5.30. This is due to the addition of the solid ground connection on the negative pole which provides an alternate path for the current to flow through the ground. This effectively reduces the termination impedance seen by the travelling wave approaching the fault, resulting in a better reflection coefficient and a resultant positive wave at the relaying point.

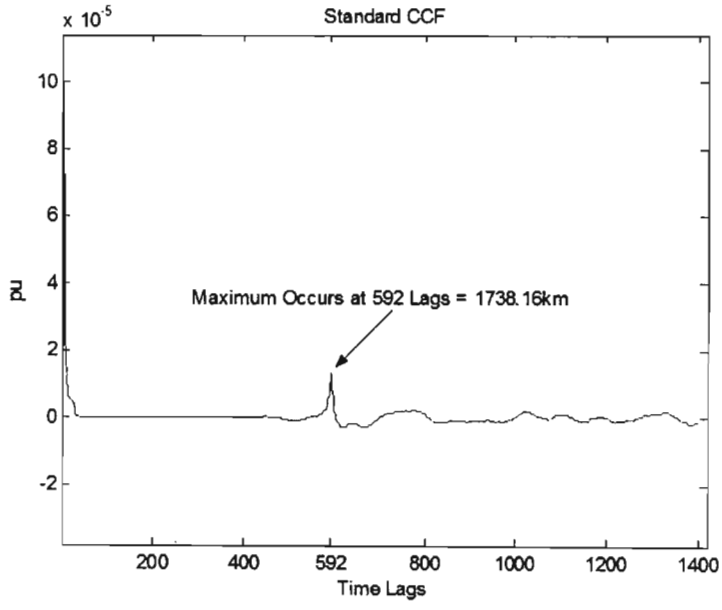

Fig 5.33. SCCF Output for unbalanced P-P-G Fault with 400Ω between poles at 1750kms

The same fault was again applied in the middle of the line, but this time with both a 400Ω fault resistance between the poles and a 400Ω ground fault resistance. The SCCF output of this is shown in Fig 5.34. Notice that in this case, the refracted wave has once again caused a minimum in the standard CCF at the fault point. The method of getting around this problem to allow the fault to be correctly detected has already been discussed.

The results of the bipole fault located at the centre of the transmission line has been discussed in detail here because this seems to be the only location on the transmission line, out of those considered, were the CCF encounters some problems. For bipole

faults at all other locations simulated, the faults have been located with a relatively high accuracy with all the bipole faults being correctly located by the standard CCF. Tables 5.8 and 5.9 indicate the results obtained for bipole faults at 25% and 95% of the line length respectively. Clearly from the results the standard CCF has been able to correctly locate the fault even with fault resistances as high as 400Ω.

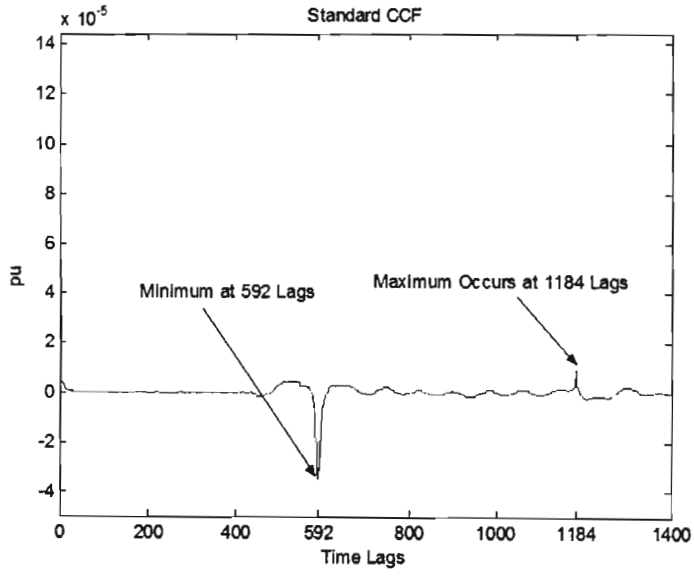

Fig 5.34. SCCF Output for unbalanced P-P-G Fault with 400Ω in both fault paths at 1750kms

Table 5.8. Fault Location Results for a Bipole Faults located at 875kms.

BIPOLE FAULTS AT 875KM (25% OF LL)						
Fault Resistance		Fault Type	Fault Location			% Error
Bipole	Ground		SCCF Equation (22)	ACCF Equation (46)	Final	
0Ω	Infinite	Bal	869.1km	N/A	869.1km	0.67%
0Ω	0Ω	Bal	869.1km	N/A	869.1km	0.67%
0Ω	400Ω	Bal	869.1km	N/A	869.1km	0.67%
400Ω	Infinite	Bal	869.1km	N/A	869.1km	0.67%
400Ω	0Ω	Bal	869.1km	N/A	869.1km	0.67%
400Ω	400Ω	Bal	869.1km	N/A	869.1km	0.67%
400Ω	0Ω	Unbal	869.1km	N/A	869.1km	0.67%
400Ω	400Ω	Unbal	869.1km	N/A	869.1km	0.67%

Table 5.9. Fault Location Results for a Bipole Faults located at 3325kms.

BIPOLE FAULTS AT 3325KM (95% OF LL)						
Fault Resistance		Fault Type	Fault Location			% Error
Bipole	Ground		SCCF Equation (22)	ACCF Equation (46)	Final	
0Ω	Infinite	Bal	3303.10km	170.3km	3303.10km	0.66%
0Ω	0Ω	Bal	3303.10km	170.3km	3303.10km	0.66%
0Ω	400Ω	Bal	3303.10km	170.3km	3303.10km	0.66%
400Ω	Infinite	Bal	3303.10km	170.3km	3303.10km	0.66%
400Ω	0Ω	Bal	3303.10km	170.3km	3303.10km	0.66%
400Ω	400Ω	Bal	3303.10km	170.3km	3303.10km	0.66%
400Ω	0Ω	Unbal	3303.10km	170.3km	3303.10km	0.66%
400Ω	400Ω	Unbal	3303.10km	170.3km	3303.10km	0.66%

5.4.3. Startup Faults

5.4.3.1. Faults existing prior to Startup\Restart

On detection of a fault, a fault clearance process is initiated to de-energize the faulted pole. Normally at least one attempt is made to re-energize the pole after a short pole deionization time. So in the case of a permanent fault if an attempt to re-energize the pole is made, the pole will be energized onto an existing fault.

In order to determine whether a restart is successful or not the dc line voltage is monitored. In the case of an existing fault, the fault clearance control system will detect a collapse in the dc line voltage and would then immediately initiate the fault clearance process. So clearly the protection system is not really required to be able to detect a fault that exists prior to the restart or startup process.

The author still, however, conducted simulations to check the protection system's ability to detect faults existing prior to restart. In order to simulate the above

condition, permanent faults were placed at various locations prior to startup. The HVDC system was then started up from a de-energized state with the permanent faults applied. The fault location results obtained are tabled in Table 5.10.

Table 5.10. Fault Location Results for a Fault Existing Prior to Startup

POLE TO GROUND FAULTS EXISTING PRIOR TO STARTUP					
Faulted Pole	Fault Distance	Fault Location Using Standard CCF Equation (22)	Fault Location Using Auxiliary CCF Equation (46)	Final Fault Location	Percentage Error
Positive	700km	692.92km	N/A	692.92km	-1.01%
Negative	700km	692.92km	N/A	692.92km	-1.01%
Positive	1400km	1388.77km	N/A	1388.77km	-0.80%
Negative	1400km	1388.77km	N/A	1388.77km	-0.80%
Positive	2100km	2084.62km	N/A	2084.62km	-0.73%
Negative	2100km	2084.62km	N/A	2084.62km	-0.73%
Positive	2800km	2780.47km	N/A	2780.47km	-0.69%
Negative	2800km	2780.47km	N/A	2780.47km	-0.69%
Positive	3150km	3129.87km	2780.47km	3129.87km	-0.64%
Negative	3150km	3129.87km	2780.47km	3129.87km	-0.64%

The results in Table 5.10 indicate that the protection system is capable of detecting and locating the above type of fault if necessary.

5.4.3.1. Faults Occurring During Startup

Faults may occur at anytime including during the HVDC system startup process. In order to ensure that the proposed protection system will be able to detect and locate faults occurring during startup, faults were placed on the system at various locations and times during startup.

Table 5.11 shows the simulation results obtained for P-G faults placed at various locations at time t equal to 100ms. This corresponds to 60ms after startup has been

initiated considering the converters are only deblocked at time t equal to 40ms. The results obtained are identical to that of table 5.10 above.

Table 5.12 shows the simulation results when pole to pole faults were applied at different locations during startup. From the simulation results in Tables 5.11 and 5.12, it is clear that the protection system is capable of locating faults occurring at startup just as accurately as it can locate faults occurring during steady state conditions.

Table 5.11. Fault Location Results for a P-G Faults occurring at Startup

POLE TO GROUND FAULTS OCCURING DURING STARTUP					
Faulted Pole	Actual Fault Location	Fault Location Using Standard CCF Equation (22)	Fault Location Using Auxiliary CCF Equation (46)	Final Fault Location	Percentage Error
Positive	700km	692.92km	N/A	692.92km	-1.01%
Negative	700km	692.92km	N/A	692.92km	-1.01%
Positive	1400km	1388.77km	N/A	1388.77km	-0.80%
Negative	1400km	1388.77km	N/A	1388.77km	-0.80%
Positive	2100km	2084.62km	N/A	2084.62km	-0.73%
Negative	2100km	2084.62km	N/A	2084.62km	-0.73%
Positive	2800km	2780.47km	N/A	2780.47km	-0.69%
Negative	2800km	2780.47km	N/A	2780.47km	-0.69%
Positive	3150km	3129.87km	2780.47km	3129.87km	-0.64%
Negative	3150km	3129.87km	2780.47km	3129.87km	-0.64%

Table 5.12. Fault Location Results for a Pole to Pole Faults occurring at Startup

BIPOLE FAULTS OCCURING DURING STARTUP				
Actual Fault Location	Fault location Using Standard CCF Equation (22)	Fault location Using Auxiliary CCF Equation (46)	Final Fault Location	Percentage Error
350km (10%)	346.46km	N/A	346.46km	-1.01%
1050km (30%)	1042.31km	N/A	1042.31km	-0.73%
1750km (50%)	1738.16km	N/A	1738.16km	-0.68%
2450km (70%)	2434.02km	N/A	2434.02km	-0.66%
3150km (90%)	3129.87km	2780.47km	3129.87km	-0.64%

5.4.4. Close in Faults

Let us consider a close in P-G fault located 20kms from the relaying point, Fig 5.35 and Fig 5.36 show the SCCF outputs for a P-G fault with zero and 400Ω fault resistance respectively. In both cases the faults are located relatively accurately with the SCCF output for the 400Ω case being much more flat due to the low reflection coefficient and high attenuation caused by the high resistance fault.

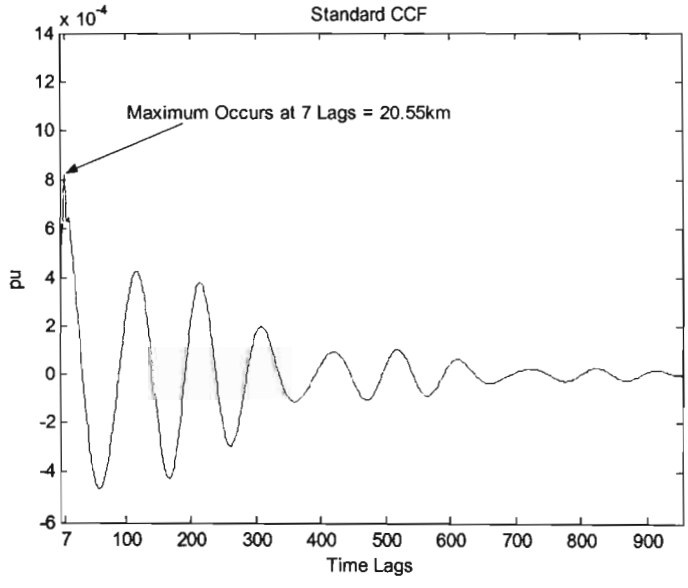

Fig 5.35. SCCF Output for P-G Fault at 20kms

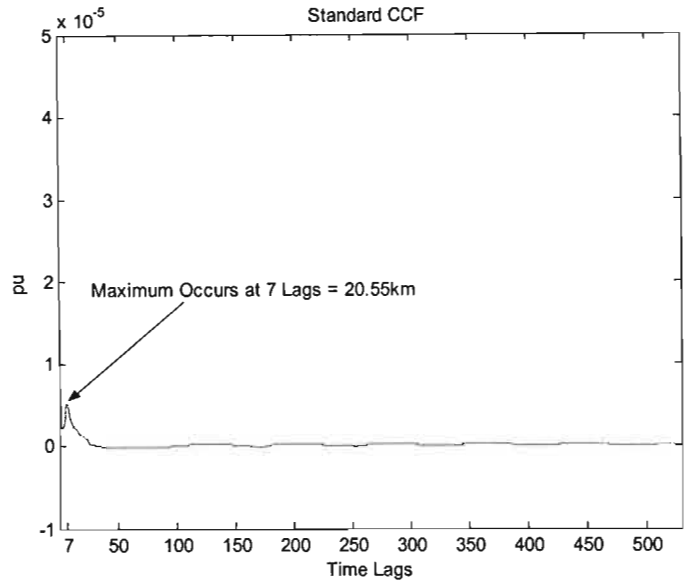

Fig 5.36. SCCF Output for P-G Fault with a 400Ω Fault Resistance at 20kms

Note there is a minimum fault location that the SCCF can report. This occurs at 1 time lag, with the actual minimum distance being dependent on the sampling rate and propagation velocity. With a sampling rate of 50 kHz and propagation velocity of 293.61 km/ms the minimum distance will be approximately 2.94km. Therefore any fault closer to the relay than 2.94km will report a distance of 2.94km or 5.88km (including a possible error of 1 time lag). The results obtained for close up fault simulations are given in Table 5.13.

Table 5.13. Fault Location Results for Close up Faults

FAULT LOCATION FOR CLOSE UP FAULTS					
Fault Type	Actual Fault Location	Fault Location Using Standard CCF Equation (22)	Fault Location Using Auxiliary CCF Equation (46)	Final Fault Location	Percentage Error
P-G	3km	5.88km	N/A	5.88km	96.00%
P-P	3km	5.88km	N/A	5.88km	96.00%
P-G	2.5km	5.88km	N/A	5.88km	135.20%
P-P	2.5km	5.88km	N/A	5.88km	135.20%
P-G	1km	2.94km	N/A	2.94km	194.00%
P-P	1km	2.94km	N/A	2.94km	194.00%
P-G	10m	2.94km	N/A	2.94km	29300%
P-P	10m	2.94km	N/A	2.94km	29300%
P-G	0m	2.94km	N/A	2.94km	Inf
P-P	0m	2.94km	N/A	2.94km	Inf

Clearly for the close up faults given in Table 5.13, the fault location reported by the protection system is incorrect. However, although the fault location maybe incorrect, the protection system is still able to detect a fault on the line and initiate fault clearance. The minimum fault location distance and the overall accuracy of the CCF can be improved by using a higher sampling rate if possible, however, this has other implications as explained earlier.

It will be desirable to detect and clear these close up faults as fast as possible. The proposed protection system can be used alone to detect and clear these faults, however, it will only detect the fault after the entire correlation process and fault location calculations are complete, which will take more than 28ms.

It is, therefore, proposed that this protection system be used in conjunction with the existing voltage derivative protection which is capable of detecting close up faults within a few milliseconds. Since the protection systems are not physically made up of different devices but are merely algorithms running on the HVDC system computer,

these two protection systems can easily be combined without any additional hardware. The above can be accomplished by incorporating the voltage derivative algorithm into the proposed protection system in order to enhance the protection response times for both close up and distant faults.

5.4.5. External Faults

So far all simulations conducted have been done to established the protection system's ability to accurately detect and locate faults occurring on the HVDC transmission line. Now let us look at the protection system's ability to recognize an external fault and act appropriately. Two types of external faults exist i.e. faults beyond the transmission line in front of the relaying point and faults behind the relaying point. Let us now look at the systems response to each type of fault.

5.4.5.1. External Faults behind the Relaying Point

In order to determine the protection response to this type of disturbance the following faults were simulated behind the relaying point.

- PP-G fault in DC yard.
- NP-G fault in DC yard.
- Bipole fault in DC yard.
- Three phase fault on AC System.
- Single phase fault on AC System.

Common to all these faults is the fact that they cause changes in the dc line voltage and current in the same direction, therefore, making it impossible for the starter threshold to be exceeded. The protection system is therefore stable for this case as none of these faults are capable of activating the protection system. Fig 5.37 shows the modal quantities for a NP-G fault behind the relaying point. Note the voltage and current waveforms change in the same direction when the fault occurs at 0.85s.

Fig 5.38 indicates that the starter has not picked up for this fault. Also note that in Fig 5.38 the fact that the relaying signals do not change simultaneously, is another clear indication, as explained in 3.2.4, that the fault is located behind the relaying point. Clearly a fault behind the relaying point poses no problem for the proposed protection system.

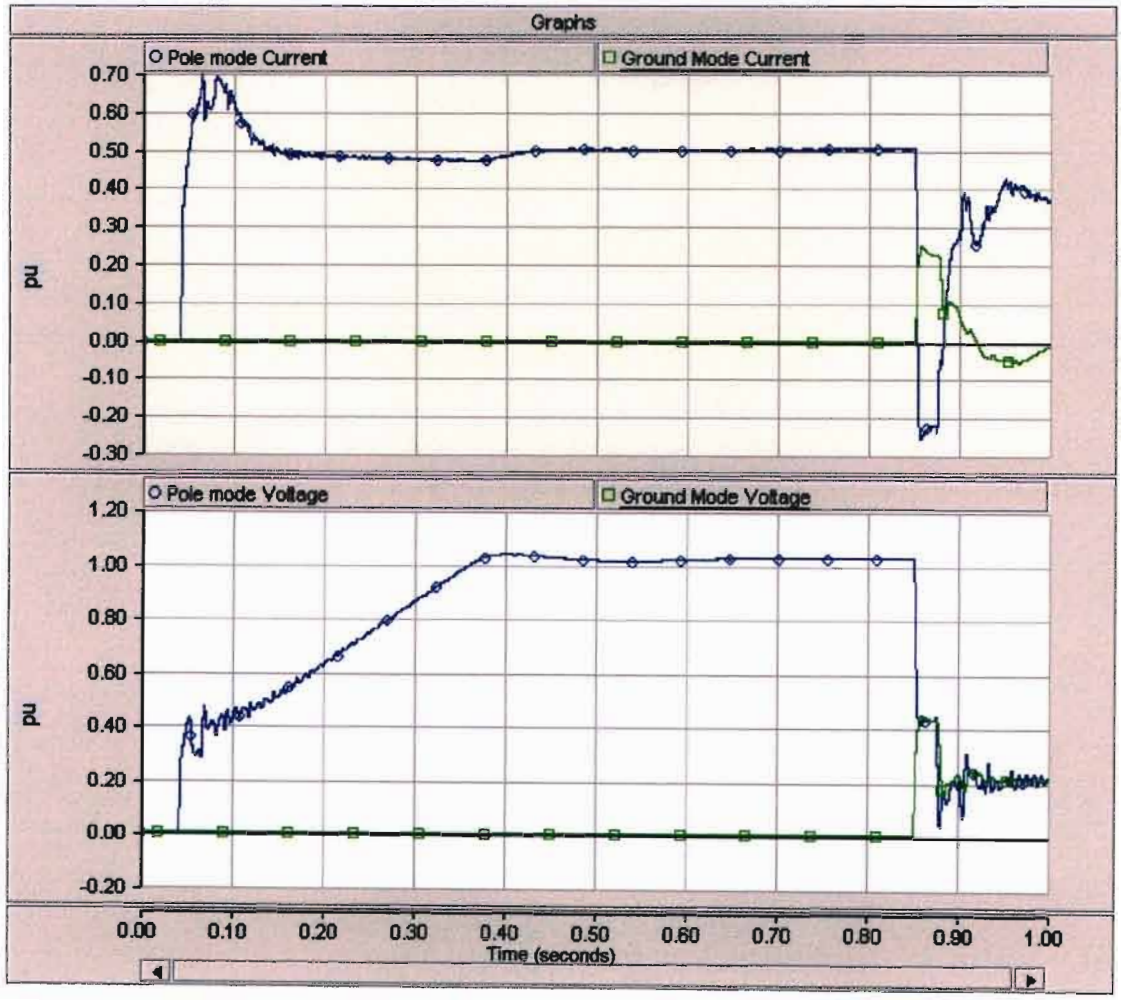

Fig 5.37. Modal Quantities for a Fault behind the Relaying Point

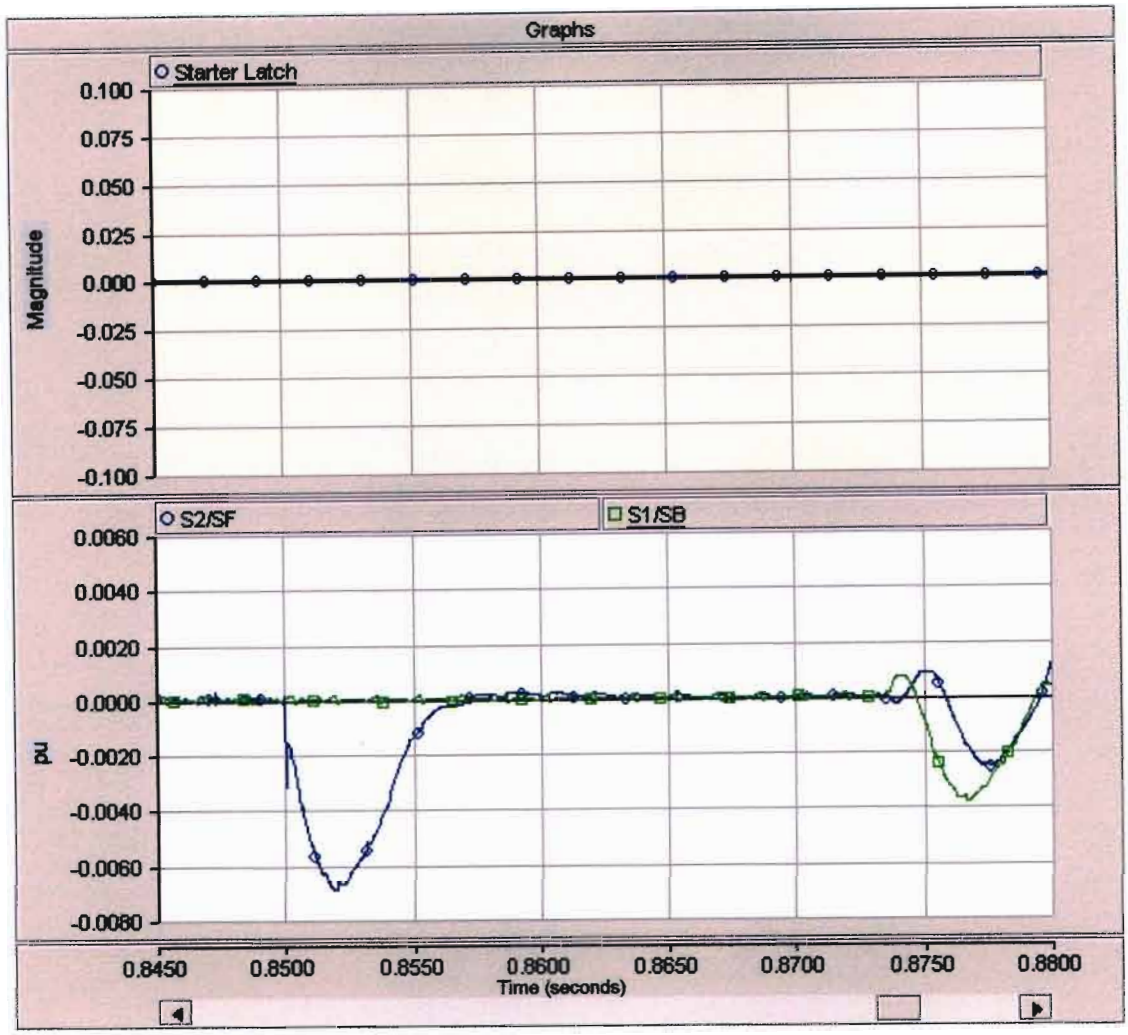

Fig 5.38. Starter and Relaying Signals for Fault behind the Relaying Point

5.4.5.2. External Faults in Front of the Relaying Point

External faults in front of the relaying points are not as easily determined as faults behind the relaying point as the changes in dc line voltage and current are the same as they are for faults on the line. The same faults as applied in 5.4.5.1 have been applied here except that the faults are now applied in front of the relaying point beyond the transmission line.

It should be noted that in this case none of the faults were able to cause enough changes in the dc line voltage and current to exceed the starter threshold. The above was possible because of the wave damping caused by the dc reactor, as the travelling

wave initiated by the external fault passed through the reactor. Therefore, the protection system in this case would not be started for these external faults.

Let us, however, say that the external fault managed to exceed the starter threshold and start the protection. The SCCF and ACCF output for a P-P fault in the DC yard would then be given by Figs 5.39 and 5.40 respectively. Since the ACCF indicates a distance greater than that of the SCCF, the ACCF is ignored and the final fault location is given by the SCCF.

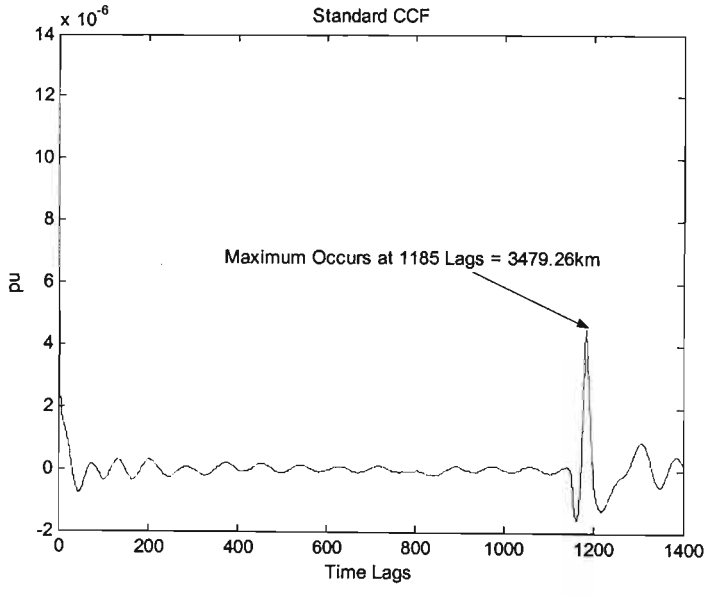

Fig 5.39. SCCF Output for External P-P Fault in Front of the Relaying Point

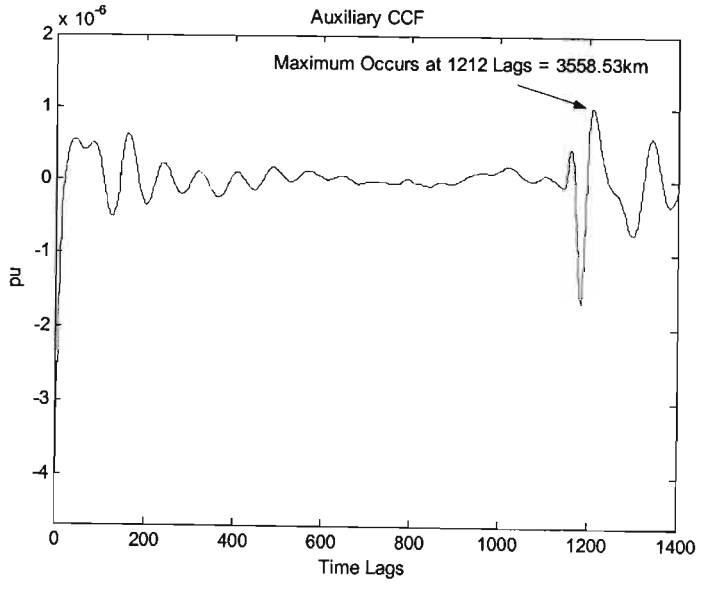

Fig 5.40. ACCF Output for External P-P Fault in Front of the Relaying Point

As expected, the SCCF returns a distance to fault approximately equal to the length of the line. The reason for the SCCF returning a distance to fault approximately equal to the length of the line is explained in 3.2.3. Since the returned distance is greater than 80% or 90% (depending on the setting) of the line, a timer will be started to give the converter station protection a chance to clear the fault. If the starter does not drop off before the timer expires, the protection system will assume the fault is still present and take the necessary action. In this case the line protection provides backup to the station protection.

5.4.6. Effect of the DC Filters on the Correlation Function.

All simulations conducted above were redone this time with the dc filters off. The results revealed that the dc filters did affect the magnitude of the CCF output. This could be expected since the reflection coefficients at the termination have changed. However the peaks were detected at the same time lag and therefore had no effect on the CCF ability to correctly locate the fault. This is illustrated in Figs 5.41 and 5.42 were the output of the SCCF is given for P-G faults at 80% of line with and without DC filters respectively. Clearly both provide the same result with the peak occurring at 946 time lags.

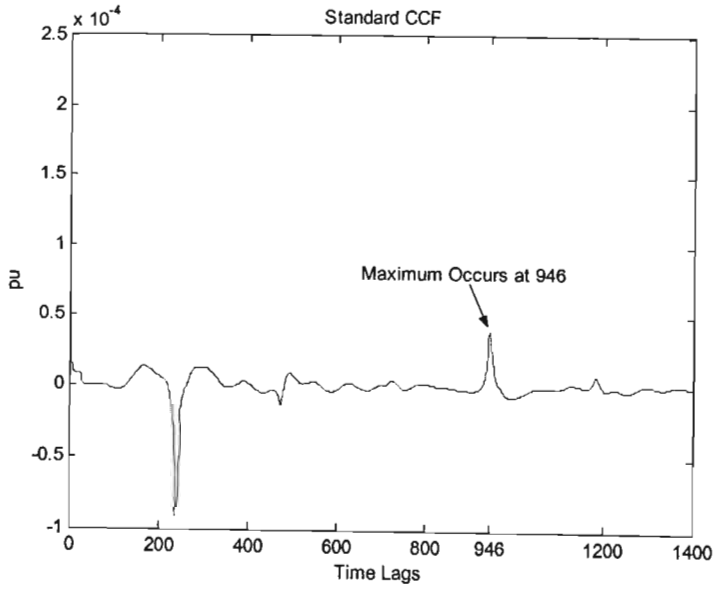

Fig 5.41. SCCF Output for P-G Fault at 80% of Line with DC Filters

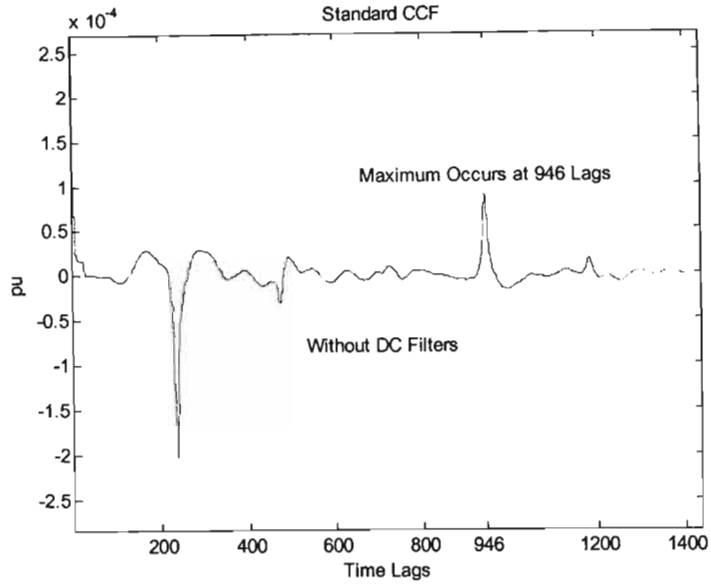

Fig 5.42. SCCF Output for P-G Fault at 80% of Line without DC Filters

It should be noted that the addition or removal of the DC filters may not only affect the magnitude of the reflection coefficient but may more importantly change the sign of the reflection coefficient at the termination. This may indeed have a negative impact on the performance of the correlation function and should be investigated further.

5.4.7. Effect of the Control System on the Correlation Function.

The control system of the HVDC system under study takes around 12ms to response to changes in the measured current. Since the proposed protection system takes longer than this time to detect and locate the fault, the author wished to investigate what effect the control system had on the standard CCF. Clearly from the simulation results obtained, the SCCF and ACCF have had very little difficulty in detecting the faults and the author just wished to compare the results of the standard CCF with and without the control system active.

In order to simulate the effect of no control action on the SCCF, all control action was blocked on detection of a fault and stayed blocked for the duration of the fault to insure that the changes in the relaying signals were only caused by the travelling waves setup by the fault. The effect of the control system would be more pronounced in distant faults where the maximum in the SCCF occurs after control action has

started. Therefore faults at 80, 90 and 100% of the line were used to make a comparison. The SCCF outputs for both the cases, with and without control action, were almost identical for faults at 80 and 90% of the line length.

Figs 5.43 and 5.44 show the results obtained for a fault at the end of the line with and without control action respectively. From the results obtained, it is clear that for this working case, control action has only reduced the magnitude of the SCCF and has had no effect on the fault location ability of the CCF.

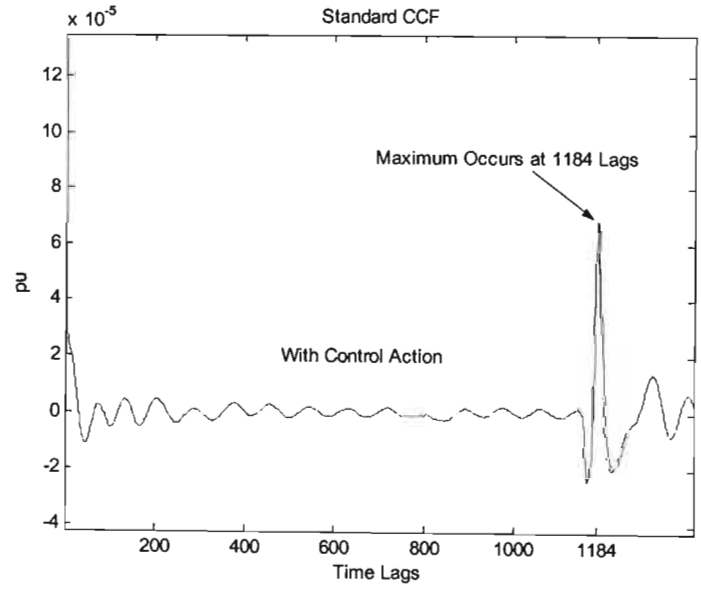

Fig 5.43. SCCF Output for P-G Fault at 100% of Line with Control Action

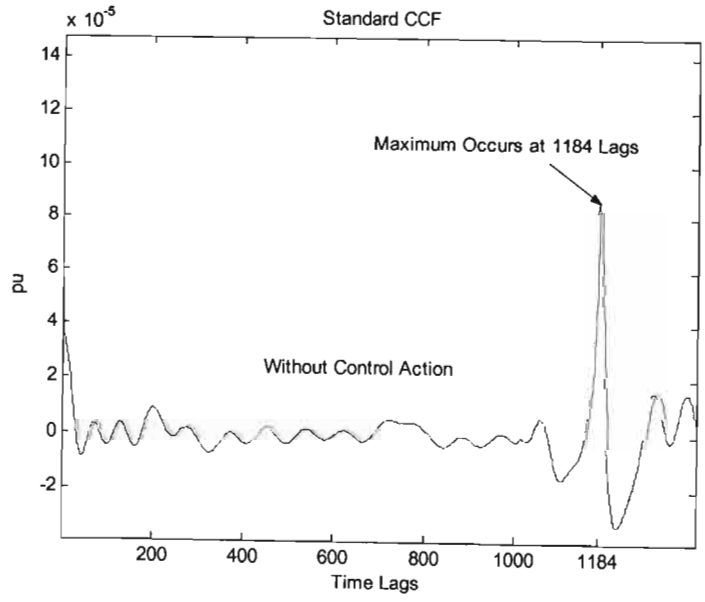

Fig 5.44. SCCF Output for P-G Fault at 100% of Line without Control Action

5.4.8. Fault Detection using Telecommunications Method

At the end of chapter 3 the author proposed a method of using the telecommunication infrastructure (TI), when available, to optimize the protection system. Lets us now examine the response of this method to various fault conditions.

Let us first consider a fault located 350kms from the rectifier. Figs 5.45 and 5.46 show the calculated starter values at the rectifier and inverter end for this fault respectively.

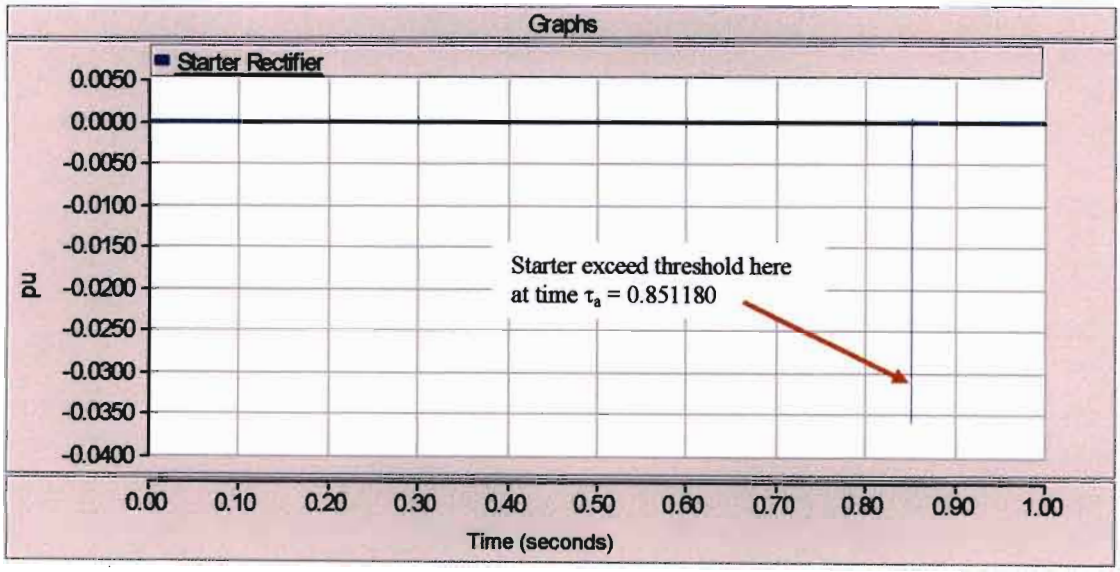

Fig 5.45. Calculated Rectifier Starter Values for a Fault at the 350kms

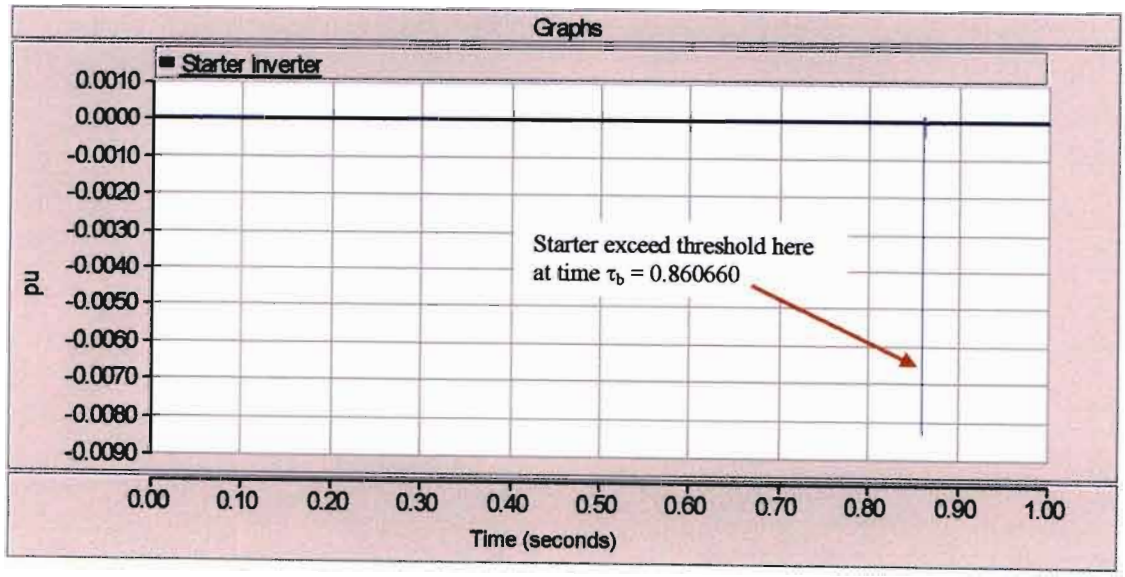

Fig 5.46. Calculated Inverter Starter Values for a Fault at the 350kms

The protection starters above are used to determine the arrival time of the incident travelling waves at the relaying point. The time at which the protection starter thresholds are exceeded are tagged for used by the protection system as shown in Figs 5.45 and 5.46. These times will now be used in (47) and (48) to locate the fault. Note in this case side *A* represents the rectifier end and side *B* represents the inverter end.

$$D_A = \frac{\ell + v(\tau_a - \tau_b)}{2} = \frac{3500 \times 10^3 + 293608598\ (0.851180 - 0.860660)}{2}$$

$$= 358.30\text{km}$$

$$D_B = \frac{\ell - v(\tau_a - \tau_b)}{2} = \frac{3500 \times 10^3 - 293608598\ (0.851180 - 0.860660)}{2}$$

$$= 3141.70\text{km}$$

Now D_{AB} can be calculated using (49) as follows

$$D_{AB} = \ell - D_B = 3500\text{km} - 3141.70\text{km} = 358.30\text{km}$$

Since D_A and D_{AB} are equal, condition (50) is met and a fault is located at 358.30km. Now if 358.30km is less than the threshold setting, condition (51) will also be met and the protection will initiate fault clearance. The polarity of the ground mode current will again be used to identify the faulted pole.

Faults were now applied at the same location (350km) with 50Ω, 100Ω, 200Ω and 400Ω fault resistances and exactly same results were acquired as shown in Table 5.14. It should be noted that this detection method will not be affected by fault impedance as the method is based on the detection of the incident pole mode quantities arriving at the relaying point due to the fault. The pole mode propagation velocities are not affected by fault resistance and, therefore, reach the relaying point at the same time irrespective of the fault resistance. Therefore, this protection method's ability to detect a fault on the transmission line is only limited by its starter threshold setting.

Bipole faults were also simulated at the same location and the results are tabled in Table 5.15. Again exactly the same results were obtained irrespective of the fault resistance.

Table 5.14. Fault Location Results using the TI for P-G Faults at 350kms

POLE TO GROUND FAULTS AT 350KM (10% OF LL)					
Faulted Pole	Fault Resistance	Incident Wave Time of Arrival at Rectifier	Incident Wave Time of Arrival at Inverter	Calculated Fault Location	Percentage Error
Positive	50 Ω	0.851180s	0.860660s	358.30km	2.37%
Negative	50 Ω	0.851180s	0.860660s	358.30km	2.37%
Positive	100 Ω	0.851180s	0.860660s	358.30km	2.37%
Negative	100 Ω	0.851180s	0.860660s	358.30km	2.37%
Positive	200 Ω	0.851180s	0.860660s	358.30km	2.37%
Negative	200 Ω	0.851180s	0.860660s	358.30km	2.37%
Positive	400 Ω	0.851180s	0.860660s	358.30km	2.37%
Negative	400 Ω	0.851180s	0.860660s	358.30km	2.37%

Table 5.15. Fault Location Results using the TI for Bipole Faults at 350kms

BIPOLE FAULTS AT 350KM (10% OF LL)						
Fault Resistance		Fault Type	Incident Wave Time of Arrival at Rectifier	Incident Wave Time of Arrival at Rectifier	Calculated Fault Location	% Error
Bipole	Ground					
0 Ω	Infinite	Bal	0.851180s	0.860660s	358.30km	2.37%
0 Ω	0 Ω	Bal	0.851180s	0.860660s	358.30km	2.37%
0 Ω	400 Ω	Bal	0.851180s	0.860660s	358.30km	2.37%
400 Ω	Infinite	Bal	0.851180s	0.860660s	358.30km	2.37%
400 Ω	0 Ω	Bal	0.851180s	0.860660s	358.30km	2.37%
400 Ω	400 Ω	Bal	0.851180s	0.860660s	358.30km	2.37%

400 Ω	0 Ω	Unbal	0.851180s	0.860660s	358.30km	2.37%
400 Ω	400 Ω	Unbal	0.851180s	0.860660s	358.30km	2.37%

The results of faults simulated at other locations on the transmission line are summarized in Table 5.16. Note that the fault location estimates were the same irrespective of the fault resistance and, therefore, only the results obtained for solid faults are shown in Table 5.16.

Table 5.16. Fault Location Results using TI for Faults at different locations.

FAULTS AT VARIOUS LOCATION ON THE TRANSMISSION LINE					
Faulted Type	Fault Location	Incident Wave Time of Arrival at Rectifier	Incident Wave Time of Arrival at Inverter	Calculated Fault Location	Percentage Error
P-G	1050km	0.853560s	0.858300s	1054.15km	0.40%
P-P/P-P-G	1050km	0.853560s	0.858300s	1054.15km	0.40%
P-G	1750km	0.855920s	0.855920s	1750.00km	0.00%
P-P/P-P-G	1750km	0.855920s	0.855920s	1750.00km	0.00%
P-G	2450km	0.858300s	0.853560s	2445.85km	-0.17%
P-P/P-P-G	2450km	0.858300s	0.853560s	2445.85km	-0.17%
P-G	3150km	0.860660s	0.851180s	3141.70km	-0.26%
P-P/P-P-G	3150km	0.860660s	0.851180s	3141.70km	-0.26%

Faults at various locations were also applied during startup (100ms) to examine the protection system's ability to locate faults developing during startup. The results obtained are shown in Table 5.17. Clearly no problems have been experienced locating these faults at startup. In fact all the faults simulated so far have been accurately located with no problem by this method that uses the telecommunications infrastructure.

External faults will pose no problem to this method because in the case of external faults, the fault will be located behind one of the relaying points. Therefore, the starter

at that relaying point will not pickup, thereby not allowing the protection system to become active.

Table 5.17. Fault Location Results using TI for Startup Faults at different locations.

STARTUP FAULTS AT VARIOUS LOCATION ON THE TRANSMISSION LINE					
Faulted Type	Fault Location	Incident Wave Time of Arrival at Rectifier	Incident Wave Time of Arrival at Inverter	Calculated Fault Location	Percentage Error
P-G	350km	0.101180s	0.110660s	358.30km	2.37%
P-P/P-P-G	350km	0.101180s	0.110660s	358.30km	2.37%
P-G	1050km	0.103560s	0.108300s	1054.15km	0.40%
P-P/P-P-G	1050km	0.103560s	0.108300s	1054.15km	0.40%
P-G	1750km	0.105920s	0.105920s	1750.00km	0.00%
P-P/P-P-G	1750km	0.105920s	0.105920s	1750.00km	0.00%
P-G	2450km	0.108300s	0.103560s	2445.85km	-0.17%
P-P/P-P-G	2450km	0.108300s	0.103560s	2445.85km	-0.17%
P-G	3150km	0.110660s	0.101180s	3141.70km	-0.26%
P-P/P-P-G	3150km	0.110660s	0.101180s	3141.70km	-0.26%

Control action should have little or no effect on this particular system as the detection is based on incident waves which in the HVDC system under study should reach the terminations before control action can be initiated.

As explained in 5.4.6, the DC side filters connected to the transmission line change the reflection coefficients at the terminations. Now since the relaying points are located at the terminations, the changes in voltage and current seen by the relaying point are due to the combination of the incident and reflected wave. This fact must be taken into account when setting the starter thresholds.

Note that if the protection range becomes limited by the use of the existing starter, then the changes in relaying signals (S_F *and* S_B) can be used as alternate starters. The above starter will provide the advantage of being able to distinguish between changes

caused incident and reflected wave and will, therefore, be independent of the type or configuration of dc filters used.

5.4.9. Fault Detection with One Pole Out of Service

Bipole HVDC Systems are designed to operate in monopole mode. This becomes necessary when one pole needs to be isolated due to maintenance or a permanent fault on the pole. In this case the respective converters are blocked and the pole is isolated and earthed. Power flow is then restored on the other pole with the ground providing the return path.

It is, therefore, essential that both proposed protection methods viz. the local detection method and the telecommunications method, be able to detect and locate a fault on the healthy pole under this contingency. In order to establish the protection system's ability to achieve this, the above contingency was simulated for both the positive and negative poles being out of service in turn. The same P-G faults as given in 5.4.1, 5.4.3, 5.4.4 and 5.4.8 were then simulated.

The fault location results obtained under this monopole contingency were identical to the results obtained in 5.4.1, 5.4.3, 5.4.4 and 5.4.8 for the respective P-G faults. The above indicates that both protection methods experienced no problems in locating these faults. Therefore, the overall protection system has no problem detecting faults under this contingency. Fig 5.47 shows the result obtained for a solid fault located at the centre of the line.

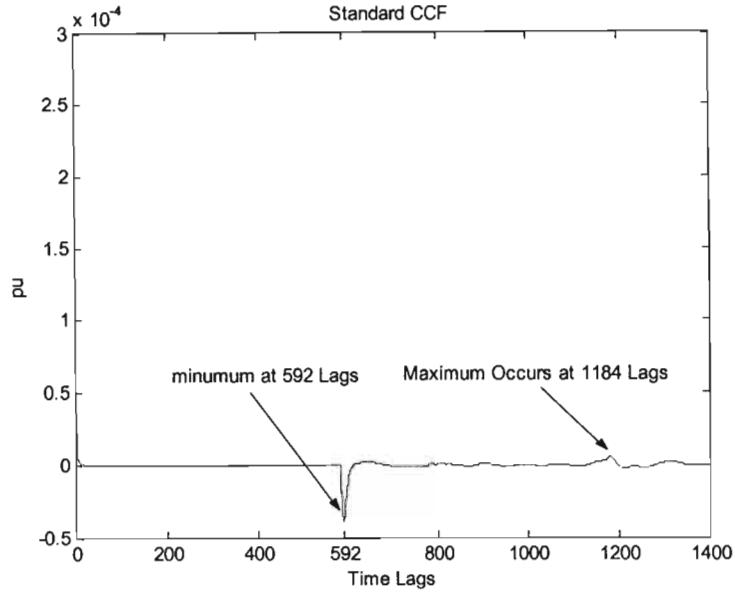

Fig 5.47. SCCF for P-G Fault at 1750kms under Monopole Condition.

It should be noted that in a true monopole system, a solid fault in the centre of the line will not cause a minimum peak but a maximum peak at the fault location as there is no refracted wave present for the above condition. However, as fault resistance is introduced, refraction starts to occur, and a local minimum can occur at the fault location when the fault resistance produces a refraction coefficient that is greater than the reflection coefficient.

The reason for the SCCF in Fig 5.47 still showing a minimum peak at the fault location under this monopole contingency, is that although the other pole conductor is not energized, it is still physically located in close proximity to the energized conductor. Therefore, coupling between the poles still occurs implying that the positive mode surge impedance is still terminated through the ground mode surge impedance at the fault point. This results in a high refraction coefficient that causes the minimum peak at the fault location in the SCCF. The only difference in this case (one pole out of service) as opposed to the normal bipole case, is that in this case the induced surges on the dead pole are shunted to ground and thus not allowed to reach the terminations.

Chapter 6: Conclusion and Recommendations

6.1. Conclusion

The initial part of the research work involved reviewing the current dc line protection systems and philosophies to assess their ability to adequately protect an ultra long HVDC transmission line. Upon reviewing the different types of currently used dc line protection systems, the author discovered that both the currently used dc line main protection systems are dependent on the fault loop impedance and, therefore, have limited protection coverage. This represents a major drawback in the dc line main protection systems which render them unsuitable for the protection of ultra long transmission lines.

The challenge and main focus of this research was to develop a dc line main protection system that is capable of protecting an ultra long HVDC transmission line. Also in order to improve the reliability of the protection system, the proposed system was to have the capability of detecting and clearing faults based solely on locally available quantities.

In order to address this challenge, the author first investigated the fault phenomena as applicable to HVDC transmission systems and then researched possible methods of identifying these faults. The author then used all this information to propose and develop a protection system that was suitable for protecting ultra long HVDC transmission lines.

As required the protection system is capable of detecting and locating faults using only the quantities available at the local relaying point. The author, however, suggested that when the telecommunication infrastructure is available it should be used to try and optimize the overall response of the protection system. The author also proposed and developed a method of accomplishing this.

The author then finally recommended that the above protection system be used in conjunction with the existing voltage derivative protection which is capable of

detecting close up faults within a few milliseconds. The above recommendation can be accomplished by incorporating the voltage derivative algorithm into the proposed protection system in order to enhance the protection response times for both close up and distant faults.

The proposed protection system was tested on a 500kV Bipole, HVDC System Model, using computer simulations in EMTDC™ and Matlab®. Extensive fault simulations covering various scenarios were conducted in order to evaluate the performance of the protection system.

With regards to local detection method, the cross-correlation function produced excellent results, locating the faults with high accuracy for all scenarios except for a fault located at the centre of the line. The reason for this has been explained and a solution to overcome this problem has been discussed and implemented. The only drawback of the solution is that it involves the use of both the standard and auxiliary CCF, which effectively doubles the protection response time, even for solid faults located in the middle of the line.

The simulated faults were again located with a very high accuracy when the telecommunication assisted method was used. This method had no problem locating any of the fault conditions simulated.

It should be noted that both the local detection and telecommunication methods have a minimum distance that they can detect which is dependent on the sampling rate and propagation velocity. All this implies is that when a fault is located closer than this minimum distance, the protection system will return a distance to fault equal to the minimum distance. This poses no problem as the fault will still be detected and cleared correctly, only the distance to fault may be incorrect.

The various faults were also simulated with dc filters removed. This proved to have no effect on the fault location ability of the overall protection system for this study case. The effect of the control system was also investigated and again proved to have

no effect on the fault location estimates provided by the protection system for the case under study.

The overall performance of the proposed protection system is extremely good. It is the opinion of the author that the proposed protection scheme can be successfully applied to but not limited to HVDC systems with ultra long transmission lines.

6.2. Recommendations for Further Work

1. The size of the sample or template used in the CCF was arbitrarily chosen in this work. Although this produced acceptable results, research into ways of determining the optimal sample size should be untaken.

2. The CCF experiences a problem when both the reflected and refracted waves reach the relaying point at the same time. Although a solution to this has been implemented, it has certain drawbacks. The author, therefore, suggests that other signal processing techniques (e.g. wavelet transforms, pattern recognition) be investigated to determine the most appropriate method for use with this protection system.

3. Although the addition and removal of DC filters in this case study has not affected the ability of the protection system to locate faults, the author recommends that further research be conducted into the effects of different dc filter types and configuration, on the protection system since dc filters and shunt capacitors can change not only the magnitude of the reflection coefficient but also its sign, which may have a negative impact on the CCF.

4. The control system in this case study has only a minimal effect on the magnitude of the CCF at distant faults. It has in no way affected the fault location estimates. The author however recommends further investigation when longer lines or faster control systems are adopted.

5. The protection system should also be tested on HVDC systems with different voltage and power levels as well as different line configurations in order to determine its versatility.

6. This research has assumed that the noise present in the physical voltage and currents signals could be effectively filtered out prior to the correlation process. Further research regarding the noise filtering process is required.

References

1. R. Rudervall, J.P. Charpentier and R. Sharma, "High Voltage Direct Current (HVDC) Transmission Systems Technology Review Paper", Energy Week 2000, March 2000.

2. L. Carlsson, "Classical HVDC: Still Continuing to Evolve", Modern Power Systems, June 2002, pp 19-21.

3. K.A. Folly, "Power System Modelling and Analysis Course Notes", University of Durban-Westville, Faculty of Engineering, HVDC Centre, 2003.

4. J.J. Grainger and W.D. Stevenson, "Power System Analysis", Electrical Engineering Series, McGraw-Hill, 1994.

5. J. Ammon, H. Huang, A. Kumar, H.P. Lips, M. Pereira, K. Sadek and G. Wild, "Innovations in HVDC Technology", October 2000.

6. F. Venter, "HVDC Design and Operation Course Notes", University of Durban-Westville, Faculty of Engineering, HVDC Centre, 2003.

7. "High Voltage Direct Current Handbook", First Edition, EPRI, 1994.

8. U. Astrom, B. Westman, V. Lescale and G. Asplund, "Power Transmission with HVDC at Voltages Above 600kV", Conference Proceedings, IEEE PES2005 Conference and Exposition in Africa, Durban, July 2005, pp. 44-50.

9. G. Asplund, U. Astrom and D. Wu, "Advantage of HVDC transmission at 800kV", Conference Proceedings, XIV International Symposium on High Voltage Engineering, Beijing, August 2005, Paper K03.

10. W. Breuer, D. Povh, D. Retzmann, E Teltsch and X. Lei, "Role of HVDC and FACTS in future Power Systems", Conference Proceedings, CEPSI 04, Shanghai, 2004, pp. 1-21.

11. P. Naidoo, B. Mbuere, G. Kelesitse, J. Ventura and M. Musanda, "The Western Corridor Project – The Planning for Large Scale Hydro Electric Power Generation and Transmission across Southern Africa", Conference Proceedings, IEEE PES2005 Conference and Exposition in Africa, Durban, July 2005, pp. 2-6.

12. "DPL 100 Series – Performance Testing and Evaluation", ABB Technical Report, Internal Document No. JN000435, 2002.

13. E. Francocci, "Automatic Control for a HVDC Transmission Scheme", MSc Dissertation, University of Witwatersrand, 1986.

14. J. Arrillaga, "High Voltage Direct Current Transmission", Power Engineering Series 6, London: Peter Peregrinus Ltd, 1983.

15. "DLP 100 Series (DC High Voltage/Cable Protections)", ABB Guidelines, March 2002.

16. "DLP 120 DC line protection (Travelling Wave)", ABB Guidelines, March 2002.

17. D.C. Smith, "The Telecommunications System installed on the Apollo-Cahora Bassa HVDC Scheme", Transmission Engineering, Eskom, 2000.

18. J. Kauferle and D. Povh, "Concepts of Overvoltage and Overcurrent Protection of HVDC Converters", CIGRE 1979, Paper 14-08.

19. S. Madan, K.E. Bollinger and S.K. Banerjee, "Microprocessor Based HVDC Converter Protection", Conference Proceedings, Canadian Conference on Electrical and Computer Engineering, Vol.2, 1996, pp. 750-753.

20. F. Ming, J. Shufei, J. Lianwei, C. Shousun, Z. Wang, G. Hongguang and C. Jie, "HVDC Protection System Based Multiprocessor", Conference Proceedings, ICEE International Conference on Electrical Engineering, Vol 1, 1996, pp. 619-623.

21. W. Becker, S. Ranade, E. Rumpf and T.Wess, "Control System for the Cahora Bassa HVDC Scheme Design Criteria – Simulator Studies", CIGRE 1976, Paper 14-06.

22. A. Ekstrom and G. Liss, "Basic Problems of Control and Protection of Multiterminal HVDC Schemes with and without DC Switching Devices", CIGRE 1977, Paper 14-08.

23. G. Mazur, R. Carryer, S.T. Ranade, T Weß, "Converter control and protection of the Nelson River HVDC Bipole 2 – Commissioning and first year of commercial operation", IEEE Transactions on Power Apparatus and Systems, Vol. PAS - 100, No.1, January 1981, pp. 327-335.

24. L.V. Bewley, "Travelling Waves on Transmission Systems", Second Edition, John Wiley & Sons, Inc, New York, 1951.

25. E.W. Kimbark, "Transient Overvoltages caused by Monopolar Ground Fault on Bipole DC Line: Theory and Simulation", IEEE Transactions on Power Apparatus and Systems, Vol. PAS - 89, No.4, April 1970, pp. 584-592.

26. H.G. Hingorani, "Transient Overvoltage on Bipolar HVDC Overhead Line caused by DC Line Faults", IEEE Transactions on Power Apparatus and systems, Vol. PAS - 89, No.4, April 1970, pp. 592-610.

27. H. Takeda, H. Ayakawa, M. Tsumenaga and M. Sanpel, "New Protection Method for HVDC Lines including Cables", IEEE Transactions on Power Delivery, Vol. 10, No.4, October 1995, pp. 2035-2039.

28. Y. Kato, A. Watanabe, H. Konishi, T. Kawai, Y. Inoue and M. Sanpei, "Cable Section Fault Detection For HVDC Line Protection", IEEE Transactions on Power Delivery, Vol.1, No.3, July 1986, pp. 332-336.

29. S. Jamali and A. Ghezeljeh, "Fault Location on Transmission Line Using High Frequency Travelling Waves", Conference Proceedings, International Conference on Power Systems Transients, New Orleans, 2003.

30. J. D. Glover, M.S. Sarma, "Power System Analysis and Design", Third Edition, Thomson Learning, Inc, 2002.

31. "Travelling wave fault location in Power Transmission Systems", HP Application Guide 1285, February 1997.

32. E.H. Shehab-Eldin and P.G. McLaren, "Travelling wave distance protection - Problems areas and solutions", IEEE Transactions on Power Delivery, Vol.3, No. 3, July 1988, pp.894-902.

33. M. Chamia and S. Liberman, "Ultra high speed relay for EHV/UHV transmission lines-development, design and application", IEEE Transactions on Power Apparatus and Systems, Vol. PAS-97, No.6, November/December 1978, pp. 2104-2116.

34. G.W. Swift, "The spectra of fault induced transients", IEEE Transactions on Power Apparatus and Systems, Vol. PAS.98, No.3, May/June 1979, pp. 940-947.

35. M. Vitins, "A correlation method for transmission line protection", IEEE Transactions on Power Apparatus and Systems, Vol. PAS-97, No.5, September/October 1978, pp.1607-1617.

36. P.A. Crossley, and Mclaren, "Distance protection based on travelling waves", IEEE Transactions on Power Apparatus and Systems, Vol. PAS-102, No.9, September 1983, pp. 2971-2983.

37. L. Jie, S. Elangovan and J.B.X. Devotta, "Adaptive Travelling Wave Protection Algorithm Using Two Correlation Functions", IEEE Transactions on Power Delivery, Vol.14, No.1, January 1999, pp.126-131.

38. E.C. Ifeacher and B.W. Jervis, "Digital Signal Processing, A Practical Approach", Second Edition, Prentice Hall, 2002.

39. C. Christopoulos, D.W.P. Thomas and A. Wright, "Signal Processing and Discriminating Techniques Incorporated in a Protective Scheme based on Travelling Waves", IEE Proceedings, Vol. 136, No. 5, September 1989, pp. 279-288.

40. "EMTDC User Guide", Manitoba HVDC Research Centre, Manitoba, Canada, 2003.

41. "PSCAD User Guide", Manitoba HVDC Research Centre, Manitoba, Canada, 2003.

42. D. Muthumuni (dharshana@hvdc.ca), "Re: HVDC Monopole and Bipole System Model for PSCAD 4.0.3", E-mail to D. Naidoo (naidoodr@eskom.co.za), 14 September 2004.

43. M. Szechtman, T. Wess and C.V. Thio, "First Benchmark Model for HVDC Control Studies", Electra, No. 135, April 1991.

44. F.J. Havran, "Fault Investigations on the Power Transmission System", Eskom Transmission, October, 1999.

45. F.J. Havran, "Protection Components Course Notes", University of KwaZulu-Natal, Faculty of Engineering, HVDC Centre, 2004.

46. C.R. Mason, "The Art and Science of Protective Relaying", John Wiley & Sons Inc, 1956.

47. "Transmission Integrated Plant Performance System (TIPS) Database", Eskom Transmission, October, 2000.

Appendix A

Matlab M Files

```
function fault = protectsystem(sf,sb,psl,numlags,v,ds,pre,post)
%Algorithm for proposed protection system.
%
% input "protectsystem(sf,sb,psl,numlags,v,ds,pre,post)" where
%
% psl is the protection starter latch signal from EMTDC.
% sf & sb are the relaying signals from EMTDC.
% numlags is the number of lags to be calculated.
% v is the propagation velocity in m/s.
% ds is the distance protection setting in km.
% pre and post represent the number of pre and postfault samples taken.
[b,f,t] = datainput(psl,sf,sb,pre,post,numlags);
%b is the backward travelling wave.
%f is the forward travelling wave.
%t is the sample to be using for the standard crosscorrelation function.
[standard,auxiliary,index] = comcorr(b,f,t,numlags,'y'); % calls comcorr.m to calculate the CCF's.
samplerate = 50000; % sampling rate set to 50kHz.
traveltime = ((index-1)/samplerate);
df1 = (v*traveltime)/(2*1000); % first distance to fault calculation.

if df1 < ds % checks distance against threshold setting to determine if fault is to be cleared instantaneously.
   instfault = sprintf('Fault detected at %4.2fkm and cleared instantaneously',df1); % sets display format for output.
   disp(instfault); %display fault detection information
 else
   auxiliarymax = 0;
   a = numlags;    % determine size of correlation window.
   for auxcounter = 2:a %proceedure to determine the maximum in the auxiliary CCF.
      if auxiliary(auxcounter)>auxiliary(auxcounter-1) & auxiliary(auxcounter)>auxiliary(auxcounter+1)
         if auxiliary(auxcounter)>auxiliarymax
          auxiliarymax = auxiliary(auxcounter); %determines index at which maximum occurs.
          auxindex = auxcounter-1; % 1 is substracted from the index because zerolags corresponds to auxiliary(1)
         end
      end
   end
   df2 =(v*((index-auxindex-2)/samplerate))/2000; % second distance to fault calculation
    if df2 < 0 % if df2 is negative, df1 estimates are used.
      question = input('Is the protection starter still active (y/n) : ');
      if question == 'y' % if protection starter still active, fault cleared after time delay.
         timefault =sprintf('Fault detected at %4.2fkm and cleared after set time delay',df1);
         disp(timefault); %display fault detection information
      else
         disp('Fault not detected on transmission line');
      end
   else
      hr = (index-auxindex-1); %should be a local max in SCCF here if high resistance fault.
      std = standard; % just used to shorten the name for the next line.
      if (std(hr)>std(hr-1) & std(hr)>std(hr+1))|(std(hr+1)>std(hr) & std(hr+1)>std(hr+2))|(std(hr-1)>std(hr-2) & std(hr-
1)>std(hr))
         hrfault = df2; % This procedure checks if the is a local max around df2 in the SCCF. An error of +- one time lag allowed.
         if df2 < ds %checks distance against threshold setting.
```

```
        timefault =sprintf('High resistance fault detected at %4.2fkm and cleared without additional time delay',df2);
        disp(timefault); %display fault detection information
      else
        question = input('Is the protection starter still active (y/n) : ');
          if question == 'y' % if protection starter still active, fault cleared after time delay.
            timefault =sprintf('High resistance fault detected at %4.2fkm and cleared after set time delay',df2);
            disp(timefault); %display fault detection information
          else
            disp('Fault not detected on transmission line');
          end
        end
    elseif abs(1-(auxindex/(index-1-auxindex)))< 0.005 % checks if ACCF Max approx equal to df2, 0.5% error allowed.
      midfault = sprintf('Midpoint fault detected at %4.2fkm and cleared without additional timedelay',df2);
      % if above true midpoint fault assumed.
      disp(midfault); %display fault detection information
    else
      question = input('Is the protection starter still active (y/n) : ');
          if question == 'y' % if protection starter still active, fault cleared after time delay.
            timefault = sprintf('Fault detected at %4.2fkm and cleared after set time delay',df1);
            disp(timefault); %display fault detection information
          else
            disp('Fault not detected on transmission line');
          end
      end
  end
end
```

```
function [b,f,t] = datainput(psl,sf,sb,pre,post,corrtime)
%DATAINPUT Summary of this function goes here
%input as follows datainput(psl,sf,sb,pre,post,corrtime) where
% psl is the protection starter latch signal from EMTDC.
% sf & sb are the relaying signals from EMTDC.
% pre and post represent the number of pre and postfault samples taken.
% corrtime is duration of correlation process
x=length(psl);
activetest = 0; % used to test if protection starter is activated.
for counter = 1:x
   activetest = activetest + psl(counter);
   if psl(counter)==1 % determines when the starter has been activated.
      startlatch = counter;
      break;
   end
end

if activetest < 1 % check to see if protection starter has been activated.
   disp('Protection starter not activated');
   break;
end

storestart = startlatch - pre; % time from which template will be stored based on prefault data required.
templength = pre + post; % determines template length
for tempcount = 1:templength
   t(tempcount) = -sf(tempcount+storestart-1); % storing of templated with required prefault data. Note -sf used as template
end
correlationtime = corrtime; % correlation time used
relayfunlength = templength + correlationtime + 1; % sets length of relaying functions to be used by the protection system
for relay = 1:relayfunlength
   f(relay)= sf(relay+storestart-1); % determines section of forward travelling wave to be used for ACCF process
   b(relay) = sb(relay+storestart-1); % determines section of backward travelling wave to be used for SCCF process
end
```

```
function [standard,auxiliary,index] = comcorr(b,f,t,numlags,auto)
%calculates both the standard and auxiliary crosscorrelation function using
%samplecorr.m developed for sampled mean removed crosscorrelation.
% input as follows comcorr(b,f,t,numlags,auto)
%b is the backward travelling wave
%f is the forward travelling wave
%t is the sample to be using for the standard crosscorrelation function
%numlags is the number of lags to be calculated.
%auto – set to 'y' to automatically calculate the auxiliary crosscorrelation function otherwise set to 'n'
standard = samplecorr(b,t,numlags); % performs sampled crosscorrelation.
s = length(standard); % determine size of correlation vector.
standardmax = 0; % sets value for maximum comparison equal to zero.
if auto == 'n' % allows maximum at which aux function is calculated to be manually selected.
   question = input('Enter Lag at which Maximum Correlator output is assumed : ');
   index = question + 1;
else
   for counter = 2:numlags % standard(1) will be the global max as this represent the autocorrelation of the template. Therefore,
counter started from 2.
      if standard(counter)>standard(counter-1) & standard(counter)>standard(counter+1)
         if standard(counter)>standardmax
          standardmax = standard(counter); %determines index at which max correlation occurs.
          index = counter;
         end
      end
   end
end
inc = 1; % index for template2
incsize= length(t); % size of original template
templength = index + incsize; % calculates last index of template2
for counter2 = index:templength
   template2(inc) = b(counter2); %creation of template2
   inc = inc+1;
end
auxiliary = samplecorr(f,template2,numlags); %performs auxiliary crosscorrelation function.
```

```
function result = samplecorr (a,template,numlags)
% Function to calculate mean value removed crosscorrelation from a sample
% "template" is the sample data while "dataset" is the data vector to be time shifted
% "maxlags" represents the max number of lags to be applied
% INPUT as follows samplecorr(dataset,template,maxlags)
% NOTE THAT RESULT(1) REPRESENTS NO LAG
% THEREFORE WHEN READING DATA NOTE THAT THE LAG IS ALWAYS THE NUMBER
% MINUS 1, These is due to the fact that RESULT(0) does not exist
% THE PLOT HAS BEEN CORRECTED TO INDICATE THE CORRECT VALUES

n = length(template); % determines the size of data sample
m = n-1; % amount by which data sample should be extended
x = length(a); % determines size of correlation window
templatemean = mean(template); % calculated template mean
templatecorr = template - templatemean; % mean removed template for correlation

if numlags > x-1 % check if max number of lags are not exceeded
   disp('Error : Number of Lags greater than data sample size??????????');
   return
end

if numlags > x-n % Warning of possible errors
   disp('Warning : The number of lags entered required requires extension of dataset, possible errors may occur at the later lags')
   disp('Extension of dataset will solve this problem')
end

for extend = 1:m
   a(x+extend)= 0; % extend the data sample to cover the correlation window%
end

for shift = 1:numlags+1 %numlags extended by 1 since starting value = 1 instead of zero
   correlation = 0; % initializes the variable correlation
   for count = 1:n
      temp(count) = a(count+shift-1); % development of matched data sets%
   end
   datamean = mean(temp);
   datacorr = temp - datamean;

      for sumcount = 1:n
         increment =templatecorr(sumcount)*datacorr(sumcount);
         correlation = correlation + increment;
      end

   result(shift) = correlation/n; % Correlation Coefficent Calculation%
   lag(shift)=shift-1; % Shifts the plot by one to correct the number of lags%
end
figure;
plot(lag,result); % plots the correlation outputs %
result = result';
return
```

Appendix B

EMTDC Models

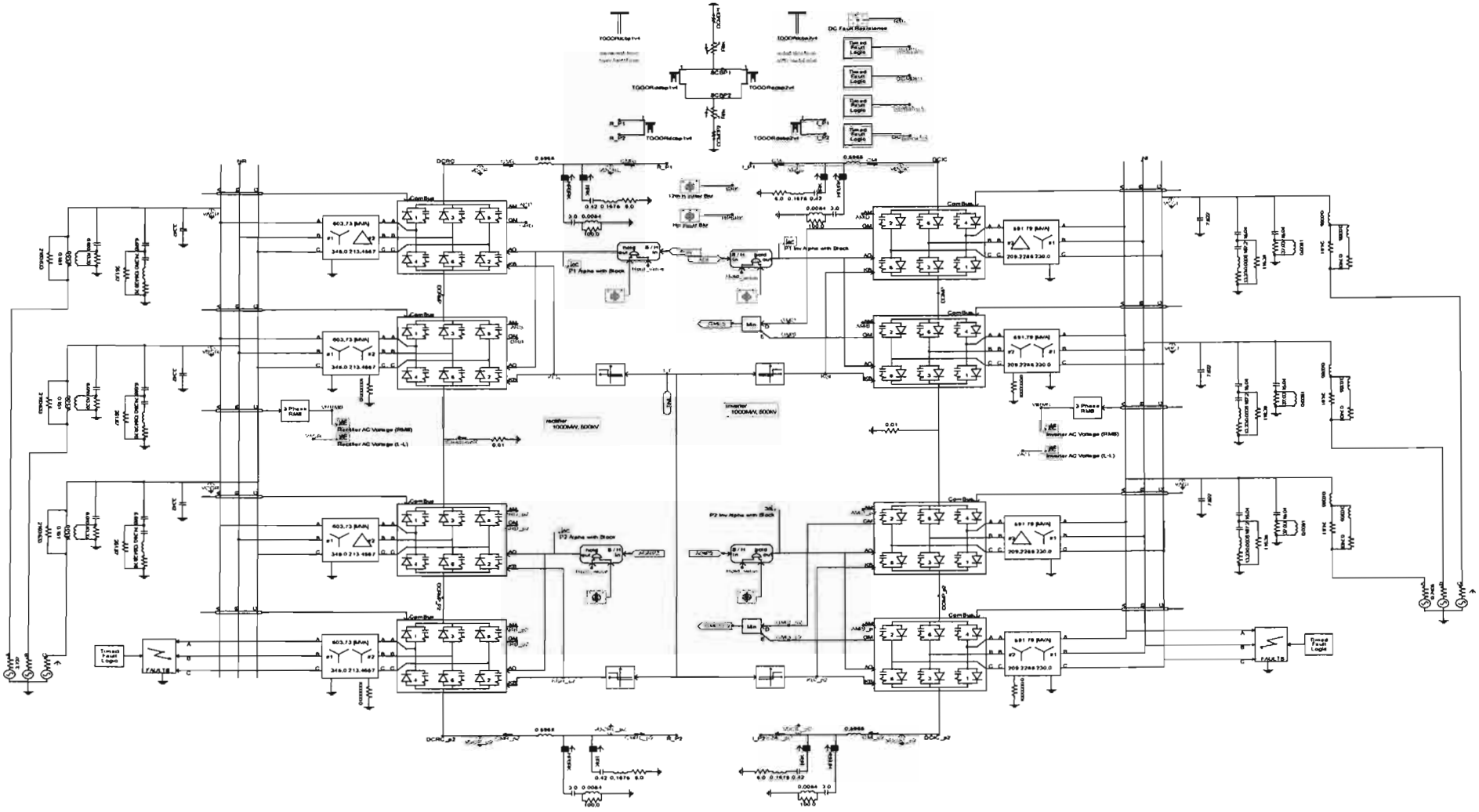

Fig B.1. Modified HVDC System Model.

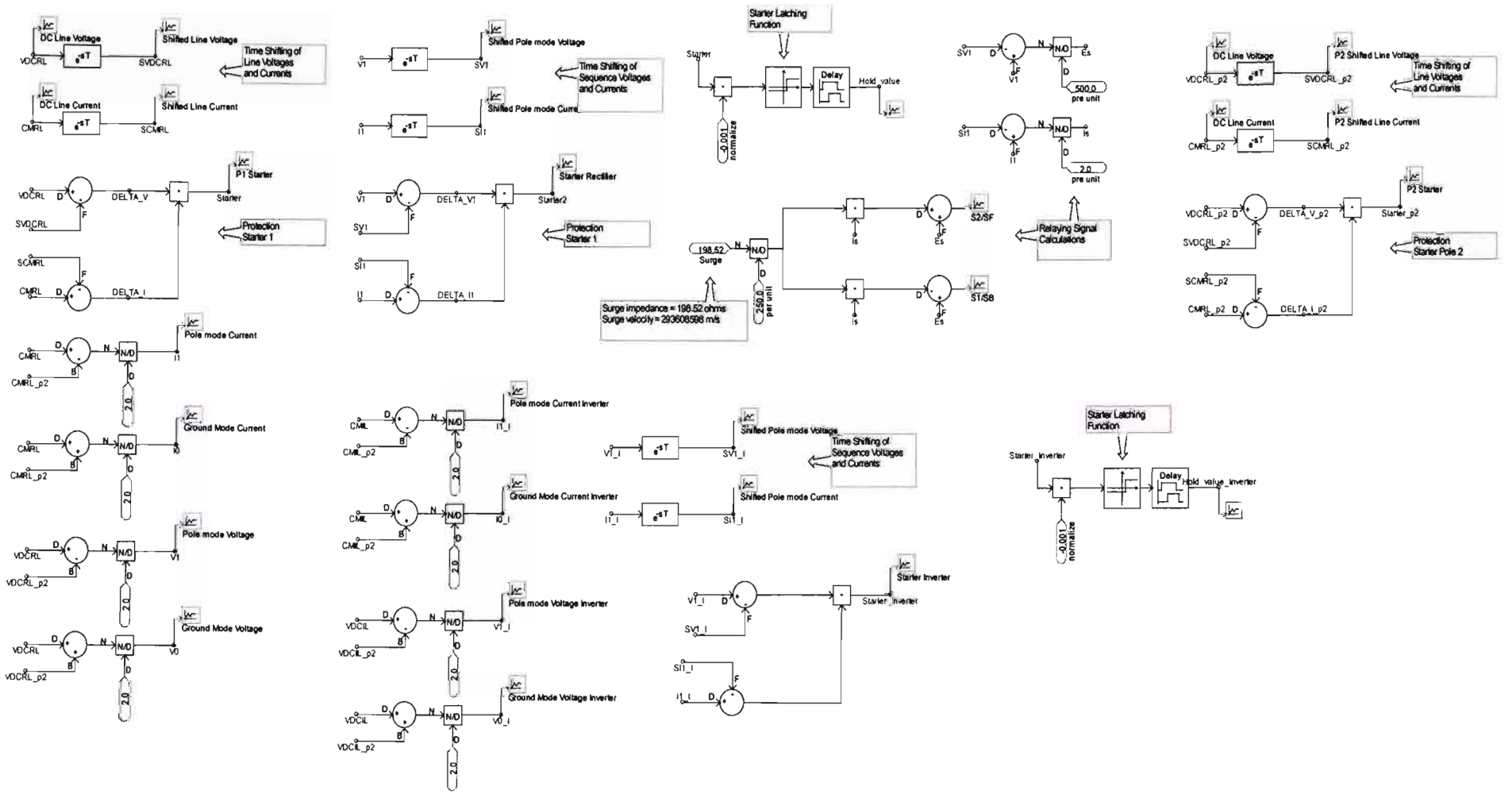

Fig B.2. Protection System Modelling.

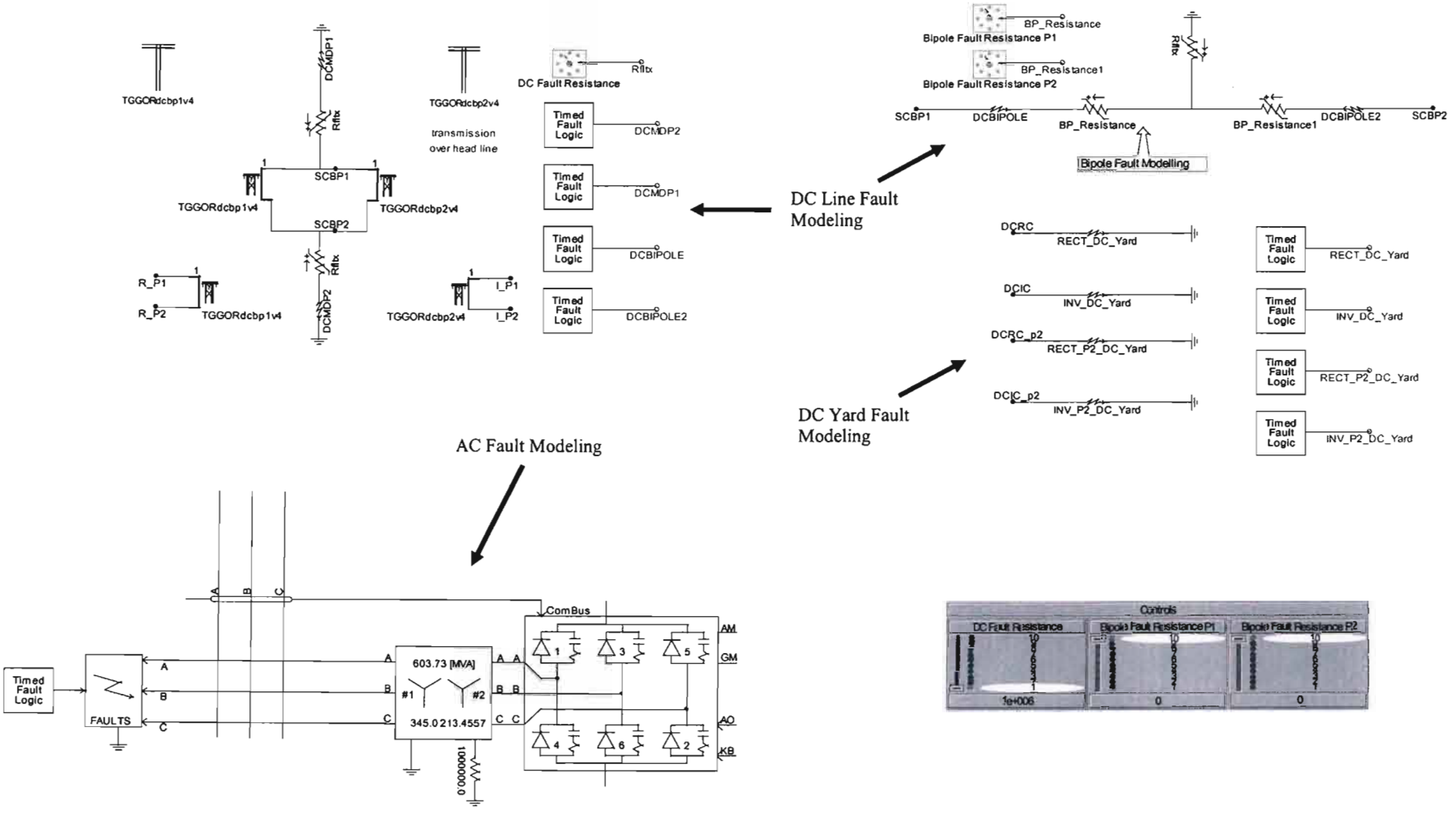

Fig B.3. AC and DC Fault Modelling.

Appendix C

Standard and Auxiliary Cross-Correlation Results

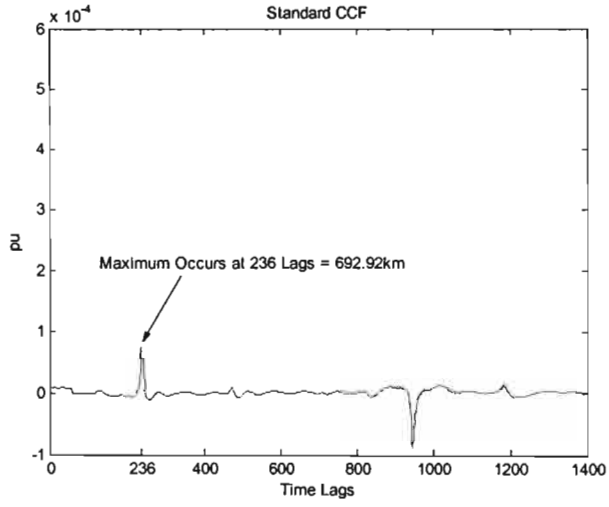

Fig C.1. SCCF output for a P-G Fault located at 700kms.

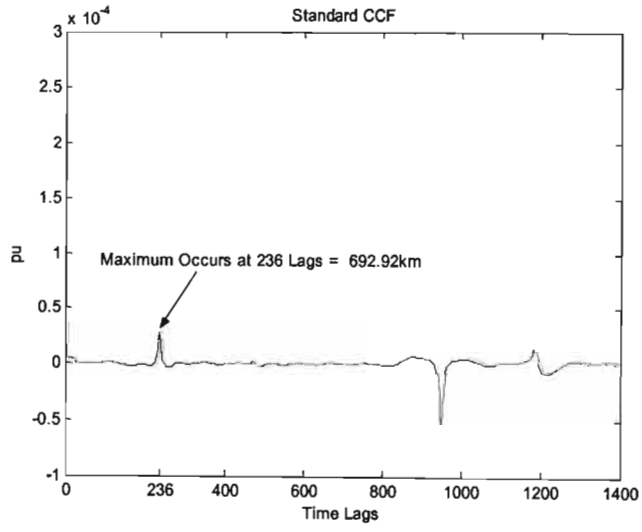

Fig C.2. SCCF output for a P-G Fault located at 700kms with 50Ω fault resistance.

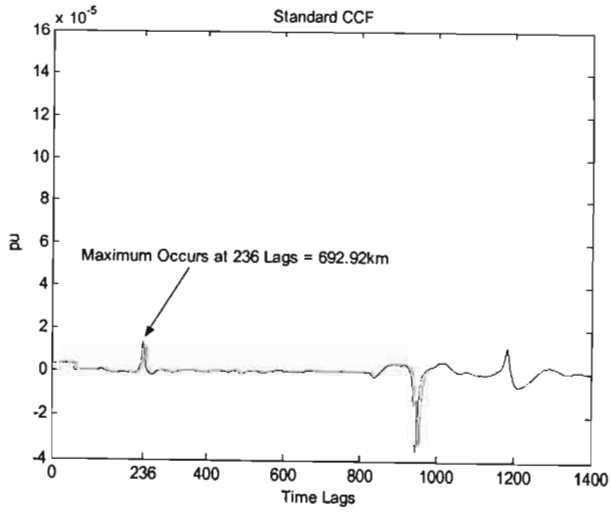

Fig C.3. SCCF output for a P-G Fault located at 700kms with 100Ω fault resistance.

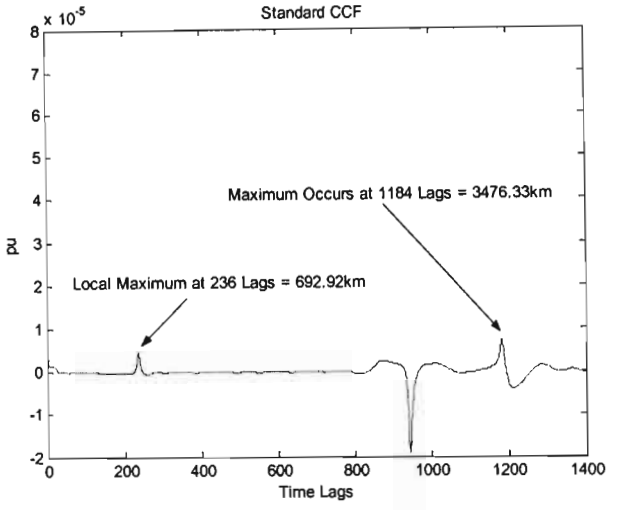

Fig C.4. SCCF output for a P-G Fault located at 700kms with 200Ω fault resistance.

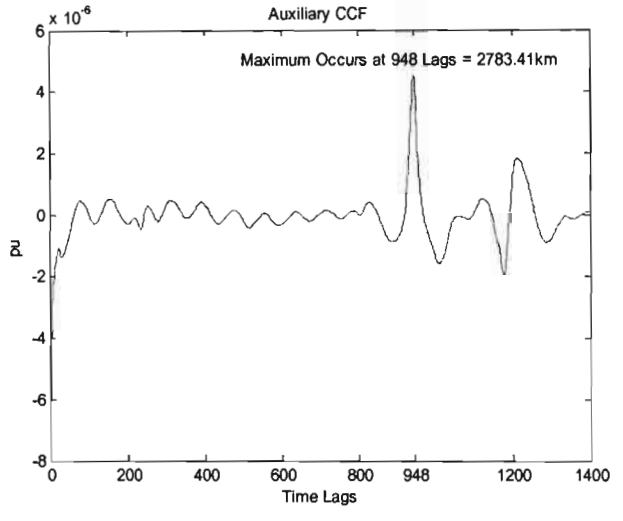

Fig C.5. ACCF output for a P-G Fault located at 700kms with 200Ω fault resistance.

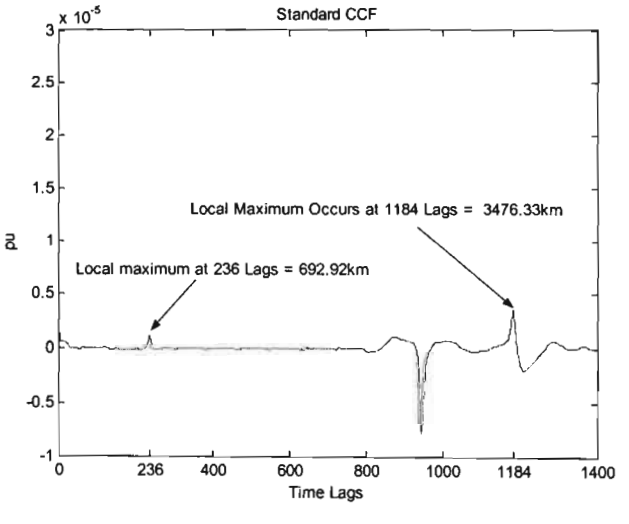

Fig C.6. SCCF output for a P-G Fault located at 700kms with 400Ω fault resistance.

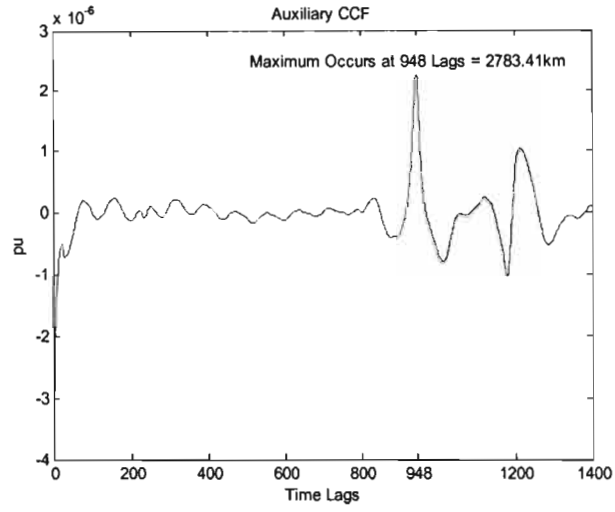

Fig C.7. ACCF output for a P-G Fault located at 700kms with 400Ω fault resistance.

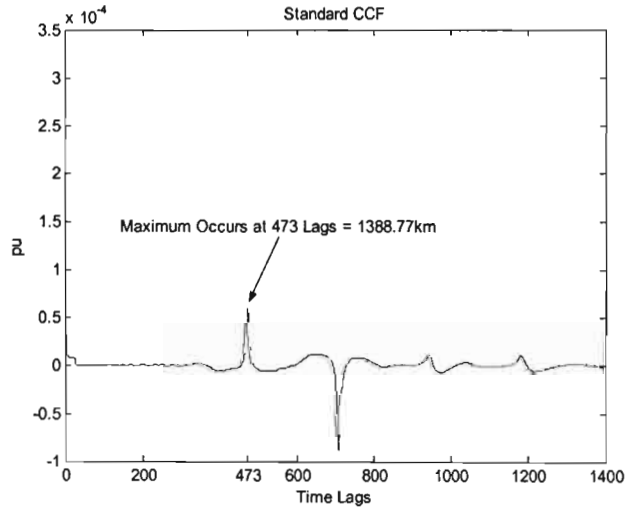

Fig C.8. SCCF output for a P-G Fault located at 1400kms.

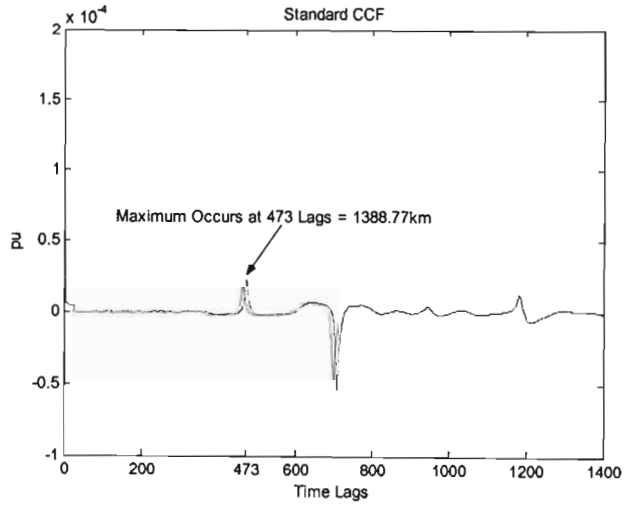

Fig C.9. SCCF output for a P-G Fault located at 1400kms with 50Ω fault resistance.

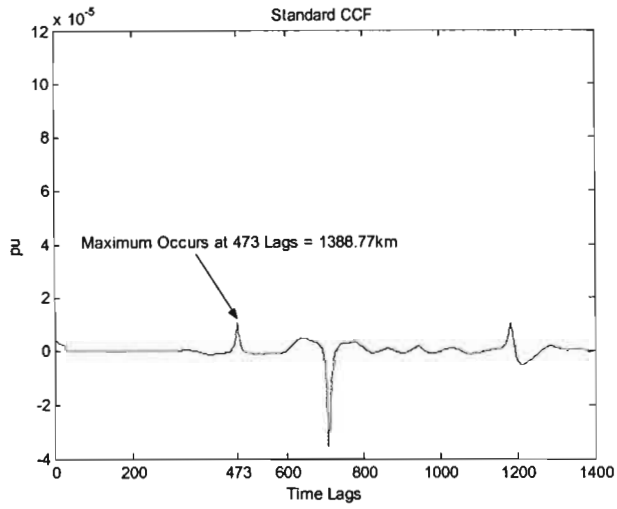

Fig C.10. SCCF output for a P-G Fault located at 1400kms with 100Ω fault resistance.

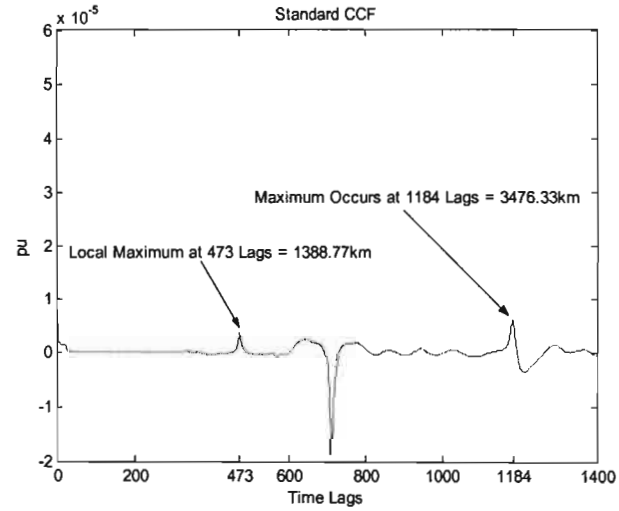

Fig C.11. SCCF output for a P-G Fault located at 1400kms with 200Ω fault resistance.

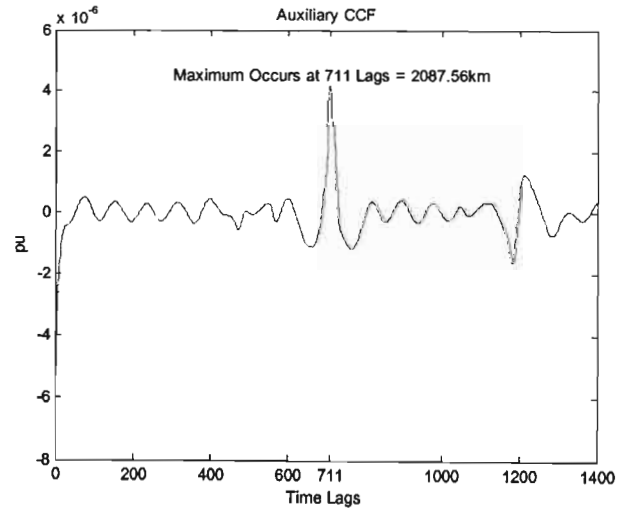

Fig C.12. ACCF output for a P-G Fault located at 1400kms with 200Ω fault resistance.

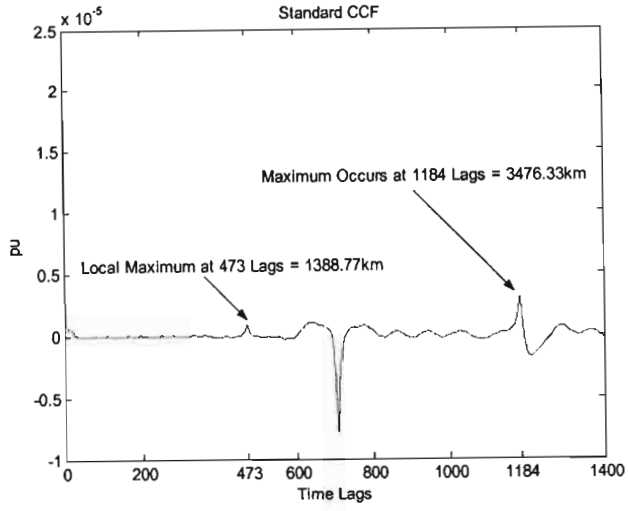

Fig C.13. SCCF output for a P-G Fault located at 1400kms with 400Ω fault resistance.

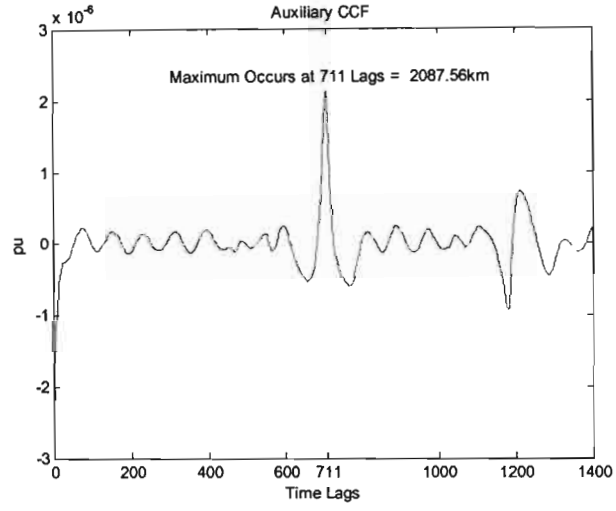

Fig C.14. ACCF output for a P-G Fault located at 1400kms with 400Ω fault resistance.

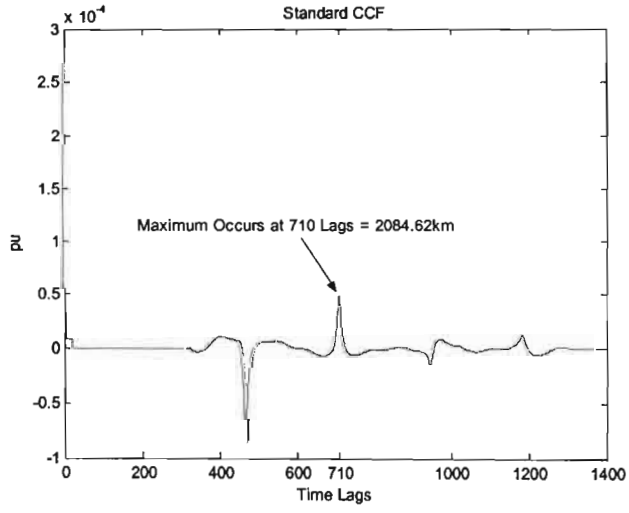

Fig C.15. SCCF output for a P-G Fault located at 2100kms.

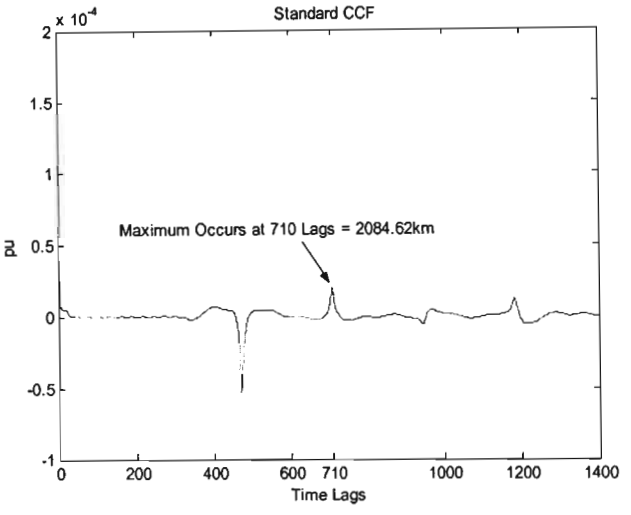

Fig C.16. SCCF output for a P-G Fault located at 2100kms with 50Ω fault resistance.

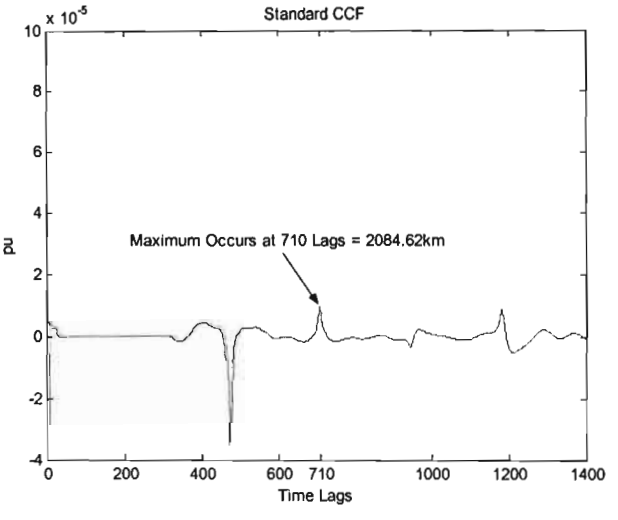

Fig C.17. SCCF output for a P-G Fault located at 2100kms with 100Ω fault resistance.

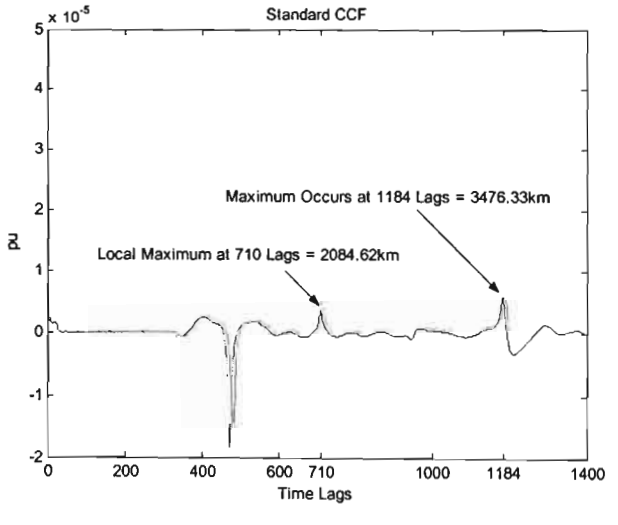

Fig C.18. SCCF output for a P-G Fault located at 2100kms with 200Ω fault resistance.

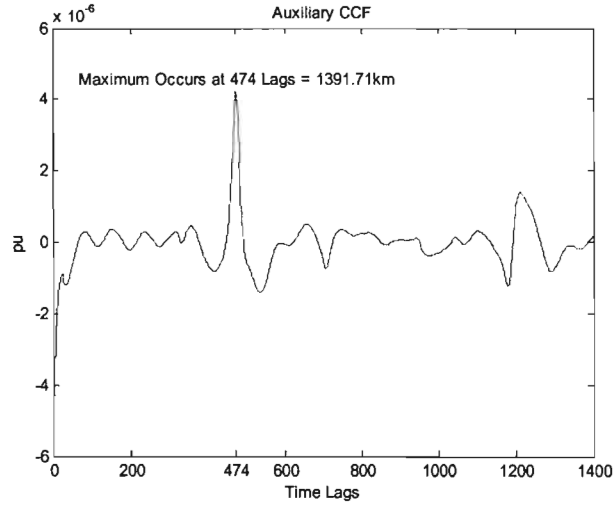

Fig C.19. ACCF output for a P-G Fault located at 2100kms with 200Ω fault resistance.

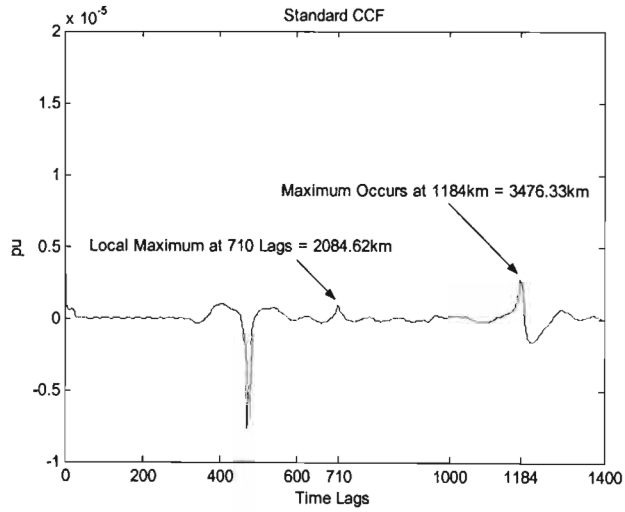

Fig C.20. ACCF output for a P-G Fault located at 2100kms with 400Ω fault resistance.

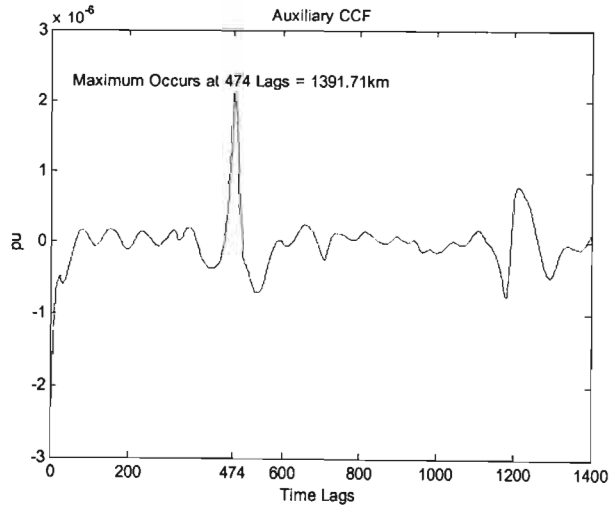

Fig C.21. ACCF output for a P-G Fault located at 2100kms with 400Ω fault resistance.

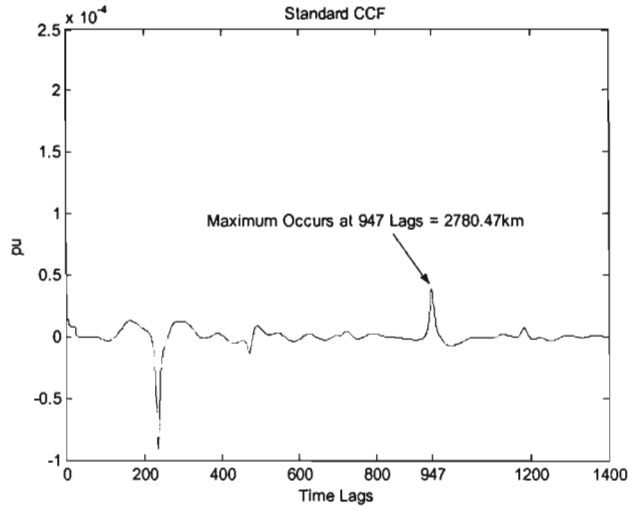

Fig C.22. SCCF output for a P-G Fault located at 2800kms.

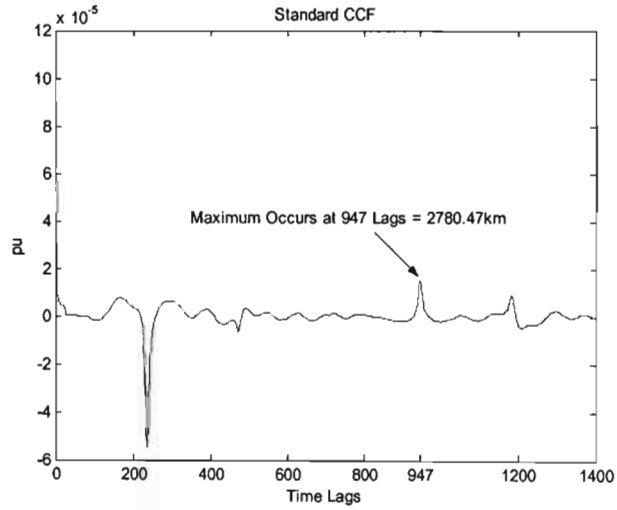

Fig C.23. SCCF output for a P-G Fault located at 2800kms with 50Ω fault resistance.

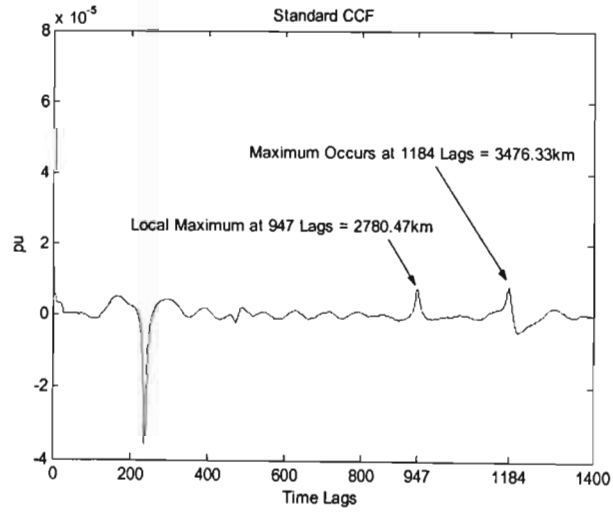

Fig C.24. SCCF output for a P-G Fault located at 2800kms with 100Ω fault resistance.

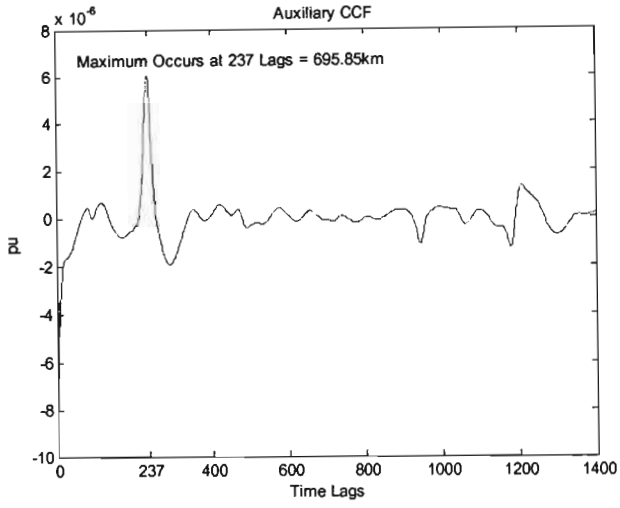

Fig C.25. ACCF output for a P-G Fault located at 2800kms with 100Ω fault resistance.

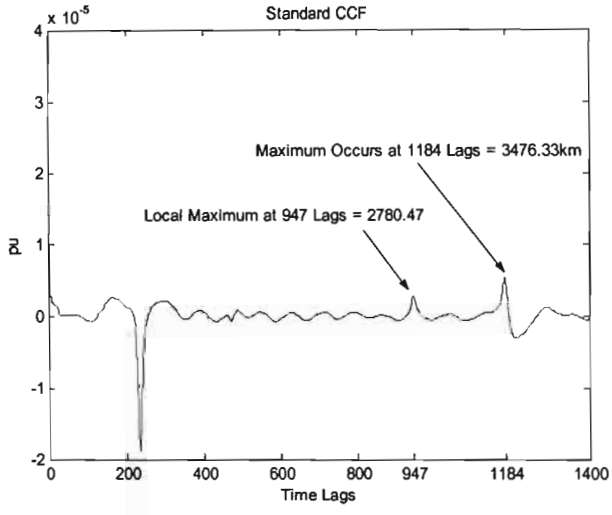

Fig C.26. SCCF output for a P-G Fault located at 2800kms with 200Ω fault resistance.

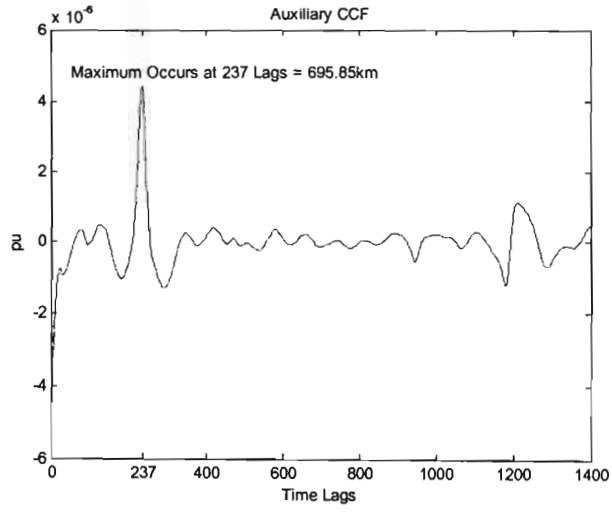

Fig C.27. ACCF output for a P-G Fault located at 2800kms with 200Ω fault resistance.

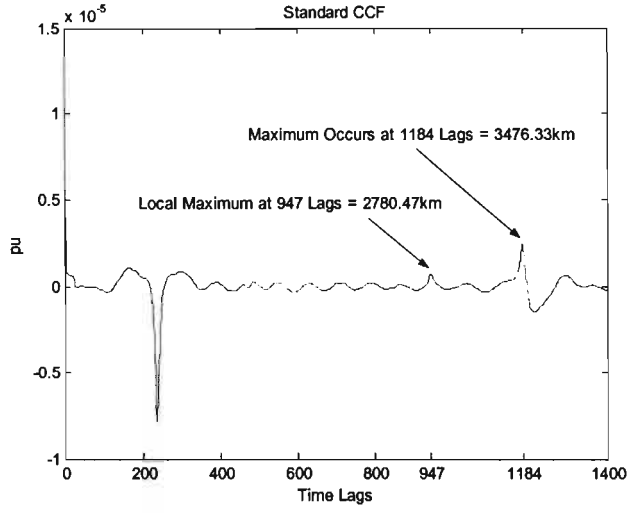

Fig C.28. SCCF output for a P-G Fault located at 2800kms with 400Ω fault resistance.

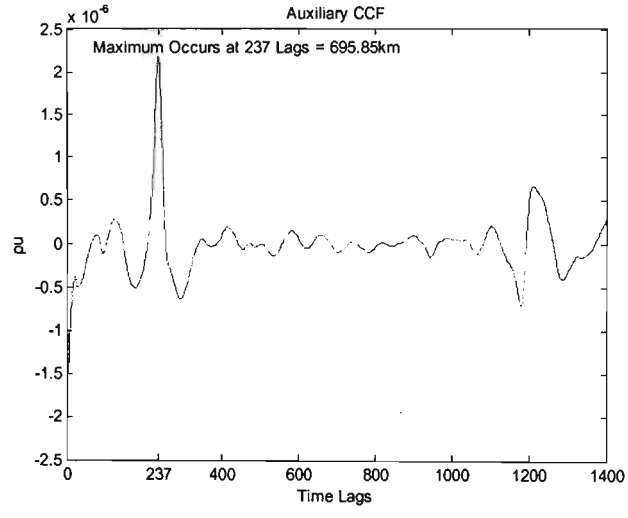

Fig C.29. ACCF output for a P-G Fault located at 2800kms with 400Ω fault resistance.